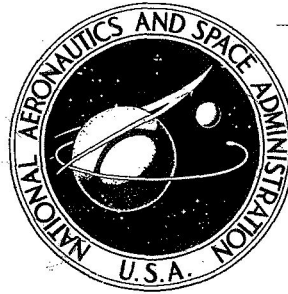NASA TECHNICAL
REPORT

NASA TR R-343

NASA TR R-343

DYNAMICAL EVOLUTION OF DISK GALAXIES

by Frank Hohl

Langley Research Center
Hampton, Va. 23365

1. Report No. NASA TR R-343	2. Government Accession No.	3. Recipient's Catalog No.
4. Title and Subtitle DYNAMICAL EVOLUTION OF DISK GALAXIES		5. Report Date July 1970
		6. Performing Organization Code
7. Author(s) Frank Hohl		8. Performing Organization Report No. L-7110
9. Performing Organization Name and Address NASA Langley Research Center Hampton, Va. 23365		10. Work Unit No. 129-02-22-01
		11. Contract or Grant No.
12. Sponsoring Agency Name and Address National Aeronautics and Space Administration Washington, D.C. 20546		13. Type of Report and Period Covered Technical Report
		14. Sponsoring Agency Code

15. Supplementary Notes

16. Abstract

     A computer model for isolated disks of stars is presented and is used to study the self-consistent motion of large numbers of point masses as they move in the plane of the galactic disk. The Control Data 6600 computer system at the Langley Research Center was used to integrate the equations of motion for each star for systems containing from 50 000 to 200 000 stars. Any initially cold balanced disk was found to be violently unstable. A sufficient amount of velocity dispersion will stabilize all small-scale disturbances. However, most disks investigated were found to be unstable against slowly growing long-wavelength modes, and after about two rotations the disks tended to assume a bar-shaped structure. It was also found that the final mass distribution for most disks could be closely approximated by an exponential variation irrespective of the initial mass distribution. To study the development of spiral structure, the model was modified to include a fixed central force similar to that in the Schmidt model of the Galaxy. The mass of the stars in the disk was taken to be from 5 to 50 percent of the total mass of the Galaxy. The evolution of a number of initial distributions of stars was investigated. The results of the calculations gave a velocity dispersion for the disk stars which was about 50 percent larger than the value of about 30 km/sec found from observation of stars in the solar neighborhood. For some of the disks investigated, a pronounced spiral structure remained even after 8.5 rotations.

17. Key Words (Suggested by Author(s)) Disk galaxies Stellar dynamics Computer model	18. Distribution Statement Unclassified – Unlimited		
19. Security Classif. (of this report) Unclassified	20. Security Classif. (of this page) Unclassified	21. No. of Pages 110	22. Price* $3.00

CONTENTS

DYNAMICAL EVOLUTION OF DISK GALAXIES

By Frank Hohl
Langley Research Center

SUMMARY

A computer model for isolated disks of stars is presented and is used to study the self-consistent motion of large numbers of point masses as they move in the plane of the galactic disk. The Control Data 6600 computer system at the Langley Research Center was used to integrate the equations of motion for each star for systems containing from 50 000 to 200 000 stars. Any initially cold balanced disk was found to be violently unstable. A sufficient amount of velocity dispersion will stabilize all small-scale disturbances. However, most disks investigated were found to be unstable against slowly growing long-wavelength modes, and after about two rotations the disks tended to assume a bar-shaped structure. It was also found that the final mass distribution for most disks could be closely approximated by an exponential variation irrespective of the initial mass distribution.

To study the development of spiral structure, the model was modified to include a fixed central force similar to that in the Schmidt model of the Galaxy. The mass of the stars in the disk was taken to be from 5 to 50 percent of the total mass of the Galaxy. The evolution of a number of initial distributions of stars was investigated. The results of the calculations gave a velocity dispersion for the disk stars which was about 50 percent larger than the value of about 30 km/sec found from observation of stars in the solar neighborhood. For some of the disks investigated, a pronounced spiral structure remained even after 8.5 rotations.

INTRODUCTION

A large fraction of the observable galaxies are spiral galaxies which have a disklike structure. De Vaucouleurs (ref. 1) finds that out of a sample of 1528 bright galaxies 61.1 percent are normal spirals. Lin (ref. 2) estimates that about 70 percent of the known galaxies are normal spirals. A normal spiral galaxy consists of a relatively thin disk-shaped spiral pattern and a central nucleus. Although the disk can be treated as a two-dimensional system, the central nucleus is a complicated three-dimensional system. In general, it is found that the nucleus rotates like a solid body and that the disk rotates with differential rotation (ref. 3). Masses of galaxies range from 10^8 to 10^{12} solar masses

and the dimensions are typically near 10^4 parsec (pc). The Galaxy has a mass of about 10^{11} solar masses. Most of the recent information on the interstellar matter and the structure of the Galaxy is contained in references 4 and 5. It appears that all spiral galaxies contain a small amount of gas, probably less than 10 percent of the total mass. The mass of gas (mostly atomic hydrogen) in the Galaxy is about 3 percent of the total mass (ref. 6). There may be some additional gas in the form of molecular hydrogen (refs. 7 and 8). Much of the gas is concentrated into a thin layer in the galactic disk between about 5 and 15 kpc (ref. 9). In the solar neighborhood, the gas constitutes about 15 to 20 percent of the total mass in the spiral arms (refs. 10 and 11). In the spiral arms the gas density is about three times larger than in the interarm regions. Most of the bright young stars and H II (ionized hydrogen) regions are in the galactic plane near the spiral arms. It is found that many of the spiral galaxies show a two-arm spiral structure. An excellent collection of photographs of galaxies has been compiled by Sandage (ref. 12). In that publication the detailed structure of a number of spiral galaxies is shown.

Oort (ref. 13) has divided the problem concerning spiral structure into two parts. The first part is concerned with the origin of the spiral structure — namely, the mechanism that causes the spiral structure. The second part raises the question of the persistence of the spiral pattern. For example, the Galaxy is about 10 billion years old and its rotational period (in the solar region) is about 200 million years. Thus, a theory is needed which allows the spiral structure to persist even after 50 rotations of a galaxy. One difficulty in many of the early theories of spiral structure is that differential rotation will wind up any spiral structure in only a few rotations (ref. 14).

Many of the recent efforts to explain spiral structure represent the spiral galaxy by an infinitesimally thin disk (refs. 15 to 19). In such models, the galaxy is considered to be an isolated system and the collective field due to purely gravitational effects determines the motion of the stars. Lin and Shu (refs. 20 to 22) have used such a disk model to argue that the spiral structure persists because it is due to a density wave. Similar ideas were put forth earlier by Lindblad (refs. 23 to 25); however, his arguments were less convincing because they were supported primarily by his studies of individual star orbits. Recent investigations (refs. 26 and 27) show that the effects of finite thickness of the galactic disk do not change qualitatively the results obtained with the infinitesimally thin disk model.

An assumption in the present report and in much of the recent work on spiral structure is that the spiral pattern is caused primarily by gravitational effects. This assumption seems to be justified if a comparison is made of the energy density due to the different phenomena in the galaxy. For example, the ratio of the energy density in galactic rotation to that in the magnetic field (10^{-9} Wb/m^2) is about 320 (ref. 22). The energy

density corresponding to cosmic rays, radiation, and turbulent gas motion is even smaller than that of the magnetic field. Nevertheless, the magnetic field may become important (ref. 28) for the motion of gas clouds in the galactic disk (ref. 9). For example, Chandrasekhar and Fermi (ref. 29) proposed that the magnetic field may be responsible for the stability of the spiral structure. Greyber (ref. 30) assumes that matter falling inward from the galactic halo is guided into the nucleus by the magnetic dipole field of the galaxy. The gas is then ejected radially outward from the nucleus into the disk.

Since analytical methods are difficult to apply to the dynamical evolution of galaxies, computer models have been developed to investigate the evolution of self-gravitating systems. There are essentially two different types of computer models. In the first type of computer model, the binary interaction between any pair of stars is important during the evolution of the system under investigation and great care is taken to treat the near encounters of the stars very accurately. In fact, the formation of binaries is one of the difficulties in such calculations. Such a model applies to systems like globular clusters where collisional effects are important. The pioneering work in this area was done by Pasta and Ulam (ref. 31). Von Hoerner (refs. 32 and 33) made extensive calculations by following the three-dimensional motion of up to 25 stars. Aarseth (refs. 34 and 35) was able to treat the motion of 100 masses with his model for clusters of galaxies. More recently, R. Wielen (ref. 36) has used the model to perform a number of numerical experiments to study the dynamical evolution of star clusters. So far, the number of stars that have been treated with this model is only a few hundred because of the large amount of computer time required.

The second type of computer model applies to systems that can be considered collisionless. The force acting on a particular star is then determined by the mean gravitational field of the system and the effect of nearby stars can be neglected (ref. 37, p. 363). Chandrasekhar (ref. 38) points out that for the Galaxy a star can describe at least 100 rotations about the galactic center before the effects of encounters with other nearby stars become important. A galaxy can therefore be studied by using a "collisionless" computer model in which close encounters are effectively neglected. The first such models used were simple one-dimensional models, where the stars are stratified into plane parallel layers or mass sheets (refs. 39 to 43). The one-dimensional model is useful as an approximation to the motion of stars normal to the galactic plane of the Galaxy. The one-dimensional model was also useful in investigating "violent relaxation" of self-gravitating systems (ref. 44). Hénon (refs. 45 and 46) used a model of concentric spherical mass shells to study the dynamical mixing of spherical star clusters. A model of concentric mass rings was used by Toomre (ref. 18). Two-dimensional models, in which the motion of infinitely long mass rods is followed, have been used by Hockney (ref. 47) and by Hohl (refs. 48 to 50) in an attempt to investigate

galactic structure. The applicability of the two-dimensional rod model to stellar structure is questionable. The rod-star model is likely to be valid only for very few galaxies, such as the cigar-shaped galaxy NGC 2685 (ref. 12). The results in the present report were obtained with a collisionless computer model which simulates the motion of large numbers of mass points or finite-length mass rods that are confined to move in the plane of the galactic disk. The model effectively simulates the evolution of an isolated disk of stars. Lindblad (refs. 51 and 52) pioneered such calculations by following the motion of up to 192 mutually attracting mass points in the given central field of the Galaxy. By placing the mass points initially in a system of concentric rings with circular velocities, Lindblad investigated the mutual disturbances in such a system to simulate the spiral structure of galaxies. Because Lindblad was able to follow the motion of only a rather small number of stars, the model is not effective for simulating the evolution of a collisionless galaxy. Miller and Prendergast (ref. 53) developed a model to study the motion of stars in a plane for systems which are doubly periodic and the forces, star positions, and velocities are allowed only discrete (integer) values which are less than some given maximum value.

SYMBOLS

D   impact parameter

E   gravitational field, $\nabla\varphi$

G   gravitational constant

H   Green's function

h   displacement of star for epicyclic motion

$i = \sqrt{-1}$

i,j,k,l   indices

k   wave number

l rod length

M   total mass of disk, Nm

m   star mass

m_f mass of field star

m_t mass of test star

N   dimension of array of cells; total number of stars

N_c number of encounters

n   star density

P   potential energy

p   pressure

$Q = \dfrac{\sigma_r}{\sigma_{r,min}}$

R_0 radius of disk

r, θ, z cylindrical coordinates

T   kinetic energy

t   time

V   rotational velocity

v_t velocity of test star before encounter

$\Delta v_\perp$ increase in perpendicular velocity of test star

x,y,z   Cartesian coordinates

Γ angular momentum

δt time step for advancing motion of system

$\delta(z)$ Dirac delta function

κ	epicyclic frequency
λ	wavelength
λ_c	largest unstable wavelength

$$\xi = \left(1 - \frac{r^2}{R_O{}^2}\right)^{1/2}$$

ρ	mass density
σ	surface mass density
σ_r, σ_θ	velocity dispersion in radial and azimuthal direction, respectively
$\sigma_{r,min}$	velocity dispersion defined by equation (45)
τ_c	relaxation time for collisional effects
τ_r	rotational period
φ	gravitational potential
ω	angular velocity
ω_O	angular velocity of cold balanced disk

Subscripts:

n,m	cell location in x- and y-direction, respectively
max	maximum
min	minimum

Notation:

*	scaled quantity

6

~   Fourier transformed quantity

⟨ ⟩   average value

COMPUTER MODEL

The computer model used to investigate the dynamics of disk galaxies is illustrated in figure 1. The $N \times N$ array of cells shown in figure 1 is superposed over the plane of the galactic disk. The array of cells is introduced only for the purpose of calculating the gravitational potential. The cells are identified by n,m with $n = 0,1,2,...,N-1$ increasing in the x-direction and with $m = 0,1,2,...,N-1$ increasing in the y-direction. The cell in the lower left-hand corner is $0,0$ and that in the upper right-hand corner of the array is $N-1,N-1$. The stars move over this imaginary array of cells. At the center of each cell a mass density is defined which is given by the number of stars in that cell. The number of stars in a cell is usually of the order of 100 and can become much larger near condensations. The density distribution is used to obtain the gravitational potential at the center of each cell. From the gravitational potential, the force acting at the position of a star is computed. Newton's equations of motion are then used to advance the position and velocity of each star by a small time step. For the parameters of a typical galaxy, retardation or relativistic effects need not be considered.

One complete cycle for advancing the motion of the system by a time δt consists of the following procedure. First, the distribution of mass $\sigma_{n,m}$ is used to obtain the gravitational potential $\varphi_{n,m}$ by effectively summing over the density. Second, the gravitational field at the position of the stars is computed from the potential $\varphi_{n,m}$. Third, by applying Newton's laws of motion, the motion of all the stars is advanced for a small time step δt. This procedure represents one cycle and it is repeated until the desired evolution of the system is achieved.

Equations of Motion

The motion of the stars is described by the differential equations

$$\frac{dV_x}{dt} = \frac{\partial \varphi}{\partial x} \qquad \frac{dV_y}{dt} = \frac{\partial \varphi}{\partial y} \qquad (1)$$

and

$$V_x = \frac{dx}{dt} \qquad V_y = \frac{dy}{dt} \qquad (2)$$

The variable φ represents the gravitational potential and the gravitational field is given by $E = \nabla\varphi$. For a star in the (n,m)th cell, equations (1) and (2) in the time-centered finite difference form (refs. 54 and 55) are

$$\frac{1}{\delta t}\left[V_x\left(t + \frac{\delta t}{2}\right) - V_x\left(t - \frac{\delta t}{2}\right)\right] = \left(E_x(t)\right)_{n,m} \tag{3}$$

and

$$\frac{1}{\delta t}\left[x(t + \delta t) - x(t)\right] = V_x\left(t + \frac{\delta t}{2}\right) \tag{4}$$

with similar equations for the y-components. The numerical calculations can be speeded up greatly by scaling the distance so that the cell dimensions are equal to unity, that is, $\Delta x^* = \Delta y^* = 1$. If, in addition, the velocity and mass of a star are scaled as

$$V_x^* = V_x \frac{\delta t}{\Delta x} \tag{5}$$

and

$$m^* = \frac{G(\delta t)^2}{2(\Delta x)^2} m \tag{6}$$

then the potential is scaled as

$$\varphi^* = \frac{(\delta t)^2}{2(\Delta x)^2} \varphi$$

The equations of motion take on the simplified form

$$V_x^*\left(t + \frac{\delta t}{2}\right) = V_x^*\left(t - \frac{\delta t}{2}\right) + \left(E_x^*(t)\right)_{n,m} \tag{7}$$

and

$$x^*(t + \delta t) = x^*(t) + V^*\left(t + \frac{\delta t}{2}\right) \tag{8}$$

Two methods were used to obtain the gravitational field. The simple method is to let each star in a particular cell experience the same field components, namely,

$$\left(E_x^*\right)_{n,m} = \varphi_{n+1,m}^* - \varphi_{n-1,m}^* \tag{9}$$

for the x-component of the gravitational field in the   n,m   cell and

$$\left(E_y^*\right)_{n,m} = \varphi_{n,m+1}^* - \varphi_{n,m-1}^* \tag{10}$$

for the y-component of the field.   Equations (9) and (10) show that all stars in the cell (n,m) experience the same gravitational field and the value of the field will jump in crossing the cell boundaries.   A smoother variation of the field acting on a star is obtained by means of a bilinear interpolation of the fields (as given by eqs. (9) and (10) at the four cell centers surrounding the position of a particular star.   The two components of the field are then given by

$$E_x^* = (1 - \delta y)(1 - \delta x)\left(\varphi_{n+1,m}^* - \varphi_{n-1,m}^*\right) + \delta y(1 - \delta x)\left(\varphi_{n+1,m+1}^* - \varphi_{n-1,m+1}^*\right)$$

$$+ \delta x(1 - \delta y)\left(\varphi_{n+2,m}^* - \varphi_{n,m}^*\right) + \delta x\, \delta y\left(\varphi_{n+2,m+1}^* - \varphi_{n,m+1}^*\right) \tag{11}$$

and

$$E_y^* = (1 - \delta y)(1 - \delta x)\left(\varphi_{n,m+1}^* - \varphi_{n,m-1}^*\right) + \delta x(1 - \delta y)\left(\varphi_{n+1,m+1}^* - \varphi_{n+1,m-1}^*\right)$$

$$+ \delta y(1 - \delta x)\left(\varphi_{n,m+2}^* - \varphi_{n,m}^*\right) + \delta x\, \delta y\left(\varphi_{n+1,m+2}^* - \varphi_{n+1,m}^*\right) \tag{12}$$

where the pertinent parameters are defined in figure 2.   It is found that the bilinear interpolation gives a slightly more definite structure for the condensations which occurred during the initial evolution of a system.   After about one rotation, the results obtained by the two methods display essentially the same structure.

If a star should leave the   N × N   array of cells, the field acting on it is calculated by placing all the mass remaining in the system at the center of the array.   The stars outside the array will not interact among themselves, but they will be attracted by the central force due to the mass placed at the center of the array.   Whenever an appreciable number of stars leave the array, the calculations are no longer accurate and the computer run should be repeated by either increasing the array or by changing the initial conditions.

The Potential Calculation

In calculations with the two-dimensional rod model (refs. 47 and 49), the gravitational potential is easily obtained by solving the two-dimensional Poisson equation

$$\frac{\partial^2 \varphi}{\partial x^2} + \frac{\partial^2 \varphi}{\partial y^2} = 4\pi G \rho(x,y) \tag{13}$$

An attempt therefore might be made to obtain the gravitational potential for the disk model by the same method. The Poisson equation then becomes

$$\frac{\partial^2 \varphi}{\partial x^2} + \frac{\partial^2 \varphi}{\partial y^2} + \frac{\partial^2 \varphi}{\partial z^2} = 4\pi G \sigma(x,y)\,\delta(z) \tag{14}$$

where $\delta(z)$ is the Dirac delta function and $\sigma(x,y)$ is the surface density of stars in the plane of the disk. The difficulty is that no means are available to evaluate $\partial^2 \varphi / \partial z^2$. Therefore,

$$\varphi(x,y) = G \int \int \frac{\sigma(x',y')}{\sqrt{(x-x')^2 + (y-y')^2}}\, dx'\,dy' \tag{15}$$

is used to obtain the gravitational potential from the mass density (the primes denote variables over which integration is performed). Presently the density is given only at a finite number of cells separated by a unit distance so that the integral can be changed to a summation

$$\varphi_{n,m} = \sum_{i=0}^{N-1} \sum_{j=0}^{N-1} \sigma_{i,j} H_{i-n,j-m} \tag{16}$$

where N is the dimension of the array of cells and H is Green's function defined by

$$H_{i,j} = \frac{1}{\sqrt{i^2 + j^2}} \tag{17}$$

To perform directly the summation indicated by equation (16) requires the summation of N^4 terms. For $N = 100$, $N^4 = 10^8$ and the time required to obtain φ becomes excessive.

10

Summation Method

A faster approximate method to obtain the gravitational potential is illustrated in figure 3. In the summation method, the density $\sigma_{n,m}$ in each cell is first determined. Next, the density $\left(\sigma_T\right)_{n,m}$ which consists of $\sigma_{n,m}$ plus the density of the surrounding eight cells is found. The potential at the center of a particular cell is then obtained by summing the contributions of the surrounding eight cells and the contribution of σ_T at the center of each of the larger cells (fig. 3); that is,

$$\varphi_{n,m} = \left[\sigma_{n,m} + \sigma_{n,m+1} + \sigma_{n,m-1} + \sigma_{n-1,m} + \sigma_{n+1,m} + \frac{1}{\sqrt{2}}\left(\sigma_{n+1,m+1}\right.\right.$$

$$\left.\left. + \sigma_{n+1,m-1} + \sigma_{n-1,m-1} + \sigma_{n-1,m+1}\right)\right] + \sum_i \sum_j \left(\sigma_T\right)_{i,j} H_{i-n,j-m} \qquad (18)$$

where

$$H_{i-n,j-m} = \frac{1}{\sqrt{(i-n)^2 + (j-m)^2}} \qquad \left((i-n)^2 + (j-m)^2 > 0\right) \qquad (19a)$$

$$H_{0,0} = 0 \qquad (19b)$$

The addition of the term $\sigma_{n,m}$ in equation (18) is equivalent to setting the self-potential equal to unity. The condition $H_{0,0} = 0$ in equation (19b) simply omits the contribution of $\left(\sigma_T\right)_{n,m}$ in the double summation of equation (18). The values of $H_{i-n,j-m}$ are stored in an array and have to be calculated only once during a particular run. The indices i and j in the double summation increase in increments of 3 such that one of the values of i and of j is equal to n and to m, respectively, and the summation is over every third value of $\left(\sigma_T\right)_{n,m}$. With equation (18) the number of operations is $(N+1)^2\left[9 + (N+1)^2/9\right]$, a reduction of almost 1 order of magnitude over the number of operations required in the direct summation method. In a subsequent section the results obtained by the summation method are compared with those obtained by the Fourier method. In principle, the method could be extended to include a third class of cells containing the mass of 81 small cells $\sigma_{n,m}$ $\left(\text{or 9 large cells } \left(\sigma_T\right)_{n,m}\right)$. The number of operations would then be $(N+1)^2\left[17 + (N+1)^2/81\right]$, a reduction of nearly 2 orders of magnitude over the number of operations in the direct summation method.

.   Another method to obtain the gravitational potential makes use of the fast Fourier transform methods now available (ref. 56). The Fourier transform of the density is defined as (ref. 57)

$$\tilde{\sigma}_{k,l} = \left(\frac{1}{N}\right)^2 \sum_{n=0}^{N-1} \sum_{m=0}^{N-1} \sigma_{n,m} \exp\left[i\,\frac{2\pi}{N}(kn + lm)\right] \tag{20}$$

Similarly, the Fourier transform of Green's function is given by

$$\tilde{H}_{k,l} = \left(\frac{1}{N}\right)^2 \sum_{n=0}^{N-1} \sum_{m=0}^{N-1} H_{n,m} \exp\left[i\,\frac{2\pi}{N}(kn + lm)\right] \tag{21}$$

Applying the finite convolution theorem to equation (16) gives the result (refs. 57, 58, and 59)

$$\varphi_{n,m} = \sum_{i=0}^{N-1} \sum_{j=0}^{N-1} \sigma_{i,j} H_{i-n,j-m}$$

$$= \left(\frac{1}{N}\right)^2 \sum_{k=0}^{N-1} \sum_{l=0}^{N-1} \tilde{\sigma}_{k,l} \tilde{H}_{k,l} \exp\left[-i\,\frac{2\pi}{N}(kn + lm)\right] \tag{22}$$

From equation (22) and the definition of the Fourier transform, it is clear that

$$\tilde{\varphi}_{k,l} = \tilde{\sigma}_{k,l} \tilde{H}_{k,l}$$

Therefore, the potential $\varphi_{n,m}$ is obtained directly from the inverse Fourier transform of $\tilde{\sigma} \cdot \tilde{H}$. Such a method gives a doubly periodic system and one can expect the tidal interaction between image galaxies to be important. A similar method is used by Miller and Prendergast (ref. 53) in their investigation of doubly periodic stellar systems.

The Fourier transform method just described can be modified to obtain the potential distribution for an isolated system. This modification is achieved by increasing the number of cells by a factor of 4 and by confining the system to one-quarter of the array of cells. The mass density in the remaining three-quarters of the array will then always be identically zero.

Consider now that in addition to the array under investigation, the summation in equation (16) is extended over all the doubly infinite array of images. However, Green's

function $H_{n,m}$ is now modified so that it corresponds to the correct single particle potential for particle separation r less than $N/2$ (one-half the dimension of the array) and to zero interaction for r greater than $N/2$. Even though the system is still doubly periodic, there is no longer any interaction between adjacent image systems because their masses are separated by at least $N/2$.

Thus, to get the correct potential for an isolated system at the expense of a four-fold increase in storage, Green's function to be used in equation (22) is

$$H_{n,m} = \frac{1}{\sqrt{n^2 + m^2}} \qquad \begin{array}{l} \left(0 \leq n,m \leq \frac{N}{2}\right) \\[2mm] \left(n^2 + m^2 \neq 0\right) \end{array} \qquad (23a)$$

$$H_{N-n,m} = H_{n,N-m} = H_{N-n,N-m} = H_{n,m} \qquad (23b)$$

and

$$H_{0,0} = 1 \qquad (23c)$$

As before, setting $H_{0,0} = 1$ is equivalent to setting the self-potential of a star equal to unity. The Fourier transform of $H_{n,m}$ need be done only once. Also, because of the symmetry of $H_{n,m}$ only a finite cosine transform on a $\left(\frac{N}{2} + 1\right) \times \left(\frac{N}{2} + 1\right)$ mesh is required. The modified Fourier transform approach is described in references 58 and 59. It should be pointed out that the Fourier transform method solves equation (16) for the isolated system exactly (within computer rounding error). A computer listing and a description of the Fourier method are given in the appendix.

Arbitrary Force Law

The two methods presented for obtaining the gravitational potential can easily be extended to three-dimensional problems. Also, the force law between particles can easily be changed by simply changing Green's function H. For example, some of the effects of finite thickness of the galactic disk can be simulated by using finite-length mass rods instead of point masses to represent the stars. The force of attraction F between two mass rods of unit mass and of length l alined perpendicular to the galactic plane with their centers in the galactic plane is

$$F = \frac{2G}{l^2}\left[\sqrt{1 + \left(l^2/r^2\right)} - 1\right]$$

13

where r is the separation of the two rods. Green's function then becomes

$$H_{n,m} = \frac{2}{l}\left\{\frac{r_{n,m}}{l}\left[1 - \sqrt{1 + \left(l^2/r_{n,m}^2\right)}\right] + \log_e\left[\frac{l}{r_{n,m}} + \sqrt{1 + \left(l^2/r_{n,m}^2\right)}\right]\right\} \tag{24}$$

where $r_{n,m} = \sqrt{n^2 + m^2}$. Figure 4 shows $H_{n,m}$ for four values of l.

Comparison of Methods for Obtaining Gravitation Potential

The time required to obtain the gravitational potential by the Fourier method for a 64×64 active array (Fourier transform must be performed on 128×128 array) was 2 seconds on the Control Data 6600 computer system at the Langley Research Center. The Fourier analysis and synthesis were performed with a program written in COMPASS assembly code. The remainder of the potential solver was written in FORTRAN IV. For the summation method, the time required was 6 seconds with the program written in COMPASS assembly code. The time required for a FORTRAN IV program is increased by nearly a factor of 3.

The time required to advance the motion and to calculate the density for a 50 000-star system is 8.6 seconds when the positions and velocities of the stars are stored on magnetic disks and are placed into fast storage 10 000 at a time.

Since the star coordinates are stored on magnetic disks, the number of stars that can be handled is essentially limited only by the available computer time. With packing, the summation method only takes one-half of the storage required by the Fourier method. Since the potential array is always kept in fast storage, the summation method makes possible the use of a larger mesh.

Energy and Momentum Conservation

The angular momentum of the disk at time t is given by

$$\Gamma(t) = \sum_i m_i\left\{x_i\left[\frac{V_{y,i}\left(t + \frac{\delta t}{2}\right) + V_{y,i}\left(t - \frac{\delta t}{2}\right)}{2}\right] - y_i\left[\frac{V_{x,i}\left(t + \frac{\delta t}{2}\right) + V_{x,i}\left(t - \frac{\delta t}{2}\right)}{2}\right]\right\} \tag{25}$$

where m_i is the mass of the ith star, $V_{x,i}$ is the x-component of the velocity of that star, and the summation extends over all the stars. For most of the systems investigated, the angular momentum remained constant to within 0.15 percent during the first one-half rotation of the system.

The kinetic energy of the disk at time t is

$$T(t) = \frac{1}{2} \sum_i m_i \left\{ \left[\frac{V_{x,i}\left(t + \frac{\delta t}{2}\right) + V_{x,i}\left(t - \frac{\delta t}{2}\right)}{2} \right]^2 + \left[\frac{V_{y,i}\left(t + \frac{\delta t}{2}\right) + V_{y,i}\left(t - \frac{\delta t}{2}\right)}{2} \right]^2 \right\} \tag{26}$$

An approximate expression for the potential energy is

$$P = -\frac{1}{2} \sum_n \sum_m \sigma_{n,m} \varphi_{n,m} \tag{27}$$

A better definition of the potential energy should be devised by using the definition of potential energy as the work done on a test star and apply it to the present model. The difficulty in the use of equation (27) is that in regions of large mass condensations this equation gives a value of φ which is too large for the potential energy. During the first one-half rotation, equations (26) and (27) give a value of the total energy which remains constant within 0.5 percent.

Effect of Varying Discretization Parameters

Figure 5 shows how the evolution of the system is affected by varying the discretization parameters of the system. This figure illustrates the evolution of initially uniformly rotating (solid-body rotation) balanced disks of stars. In figure 5(b) the initially cold disk contains 50 000 stars and the gravitational potential for this disk is obtained by the summation method. The time indicated is in rotational periods. Figure 5(a) presents the evolution of an identical system but with the potential calculated by means of the Fourier transform technique. It should be pointed out that the initial perturbations present in the systems in figures 5(a) and 5(b) are identical since the initial positions for the two disks were generated by the same pseudorandom number generator. The number of time steps per rotation is 200. After a quarter rotation, the summation method is seen to give a finer structure for the condensations than the Fourier transform method. The distance between condensations in figure 5(b) is about the dimension of one large cell (3 × 3 small cells) and the condensations are within one large cell. Because of the approximation made by introducing the larger cells in the summation method, the interaction between masses separated by two (or more) cell dimensions is decreased. This effect explains the finer structure of the initial condensation in figure 5(b). A comparison of figure 5(a) and figure 5(b) shows that after one-half rotation the overall structure of the condensations is the same for the two methods. Even after one rotation the results are very similar. It should be noted that since the system is violently unstable, any

small change in method of computation or initial conditions will cause rather large deviation in the overall structure of the condensations which occur as the disk breaks up.

Figure 5(c) shows the effect of changing the time step from 200 to 400 time steps per rotation with the gravitational potential being obtained by the Fourier method. For the first one-half rotation the evolution is the same as that of figure 5(a). After one rotation the number of condensations for the two disks is the same, but the relative positions are changed somewhat. Again, it should be noted that for all disks in figure 5, the initial pseudorandom positions are identical so that the perturbations caused by them are the same.

Figure 5(d) shows the effect of increasing the number of stars to 200 000. This increase is obtained by distributing four stars in the neighborhood of the position of each of the original 50 000 stars. Thus, the perturbations caused by the initial positions of the stars should be similar to those of the previous systems. The results shown in figure 5(d) indicate that increasing the number of stars has very little effect on the evolution of the system. The effect of reducing the mesh size was also checked. It was found that on a 128×128 active mesh the condensations are much finer than those for the 64×64 mesh. This result is to be expected for the extreme case of an initially cold disk. Toomre (ref. 18) has shown that a cold disk of stars is unstable to perturbations of arbitrarily small wavelengths. Since the smallest condensations possible in the present model are of the dimensions of a cell, a decrease in the cell dimensions will allow smaller condensations to occur. It has been shown by Toomre (ref. 18) that the short-wavelength modes are stabilized by the effects of velocity dispersion. The effect of changing the cell dimension was also compared for an initial disk of stars with sufficiently large random velocities to stabilize modes of the order of a few cell dimensions. Decreasing the cell dimension by a factor of 2 had essentially no effect on the evolution of the system (ref. 59).

It was also found that using the cloud-in-cell (CIC) (ref. 60) method had little effect on the evolution of the system. In the CIC method of calculation, each star has the dimension of a cell and its mass is distributed among four cells in proportion to the fraction of particle area in a cell.

The photographs in figure 5 of the star disks were made with the model dd80B display-recorder system of the Data Display Division of Control Data Corporation. This system produces both 35-mm motion-picture film or page-size recordings.

EVOLUTION OF SELF-CONSISTENT DISK GALAXIES

The first disk galaxies to be investigated are completely self-consistent disks of stars without any imposed gravitational field. The initial conditions chosen are such that

the gravitational attraction acting on the stars is balanced by the centrifugal force due to the rotation of the stars around the center of the system.

Initial Condition

Various authors (refs. 17 and 61 to 63) have constructed time-independent models for disk galaxies. An initial condition used extensively in the present calculations corresponds to the familiar simple model of a uniformly rotating disk with a surface mass density given by

$$\sigma(r) = \sigma(0)\left(1 - \frac{r^2}{R_o^2}\right)^{1/2}$$

$$= \frac{3M}{2\pi R_o^2}\left(1 - \frac{r^2}{R_o^2}\right)^{1/2} \tag{28}$$

where r is the radial coordinate, R_o is the radius of the disk, and M is the total mass of the disk. The uniform angular velocity required to balance the gravitational attraction is then

$$\omega = \sqrt{3G\pi Nm/4R_o^3} \tag{29}$$

where $M = Nm$, N being the number of stars in the system and m the mass per star. To treat disks with a higher central condensation, Toomre suggested the use of the following generalization of equation (28):

$$\sigma_n(r) = \frac{M}{2\pi R_o^2}(2n + 1)\left(1 - \frac{r^2}{R_o^2}\right)^{n-1/2} \tag{30}$$

where $n = 1, 2, 3, \ldots$.

Dr. C. Hunter of the Massachusetts Institute of Technology has found that the angular velocity ω for such a density distribution is given by

$$\omega_n^2(\xi) = \frac{\pi GM}{R_o^3}\frac{(2n - 2)!\,(2n + 1)!}{2^{4n-1}(n!)^2\left[(n - 1)!\right]^2}\,{}_2F_1\left(1-n,\frac{3}{2};\frac{3}{2} - n;\xi^2\right) \tag{31}$$

where

$$\xi^2 = \left(1 - \frac{r^2}{R_o^2}\right) \tag{32}$$

and $_2F_1$, the usual hypergeometric function (ref. 64), is found from

$$_2F_1\left(1-n,\frac{3}{2};\frac{3}{2}-n;\xi^2\right) = 1 + \frac{(1-n)\left(\frac{3}{2}\right)}{\left(\frac{3}{2}-n\right)}\frac{\xi^2}{1!} + \frac{(1-n)(1-n+1)\left(\frac{3}{2}\right)\left(\frac{3}{2}+1\right)}{\left(\frac{3}{2}-n\right)\left(\frac{3}{2}-n+1\right)}\frac{\xi^4}{2!}$$

$$+ \frac{(1-n)(1-n+1)(1-n+2)\left(\frac{3}{2}\right)\left(\frac{3}{2}+1\right)\left(\frac{3}{2}+2\right)}{\left(\frac{3}{2}-n\right)\left(\frac{3}{2}-n+1\right)\left(\frac{3}{2}-n+2\right)}\frac{\xi^6}{3!} + \ldots \tag{33}$$

The square of the rotation speed is

$$V_n^2(r) = r^2\omega_n^2(\xi) \tag{34}$$

For the first five values of n, equation (34) has the form

$$V_1^2(r) = \frac{\pi GM}{R_0}\left(\frac{r}{R_0}\right)^2\left(\frac{3}{4}\right) \tag{35a}$$

$$V_2^2(r) = \frac{\pi GM}{R_0}\left(\frac{r}{R_0}\right)^2\left(\frac{15}{32}\right)\left(1 + 3\xi^2\right) \tag{35b}$$

$$V_3^2(r) = \frac{\pi GM}{R_0}\left(\frac{r}{R_0}\right)^2\left(\frac{105}{256}\right)\left(1 + 2\xi^2 + 5\xi^4\right) \tag{35c}$$

$$V_4^2(r) = \frac{\pi GM}{R_0}\left(\frac{r}{R_0}\right)^2\left(\frac{1575}{4096}\right)\left(1 + \frac{9}{5}\xi^2 + 3\xi^4 + 7\xi^6\right) \tag{35d}$$

$$V_5^2(r) = \frac{\pi GM}{R_0}\left(\frac{r}{R_0}\right)^2\left(\frac{24255}{65536}\right)\left(1 + \frac{12}{7}\xi^2 + \frac{18}{7}\xi^4 + 4\xi^6 + 9\xi^8\right) \tag{35e}$$

Figure 6 shows $\sigma_n(r)$ as a function of r/R_0 for the first five values of n. The corresponding curves for the values of the rotational velocity are given in figure 7. The initial density distribution for most of the disks of stars investigated corresponds to n = 1 in equation (30); a few disks with n = 3 and n = 5 were also studied. The initial positions of the stars are obtained by using a pseudorandom number generator which gives a uniform distribution between 0 and 1 to generate three numbers x_r, y_r, and z_r. If

$$x_r^2 + y_r^2 < 1 \tag{36}$$

and

$$\left(1 - x_r^2 - y_r^2\right)^{n-1/2} > z_r \tag{37}$$

the initial position of a star is given by the x, y coordinates

$$x(t = 0) = 2R_o\left(x_r - 0.5\right) \tag{38}$$

and

$$y(t = 0) = 2R_o\left(y_r - 0.5\right) \tag{39}$$

The initial circular velocity of the stars is given by equation (35a). If the stars have an initial velocity dispersion, a uniform velocity dispersion $\sigma_r = \sigma_\theta$ is superposed on the circular velocity given by equation (35a). For some of the uniformly rotating disks, the pressure effects due to the initial velocity dispersion were taken into account in determining the initial angular velocity required to balance the disk. For these disks, the velocity dispersion was taken to be a function of radius so that

$$\sigma_r(r) = \sigma_r(0)\sqrt{1 - \left(\frac{r}{R_o}\right)^2} \tag{40}$$

The angular velocity required to initially balance the warm disk for $\sigma_r = \sigma_\theta$ is given by

$$\omega^2 = \omega_o^2 + \frac{1}{r\sigma}\frac{\partial p}{\partial r}$$

$$= \omega_o^2 - \frac{3}{R_o^2}\sigma_r^2(0) \tag{41}$$

The angular velocity ω_o is that of the cold disk given by equation (29); the pressure p is found from

$$p = \sigma(r)\sigma_r^2$$

where the density σ is given by equation (28). If $\sigma_r(r) \neq \sigma_\theta(r)$, the angular velocity required to balance the disk is

$$\omega^2 = \omega_o^2 + \frac{1}{r\sigma(r)} \frac{\partial}{\partial r}\left[\sigma(r)\sigma_r^2(r)\right] + \frac{1}{r^2}\left[\sigma_r^2(r) - \sigma_o^2(r)\right] \tag{42}$$

The initial circular velocity required to balance a given density distribution, which is a function of r only, can be obtained directly from the computer model. The given initial density distribution is used to calculate the gravitational potential and the radial gravitational field. The radial field $E_r(r)$ is then used to obtain the angular velocity for stars at a radius r by equating the centrifugal acceleration to the gravitational attraction

$$\frac{V_\theta^2(r)}{r} = \left|E_r(r)\right| \tag{43}$$

or

$$\omega(r) = \sqrt{\frac{\left|E_r(r)\right|}{r}} \tag{44}$$

since

$$V_\theta(r) = r\omega(r)$$

Effect of Velocity Dispersion

All the calculations for uniformly rotating disks presented in this section were performed with disks containing 50 000 stars. There are 200 time steps per rotation and the gravitational field was calculated by equations (9) and (10). A 64 × 64 active mesh was used for the potential calculation.

By using a dimensional order-of-magnitude argument, Toomre (ref. 18) predicted that a cold (zero velocity dispersion) infinitesimally thin disk of stars is violently unstable. The growth time of the unstable modes is approximately proportional to the square root of their wavelength (ref. 16) and, therefore, the small-wavelength disturbances will be the most unstable. Toomre (ref. 18) finds that the root-mean-square radial velocity dispersion required to stabilize all axisymmetric disturbances anywhere in the disk is

$$\sigma_{r,min} = 3.36 \frac{G\sigma}{\kappa} \tag{45}$$

where σ and κ are the local values of the density and epicyclic frequency, respectively. The epicyclic frequency is given by

$$\kappa^2 = \frac{\partial^2 \varphi}{\partial r^2} + \frac{3}{r} \frac{\partial \varphi}{\partial r} \tag{46}$$

Initially the cold uniformly rotating disk is balanced and

$$\frac{\partial \varphi}{\partial r} = \frac{V_\theta^2(r)}{r} = \frac{3\pi GNm}{4R_o^2} r \tag{47}$$

where $V_\theta^2(r) = V_1^2(r)$ is given by equation (35a). Substituting equation (47) into equation (46) gives the following equation for κ^2:

$$\kappa^2 = \frac{3\pi GNm}{R_o^3} = \left[\frac{2V_\theta^2(R_o)}{R_o}\right]^2 \tag{48}$$

The expressions for the density $\sigma(r)$ and κ^2 (eqs. (28) and (48), respectively) can be used in equation (45) to obtain the radial velocity dispersion needed to stabilize the disk. Thus,

$$\sigma_{r,min} = 0.342\sqrt{1 - \left(\frac{r}{R_o}\right)^2} \, V_\theta(R_o) \tag{49}$$

The longest axisymmetric unstable wavelength of a thin pressure free disk was given by Toomre as

$$\lambda_c = \frac{4\pi^2 G\sigma}{\kappa^2} \tag{50}$$

For the uniformly rotating disk, equation (50) reduces to

$$\lambda_c = R_o\sqrt{1 - \left(\frac{r}{R_o}\right)^2} \tag{51}$$

Figure 8 shows the evolution of an initially uniformly rotating balanced disk with zero velocity dispersion. The time is in rotational periods given by

$$\tau_r = 2\pi \left(\frac{3\pi GNm}{4R_o^3}\right)^{-1/2} \tag{52}$$

The initial kinetic energy of the cold balanced disk is

$$T(t=0) = \frac{1}{2} \int_0^{R_0} \sigma(r) V_\theta^2(r) 2\pi r \; dr$$

$$= \frac{3\pi G M^2}{20 R_0}$$

where $\sigma(r)$ and $V_\theta^2(r) = V_1^2(r)$ are given by equations (28) and (35a), respectively. The initial potential energy is given by

$$P(t=0) = \frac{1}{2} \int_0^{R_0} \sigma(r) \varphi(r) 2\pi r \; dr$$

$$= -\frac{3\pi G M^2}{10 R_0}$$

where

$$\varphi(r) = \frac{3\pi G M}{8 R_0^3} r^2 - \frac{3\pi G M}{4 R_0}$$

The virial theorem is of course satisfied at $t = 0$, that is,

$$2T(t=0) + P(t=0) = 0$$

The values of $P(t=0)$ and $T(t=0)$ were found to agree with the computer generated values obtained by using equations (26) and (27). As predicted by Toomre (ref. 18) the cold disk is violently unstable and the growth time for the instabilities is a fraction of the rotational period. Since the growth time of a disturbance is approximately proportional to the square root of its wavelength, the fast appearance of the small-scale condensations is to be expected. After 1.1 rotations there remain five main condensations. The same information is contained in figure 9 which shows the evolution of the gravitational potential contours in the plane of the disk. The relative sizes of the condensations can be more easily distinguished in figure 9. The evolution displayed in figures 8 and 9 is rather violent and the stars quickly build up a large velocity dispersion. The random-ization can also be observed in the evolution of the velocity distribution for this system (fig. 10). At $t = 0.4\tau_r$, the velocity distribution displays a ringlike structure which, however, has disappeared after 1.1 rotations. The five smaller clusters which remained

after 1.1 rotations in figure 8 exist mainly because the pressure caused by the increased velocity dispersion of the stars counteracts the gravitational attraction towards the center of each cluster. If the trajectories of individual stars are plotted, it is found that they oscillate in the potential wells set up by the five condensations of stars. This fast randomization observed in figures 8 and 10 must be caused by collective effects or violent relaxation as discussed by Lynden-Bell (refs. 44 and 65).

The relaxation time for collisional effects τ_c can be estimated by summing the effects of the encounters of individual stars. This summation can be performed by applying the test star approach (ref. 38) to a plane stellar system. Consider a test star of mass m_t which encounters a field star of mass m_f. Let the impact parameter and the initial relative velocity be D and V, respectively. The orbits of the two stars are hyperbolas with asymptotes that make an angle $\pi - 2\theta$ in the center-of-gravity coordinate system, where

$$\sin \theta = \left[1 - \frac{D^2 V^4}{G^2 (m_t + m_f)^2} \right]^{-1/2} \tag{53}$$

The angular deflection of the test star is therefore 2θ. Before the encounter, the test star has a velocity

$$v_t = \frac{m_f}{m_t + m_f} V$$

in the center-of-mass coordinate system. The increase in the perpendicular velocity of the test star caused by the encounter is given by

$$\left(\Delta v_\perp \right)^2 = v_t^2 \sin^2 2\theta$$

$$= \frac{4 m_f^2}{\left(m_t + m_f \right)^2} V^2 \sin^2 \theta \cos^2 \theta \tag{54}$$

From equation (53) it is found that

$$\cos^2 \theta = \frac{D^2 V^4 / G^2 \left(m_f + m_t \right)^2}{1 + \dfrac{D^2 V^4}{G^2 \left(m_f + m_t \right)^2}}$$

Equation (54) then becomes

$$\left(\Delta v_{\perp}\right)^2 = \frac{4m_f^2 V^6 D^2}{G^2\left(m_f + m_t\right)^4\left[1 + \dfrac{D^2 V^4}{G^2\left(m_f + m_t\right)^2}\right]^2}$$

So far, the derivation is the familiar one found in many textbooks. The next step is to sum over encounters in the plane of the disk galaxy rather than sum over a volume. The number of encounters $N_c(D)$ per unit time with impact parameter between D and $D + dD$ is

$$N_c(D)\ dD = 2nV\ dD$$

where n is the number density of field stars. The total increase in the transverse velocity is then given by

$$\left\langle v_{\perp}^2 \right\rangle = \int_{D_{min}}^{D_{max}} 2nV \left(\Delta v_{\perp}\right)^2\ dD$$

$$= \frac{8GVm_f^2 n}{m_t + m_f} \left(\frac{V^2 D_{min}\Big/G\left(m_f + m_t\right)}{2\left\{1 + D_{min}^2\left[\dfrac{V^2}{G\left(m_f + m_t\right)}\right]^2\right\}} - \frac{V^2 D_{max}\Big/G\left(m_f + m_t\right)}{2\left\{1 + D_{max}^2\left[\dfrac{V^2}{G\left(m_f + m_t\right)}\right]^2\right\}} \right.$$

$$\left. + \frac{1}{2}\tan^{-1}\left[\frac{V^2 D_{max}}{G\left(m_f + m_t\right)}\right] - \frac{1}{2}\tan^{-1}\left[\frac{V^2 D_{min}}{G\left(m_f + m_t\right)}\right] \right)$$

$$\approx \frac{4G^2 m_f^2 n}{V D_{min}}$$

since

$$D_{min}\left[\frac{V^2}{G\left(m_f + m_t\right)}\right] \gg 1$$

or

$$D_{max}\left[\frac{V^2}{G\left(m_f + m_t\right)}\right] \gg 1$$

24

and

$$D_{max} \gg D_{min}$$

where D_{min} is the cell dimension and D_{max} corresponds to the dimension of the system. The time required for a $90°$ deflection corresponds to $v_{\perp}^2 = V^2$ or

$$\tau_c = \frac{V^2}{\langle v_{\perp}^2 \rangle} = \frac{V^3 D_{min}}{4G^2 m_f^2 n} \tag{55}$$

The angular velocity of the uniformly rotating disk is given by equation (29) and initially the mean quadratic difference of velocity between two stars in the disk is

$$V = R_0 \left(\frac{3\pi Nm}{4R_0^3} \right)^{1/2} \tag{56}$$

Also, the rotational period of the uniformly rotating disk is

$$\tau_r = \frac{2\pi}{\omega} = 2\pi \left(\frac{4R_0^3}{3\pi GNm} \right)^{1/2} \tag{57}$$

The ratio of the collisional relaxation time τ_c to the rotational period τ_r is then

$$\frac{\tau_c}{\tau_r} = \left(\frac{3\pi}{16} \right)^2 \left(\frac{D_{min}}{R_0} \right) 2N \approx 2 \times 10^{-2} N \tag{58}$$

where n is expressed as $N/\pi R_0^2$ and $D_{min}/R_0 \approx \frac{1}{30}$. The estimate for the collisional relaxation time τ_c given by equation (58) shows that for a 50 000-star disk, collisional effects are important only after about 1000 rotations.

The velocity given by equation (56) is probably too large, and a better estimate for the velocity to be used in equation (55) is the minimum velocity dispersion required for stabilizing the disk as calculated by Toomre (ref. 18)

$$V = 3.36 \frac{G\sigma}{\kappa}$$

The relaxation time then becomes

$$\tau_c \approx 9.5 \frac{G\sigma^2 D_{min}}{\kappa^3 m} \tag{59}$$

where $m = \frac{\sigma}{n}$ is used.

With the following approximations

$$2\omega^2 \approx \kappa^2$$

$$\frac{\pi R_0^2 G \sigma}{R_0^2} \approx \omega^2 R_0 \approx \frac{\kappa^2}{2} R_0$$

and

$$\frac{\pi R_0^2 \sigma}{m} = N$$

equation (59) can be written

$$\tau_c \approx 0.32 \, \frac{N}{\omega} \left(\frac{D_{min}}{R_0} \right) \tag{60}$$

The ratio of the relaxation time to the rotational period $\left(\text{for} \quad \tau_r = 2\pi/\omega \right)$ is

$$\frac{\tau_c}{\tau_r} = 0.052 \, N \left(\frac{D_{min}}{R_0} \right) \approx 2 \times 10^{-3} N \tag{61}$$

and for $N = 50\,000$ the system can be considered collisionless for about 100 rotations.

Toomre (ref. 18) predicted that the short-wavelength modes are stabilized by the effects of velocity dispersion. To check his predictions, all stars in the initially uniformly rotating disk were given a uniform velocity dispersion. Figure 11 shows the evolution for such a disk of stars where the root-mean-square value of the random velocity is $0.068 V_\theta \left(R_0 \right)$ or 6.8 percent of the circular velocity at the edge of the cold balanced disk. The initial positions of the stars are the same as those for the disk of stars in figure 8. The disk is still violently unstable but, when compared with the evolution of the cold disk in figure 8, it can be seen that the initial condensations take longer to form and are no longer as concentrated as those for the cold disk. The smallest condensations formed are now of the order of three cell dimensions.

The evolution of the disk with a velocity dispersion equal to 13.6 percent of the circular velocity at the edge of the cold disk is shown in figure 12. The smallest condensations formed are now of the order of six cell dimensions. The evolution of the disk shows that the small-wavelength modes have been stabilized. However, the disk is still violently unstable with respect to large-wavelength modes.

An initial velocity dispersion of 20.4 percent of the circular velocity at the edge of the cold balanced disk results in the evolution displayed in figure 13. The disk is now nearly stabilized, but it still forms a barred spirallike condensation about 10 cell dimensions across. Figure 14 shows the corresponding evolution in velocity space wherein the system quickly attains a ringlike distribution.

Finally, the velocity dispersion was increased to 27.2 percent of the circular velocity at the edge of the cold balanced disk. The resulting evolution presented in figure 15 shows that the overall system is now relatively stable. Equation (49) gives the minimum velocity dispersion to stabilize the disk at $r = 0$ as 34.2 percent of the circular velocity of the cold balanced disk. The average velocity dispersion required to stabilize the disk should be less than the maximum value. Therefore, the value of 27.2 percent found from the computer simulation is in good agreement with the predictions of Toomre (ref. 18). Figure 15 indicates that an increase in the central density occurs as the system evolves. This effect is illustrated in figure 16 where the average density is plotted as a function of radius during the evolution of the system. The density was obtained from the number of stars with radii between r and $r + \Delta r$.

For the evolution of the disks in figures 11 to 15, the velocity dispersion was super-posed on the circular velocity of the stars for the cold balanced disk. Therefore, the disks were not exactly balanced at $t = 0$, since the added velocity dispersion results in a pressure which causes the disk to expand. Also, the velocity dispersion was isotropic — that is, $\sigma_r = \sigma_\theta = $ Constant. By using a velocity dispersion $\sigma_r(r)$ as given by equation (40) and a velocity dispersion $\sigma_\theta = \sigma_r \dfrac{\kappa}{2\omega_0} = \sigma_r$ (for the present disk) the system has the velocity dispersion required by Toomre (ref. 18) for stability. The disk is initially balanced by reducing the initial solid-body rotation according to equation (41). Figure 17 presents the evolution of such a balanced disk for which the initial velocity dispersion is one-half that given by equation (49). As can be seen, the system is still unstable and quickly forms a number of condensations. The evolution is similar to that in figure 12. For a velocity dispersion equal to that given by equation (49), the evolution of the initially balanced disk is as shown in figure 18. The only structure which slowly develops is a mode with dimensions of the size of the whole disk. These long-wavelength disturbances have an azimuthal dependence and are not covered by the theory of Toomre.

For the results given in figures 8 to 18, the gravitational potential was obtained by using the Fourier transform method; also, the evolution is shown only up to 1.1 rotations. In figure 19 is presented the evolution of an initially balanced cold disk of 50 000 stars when the potential is obtained by the summation method. The evolution is shown up to 2.2 rotations. The long time evolution (from 1.4 to 2.2 rotations) is typical for unstable disks. For disks with slightly different initial conditions, it has been found that after two

to five rotations the system consisted of one large central condensation around which orbited one to three small condensations. Initially uniformly rotating disks that are stabilized against small-scale disturbances (such as the system in fig. 18) tend to assume a barlike structure after about two rotations.

Effect of Finite Thickness

Some of the effects of finite thickness of the disk of stars can be taken into consideration by representing the stars as finite-length mass rods. The main effect in using finite-length rod stars is to decrease the close range interaction for the stars as shown in figure 4. The long-range collective effects are essentially unchanged. The initial density distribution of mass rods used to investigate the effects of finite thickness is taken to be that given by equation (28). The total mass of each rod is m. Since the gravitational field resulting from a distribution of mass rods is different from that due to a distribution of point masses, the rotation required to balance the cold disk is no longer given by equation (29). Therefore, the gravitational field is calculated by the model from the given initial density and equation (44) is used to obtain the initial rotation. Figure 20 shows the evolution of a 50 000-mass-rod system; each rod has a length of two cell dimensions. The structures displayed in figures 8 and 20 are very similar to $t = 0.3\tau_r$ to $t = 0.5\tau_r$. After $t = 0.5\tau_r$, the slightly different initial conditions cause rather large deviations in the overall structure of the condensations which occur as the disks break up. These deviations are to be expected since the systems are violently unstable. The evolution of the gravitational potential in the plane of the disk is presented in figure 21. Note that the gravitational potential is scaled differently from that in figure 9. Figure 22 shows the circular velocities of the stars as a function of radius for the rod system in figure 20. At $t = 0$, it can be seen that the circular velocity increases nearly linearly with radius, except near the edge of the disk where the circular velocity becomes constant. This leveling off of the circular velocity of course will not occur when the initial velocity is obtained by using equation (29). The evolution given in figure 22 indicates that the stars quickly increase their random velocities. Figure 23 shows how the distribution of the radial velocities evolves in time. Initially all the stars have zero radial velocities. As the system breaks up, the stars gain radial velocities and move along elliptical trajectories in the V_r,r space.

When the length of the mass rods is increased to five cell dimensions, the effect of finite thickness becomes more noticeable as is shown in figure 24. The short-range interaction is now reduced appreciably and, as a result, the growth time for small-scale instabilities is decreased. Also, as can be seen from figure 24, the number of condensations which form initially has been reduced when compared with those for the zero-thickness disk (fig. 8). Figure 25 shows the evolution of the radial velocities of the

stars for the system in figure 24. Because of the decrease in the short-range inter-
actions of the mass rods, the radial (or random) velocities increase at a much slower
rate than for the point mass system. It appears that the main effect of increasing the
length of the mass rods is to slow down the growth rate of the small-scale disturbances.

Effect of Increased Central Condensation

Hunter (ref. 15) finds that increasing the central condensation of a self-gravitating
disk decreases the growth rate of some of the unstable axisymmetric oscillations. To
investigate the effect of an increased central density, an initially cold balanced disk of
stars with a density $\sigma_3(r)$, given by equation (30), is studied. The evolution of this
stellar system is shown in figure 26. As expected, the evolution displayed in the figure
indicates that an increased central condensation alone does not stabilize the system
against large-scale disturbances. The time is given in units normalized to the rotation
periods of the cold uniformly rotating disk. As can be seen from figure 7, the period
corresponding to stars at the edge of the disk is then about 25 percent larger than that
corresponding to the normalized time given in figure 26.

The effect of superposing a uniform velocity dispersion was also investigated and
the results are shown in figures 27 and 28. In figure 27, the uniform velocity dispersion
is 30 percent of the circular velocity at the edge of the cold balanced disk (see fig. 7
for $n = 3$). Most of the small-scale condensations no longer form, and after one rota-
tion the system displays an S-shape structure. If the uniform velocity dispersion is
increased to 60 percent of the circular velocity at the edge of the cold balanced disk, the
evolution displayed in figure 28 is obtained. Apparently the system initially cools by
ejecting the hot stars and it then contracts. After $t = 0.7\tau_r$, the system expands again.

The evolution of a system with an even higher central condensation given by $\sigma_5(r)$
(fig. 6) is presented in figure 29. The system is initially cold and balanced and the time
shown is normalized to the period of a uniformly rotating balanced disk with the same
total mass and radius. This system is violently unstable and quickly condenses into a
circular ring as suggested by Hunter (ref. 16). The ring-shaped condensation later
breaks up into four smaller condensations. Figure 30 shows the evolution of the same
system, but with the stars replaced by mass rods each of which has a length of five cell
dimensions. The system no longer condenses into a circular ring. After $t = 2.2\tau_r$,
most of the mass is concentrated in the large central condensation.

Gaussian Mass Distribution

One of the problems of great interest is that of a galaxy being perturbed by the
close passage of some other galaxy. An example of particular interest is the proposed
close passage of the large Magellanic Cloud at 20 kpc from the center of the Galaxy some

500 million years ago (ref. 66). However, before such a problem can be undertaken by the present methods, a stable disk galaxy must first be generated which can then be perturbed by the passage of the Magellanic Cloud. As a first attempt at a stable system, a disk with a Gaussian mass distribution is considered. The Gaussian mass distribution is given by

$$\sigma_g(r) = \sigma(0)\exp\left[-\pi \frac{\sigma(0)}{M} r^2\right] \tag{62}$$

where M is the total mass of the disk

$$M = \int_0^\infty \sigma_g(r)\, 2\pi r\, dr$$

and $\sigma(0)$ is the mass density at $r = 0$. For the present calculations, the value of $\pi\sigma(0)/M$ was taken to be 2×10^{-2}. The rotational velocity required to balance a cold disk with a Gaussian mass distribution has been calculated by Toomre (ref. 17) as

$$V_\theta^2 = \pi^2 G\sigma(0)\sqrt{\frac{\sigma(0)}{M}} r^2 \, {}_1F_1\left(1.5, 2, \frac{\pi\sigma(0)}{M} r^2\right) \tag{63}$$

where

$${}_1F_1(\alpha,\rho,z) = 1 + \frac{\alpha}{1!\rho} z + \frac{\alpha(\alpha + 1)}{2!\rho(\rho + 1)} z^2 + \frac{\alpha(\alpha + 1)(\alpha + 2)}{3!\rho(\rho + 1)(\rho + 2)} z^3 + \ldots$$

is the confluent hypergeometric function with α,ρ,z as arbitrary variables. For an initially cold balanced disk with a Gaussian mass distribution, the evolution is similar to that shown in figure 29; this was to be expected since for large n, σ_n approaches a Gaussian distribution. To determine whether Toomre's minimum velocity dispersion (ref. 18) stabilizes a disk with a Gaussian mass distribution, the initial velocity dispersion was taken to be

$$\sigma_r(r) = \sigma_{r,min}$$

and

$$\sigma_\theta(r) = \frac{\kappa(r)}{2\omega_0(r)} \sigma_{r,min}$$

30

where $\sigma_{r,min}$ and $\kappa(r)$ are given by equations (45) and (46), respectively, and

$$\omega_o^2 = \frac{1}{r}\frac{\partial \varphi}{\partial r}$$

Because of the added velocity dispersion, the initial angular velocity of the stars $\omega(r)$ for a balanced disk is lower than $\omega_o(r)$ and is given by equation (42). Figure 31 shows the variation of ω_o, ω, and κ with r for a disk of stars with a Gaussian mass distribution. The evolution of the disk is given in figure 32. There are 50 000 stars in the disk and 200 time steps per rotation. The time is given in units of the rotational period of the cold balanced disk $2\pi/\omega_o(r)$ at $r = 10$ kpc. The rectangular border enclosing the disk is at $x = \pm 19$ kpc and $y = \pm 19$ kpc. The evolution displayed in figure 32 indicates that even though the disk is stabilized against axisymmetric disturbances according to Toomre's formula, the system is still violently unstable against nonaxisymmetric disturbances. After 1.5 rotations, the system has assumed a bar-shaped structure which varies very little during the following two rotations. The change (error) in the total energy of the system is less than 1 percent for the three rotations and the change in the angular momentum is about 0.1 percent. It should also be noted that at $t = 0$ the virial theorem is satisfied, that is, $2T(t=0) = -P(t=0)$. Figure 33 shows the variation of the radial velocities of the stars for the stellar system in figure 32. It can be seen that the velocity dispersion of the stars increases with time and that the stars tend to concentrate in regions of small r (as is obvious from fig. 32). The corresponding evolution in V_x, V_y space is shown in figure 34. In order to get more quantitative information than can be obtained from figures 32 to 34, the disk was divided into a number of concentric rings each with a width of 1/2 kpc. The radial dependence of various parameters averaged azimuthally over each ring was then obtained. Figure 35 presents the radial velocity dispersion obtained in this manner for the disk of stars in figure 32. Initially, the velocity dispersion for larger r increases very rapidly as can be seen from a comparison of the results at $t = 0$ and $t = 0.25\tau_r$. Again, the time shown is in units of $2\pi/\omega_o$ at $r = 10$ kpc. After three rotations, the radial velocity dispersion in the central part of the disk has increased to about 170 km/sec from the initial value of 105 km/sec. The variation of $Q = \sigma_r/\sigma_{r,min}$ is given in figure 36. The value of $\sigma_{r,min}$ is obtained from the azimuthally averaged parameters of the disk at time t by finite difference methods. After the system has settled down at $t = 3\tau_r$, Q has a value of approximately 4 over most of the disk. Because of this large value of Q, no spiral structure is expected to appear.

In interpreting the results shown in figures 35 and 36 the nonaxisymmetric shape of the disk at certain times should be kept in mind. Figure 37 presents the azimuthally averaged mass density as a function of radius. These results show that the central mass

density of the disk increased by a factor of 4 during the first two rotations. The dash-line curve shown at $t = 3\tau_r$ corresponds to an exponential density distribution with a scale length of 1.5 kpc and was obtained from

$$\sigma(r) \propto \exp(-r/1.5)$$

It can be seen that the exponential variation closely fits the mass distribution of the disk. The variation of the radial gravitational field for the disk with an initial Gaussian distribution is shown in figure 38. The gravitational field is obtained by averaging the field for x between 0 and -15 kpc and x between 0 and +15 kpc. It should be noted that the gravitational field at $t = 3\tau_r$ is much closer to that of the Galaxy (ref. 4) than is the gravitational field for the initial Gaussian mass distribution. Four individual star orbits taken at random from the 50 000 stars in the disk are shown in figure 39. The orbits indicate that stars initially near the center of the disk have a tendency to become trapped in even tighter orbits as the central mass density increases. Stars farther out have a tendency to escape from the system. To give an indication of the time step used in the integration, orbit 4 in figure 39 is plotted as a sequence of dots, one dot at the end of each time step.

The foregoing results indicate that the disk of stars with a Gaussian mass distribution and with a given initial velocity dispersion as required to stabilize all axisymmetric modes (ref. 18) is not stable. Increasing the initial velocity dispersion by 10 percent and using a different random number sequence for the initial star positions did not change the evolution of the disk very much. The result can be seen in figure 40 which shows the evolution of such a disk. The effect of using finite-length mass rods instead of point masses is illustrated in figure 41 with an initially balanced disk having a Gaussian mass distribution and zero velocity dispersion. The length of the mass rods is 2 kpc (4 cell dimensions). The time shown is in units of $2\pi/\omega_0(r)$ at $r = 10$ kpc for the thin disk, that is, the same units used in figures 32 and 40. It is seen in figure 41 that the small-scale modes are stabilized by the reduction of the interaction potential for stars in close proximity. However, large-scale modes are still violently unstable and at $t = 2.5\tau_r$ the system has assumed a bar-shaped structure. Note that the rectangular border enclosing each frame in figure 41 is at $x = \pm17$ kpc and $y = \pm17$ kpc. The results shown in figures 32 to 41 indicate that a disk of stars with a Gaussian mass distribution is not a stable configuration.

Exponential Mass Distribution

For the disk of stars with an initial Gaussian mass distribution, it was found that the final mass density was closely described by an exponential distribution. It is

therefore of interest to investigate whether a disk of stars with an initial exponential mass distribution will remain stable. For the disk investigated, the initial mass density is given by

$$\sigma(r) = \sigma(0)\exp\left(-r/r_0\right)$$

where $\sigma(0)$ is the central density and $r_0 = 3$ kpc. Figure 42 shows the initial values of κ, ω_0, and ω as a function of r as obtained by finite difference methods from the computer model. The evolution of the disk is shown in figure 43. The initial mass density was cut off at 15 kpc (or five scale lengths). This cutoff should not affect the dynamics of the disk since only 4 percent of the total mass for the exponential distribution lies outside 15 kpc. The time step used in the calculations is very small (800 time steps per rotation at a radius of 10 kpc). The evolution of this disk is not quite as violent as the evolution of the disk with the Gaussian mass distribution. (Compare figs. 43 and and 32.) However, after only 1.5 rotations the system has also assumed a bar-shaped mass distribution with a halo of stars moving in larger orbits around the central bar. Only slow changes in the shape of the system occur after $t = 1.5\tau_r$. The variation of the velocities is shown in figure 44. A more quantitative view of the radial velocity dispersion can be obtained from figure 45 where σ_r is plotted as a function of r at different times during the evolution. At $t = 1.5\tau_r$, the radial velocity dispersion has increased by only about 50 percent over the initial value. The variation of $Q = \sigma_r/\sigma_{r,min}$ is shown in figure 46. Note that Q increases slowly to a value of about 2; compare this value with that of about 4 obtained for the disk with a Gaussian mass density (fig. 36). From the mass distribution shown in figure 47, a tendency for the central mass concentration to increase can be observed. In fact, the final mass density is closely described by an exponential distribution given by

$$\sigma(r) \propto \exp(-r/1.5)$$

as indicated by the dash-line curve at $t = 1.5\tau_r$. This is the same final density variation as was found for the disk with a Gaussian mass distribution. Many of the disk galaxies investigated approach an exponential mass distribution; this fact is significant, especially since there is observational evidence (ref. 3) that the luminosity distribution of many spiral galaxies can be approximated by an exponential distribution. The variation of the radial gravitational field with radius is shown in figure 48. As is to be expected from the increase in the central mass density, the field increases sharply near the center of the disk. The epicylic frequency κ can be obtained directly from the following equation:

$$\kappa^2 = \frac{\partial E_r}{\partial r} + \frac{3}{r} E_r$$

where $E_r = \partial \varphi / \partial r$. The variation of the epicyclic frequency with radius is presented in figure 49. As expected, the epicyclic frequency increases appreciably in the central part of the disk. The orbits of six of the 50 000 stars in the disk are shown in figure 50. Note that the initial rotation is in the clockwise direction. As was observed for the Gaussian mass distribution, stars with small initial radii tend to be trapped near the center; whereas stars with large initial radii tend to move farther away from the center.

It is of interest to compare the evolution of the "stabilized" exponential disk in figure 43 with the evolution of an initially cold (zero velocity dispersion) disk. Figure 51 shows the evolution of a cold disk of stars with the same initial exponential mass distribution as the disk in figure 43. The disk now shows many fine scale condensations and it quickly breaks up into a number of separate clusters of stars. Further work is being done on the exponential disk with the hope that a stable axisymmetric disk can be obtained.

Comparison of Disk Model With Infinite-Mass-Rod Model

It is of interest to compare the results obtained for a disk of point masses with the results obtained with cylindrical systems that consist of infinitely long mass rods (refs. 47 to 50). Figure 52 shows the evolution of an initially nonrotating cold disk of stars. The time is in units of the rotation period of a balanced uniformly rotating disk. The system is seen to quickly collapse, then expand again, and present some filamentary structure. After $t = 1.0\tau_r$, most of the mass has condensed into one large cluster of stars at the center of the system. These results are essentially the same as those obtained for the cylindrical galaxy (fig. 5 of ref. 49).

The evolution of a cold disk with an initial rotation equal to one-half that required to balance the disk is shown in figure 53. Again, the evolution is very similar to that obtained for infinitely long mass rods (fig. 7 of ref. 49). The main difference is that for the point masses any structure is formed much quicker than for the rod stars. This stronger interaction is to be expected from the two-star interaction potential shown in figure 4 as a function of rod length.

For the cylindrical galaxy (infinitely long rods), it was found that the uniformly rotating cylinder was unstable (ref. 50). By letting half of the stars rotate clockwise and half rotate counterclockwise, a stable system was obtained (fig. 16 of ref. 50). Figure 54 shows the corresponding evolution of an initially balanced disk of point stars where 25 000 stars rotate clockwise and the remaining 25 000 stars rotate counterclockwise. The system is violently unstable and quickly condenses into a ring shape. Thereafter, large random velocities quickly build up and cause the system to thermalize.

EVOLUTION OF SPIRAL STRUCTURE

To study the development of spiral structure, the computer model was modified to include a fixed central potential in addition to the self-consistent disk population of stars. The central field is taken to represent the halo population and the central core of the Galaxy, which appear to produce a relatively time-independent field. The two central potentials used correspond to circular velocities (km/sec) given by

$$V_\theta = \frac{4500r}{81 + r^2} \tag{64}$$

and

$$V_\theta = \frac{4600r}{100 + r^2} + \frac{210r}{0.25 + r^2} \tag{65}$$

In figure 55 the two velocity curves are compared with the Schmidt model (ref. 4) of the Galaxy. The evolution of a system is affected little by using one or the other of the two rotation curves. The mass corresponding to the fixed central potential was taken to be as small as 50 percent of the total mass of the system. However, for most of the calculations the self-consistent disk population contained from 10 percent to 20 percent of the mass of the system.

Figure 56 gives the evolution of a 50 000-star system with a fixed central potential corresponding to the rotation curve given by equation (64). The disk stars represent 10 percent of the total mass of the system. The time step used for this calculation is rather large, there being only 80 time steps per rotation at 10 kpc from the center of the system. Initially, the disk stars have a density of the form given by equation (28) with a disk radius of 20 kpc, zero radial velocities, and rotational velocities just sufficient to balance the gravitational attraction. It can be seen from figure 56 that the system quickly develops a multiarm spiral structure. The time shown in figure 56 and in all subsequent figures is in units of the rotational period at a radius of 10 kpc. The spiral structure remains even after 8.5 rotations, at which time the calculation was terminated. From a purely kinematical viewpoint, differential rotation should have wound up the spiral structure before 8.5 rotations. In many of the calculations, there was a tendency to form circular rings of stars in the central region of the disk. Figure 56 shows that after 2.5 rotations the system develops a number of concentric rings of stars which appear to be quite stable. In the outer parts of the system, the rings open up into a spiral structure. After 6.5 rotations the system resembles a two-arm spiral galaxy with a tightly wound spiral structure in the central part of the system. The circular velocities of the stars for this galactic system are plotted as a function of distance from the center of the system in

figure 57. The velocity dispersion builds up substantially in the region above 10 kpc but remains quite small near the center of the system. This effect can be explained by the rather low value of the self-consistent gravitational field in the central region of the galaxy.

To investigate more closely the appearance and stability of the concentric rings which appeared in figure 56, the same galactic system was investigated again but with an added initial perturbation. Equations (7) and (8) indicate that to start the calculation correctly with the given velocity of a star at time zero $V(t=0)$, the position of the star must be given at time $t = 0 + \delta t/2$ or $r(t = \delta t/2)$. The perturbation was introduced by initially placing the stars at position $r(t=0)$ with velocity $V(t=0)$; this caused a shift of the correct initial position of each star given by

$$\Delta r = r(t=0) \left\{ 1 - \exp\left[-i\omega(r)\frac{\delta t}{2}\right]\right\} \tag{66}$$

where

$$\omega(r) = \frac{V_\theta(r)}{r}$$

and

$$r = x + iy$$

The perturbation is essentially a rotation (around the disk center) of the initial star positions, about 2° from their equilibrium positions. The resulting motion of the stars in the plane of the disk is shown in figure 58. The rings are now much more pronounced and are quite stable. Again, the rings open up into a spiral structure in the outer parts of the disk. The rings are actually density waves which start at the center of the system and move radially outward. No net mass is carried radially outward by these density waves. The circular velocities of the stars for this galactic system are plotted as a function of radius in figure 59. The wavelike pattern of the distribution is caused by the epicyclic motion of the stars in the central field. This effect can be seen even more clearly in figure 60 wherein the radial velocities of the stars are plotted as a function of radius. The number of maxima and minima corresponds to the concentric rings in figure 58. This behavior can be explained in terms of the epicyclic motion of the individual stars from the following equation describing the displacement of a star $h(r,t)$ from its nearly circular orbit (ref. 38):

$$h(r,t) = r \cos\left[\kappa(r)t\right] \tag{67}$$

For the present system, the epicyclic frequency $\kappa(r)$ is approximately

$$\kappa(r) = \frac{18 \times 4500}{\left(81 + r^2\right)^{3/2}}$$

where equation (46) was used with

$$\frac{\partial \varphi}{\partial r} = \frac{V_\theta^2}{r}$$

and V_θ is given by equation (64). The radial wave number is

$$k(r,t) = -\frac{\partial}{\partial r}\left[\kappa(r)t\right] = -\left[\frac{d\kappa(r)}{dr}\right]t = \frac{54 \times 4500r}{\left(81 + r^2\right)^{5/2}}t$$

and increases linearly with time. This is exactly the behavior indicated in figures 58 to 60 where the distance between concentric rings or the wavelength given by

$$\lambda(r,t) = \frac{2\pi}{k(r,t)} = \frac{\pi\left(81 + r^2\right)^{5/2}}{27 \times 4500rt} \tag{68}$$

decreases with increasing time.

Observational evidence indicates that a ring or system of rings is a feature of many galaxies. Examples of spiral galaxies which display a structure of concentric circular rings of stars, similar to that shown in figure 58, are NGC 488 and NGC 1398 (ref. 12).

Another 50 000-star system with a fixed central potential given by equation (65) was investigated and the evolution of the system is shown in figure 61. The disk stars contain 20 percent of the total mass of the galaxy and the initial radius of the disk is 15 kpc. The time step used is such that initially there are 200 time steps per rotation at 10 kpc. The system quickly develops spiral structure which remains quite pronounced up to about four rotations. After about six rotations, the spiral structure becomes quite diffuse due to the buildup of random velocities. The buildup of the random velocities can be seen in figure 62, where the radial velocities of the stars are plotted as a function of the star radius. Initially, the disk is cold and all stars have zero radial velocities. As the evolution of the system continues, the random velocities of the stars continue to increase up to about two rotations; thereafter, there is practically no increase. The same effect can be seen in figure 63, where the circular velocities of the stars are plotted as a function of the star radius. Figures 62 and 63 are plotted to the same scale. It should be noted that

in the central part of the system the self-consistent gravitational field due to the disk stars is rather small compared with the fixed central field. This fact explains the low value of the velocity dispersion in the central region of the disk (figs. 62 and 63). To study some of the individual star orbits more closely, the orbits of four stars have been plotted in figure 64. The motion of the stars is in the clockwise direction. To determine whether the stars followed an epicyclic motion, the radius of the star at time t was subtracted from the initial radius and the difference was plotted as a function of time in figure 65. The oscillations shown occur at the epicyclic frequency and the amplitude of the oscillations increases with increasing radius of the star orbit. The variation of the mass density with radius is shown in figure 66. The density is obtained from the number of stars with radius between r and r + Δr. In the absence of the applied central field, the central increase in density would be more pronounced. Figure 67 shows the variation of the average root-mean-square radial velocities with radius. Again, after two rotations there is little further increase in the velocity dispersion. The velocity dispersion in the azimuthal direction is found to be smaller than the radial velocity dispersion by a factor given by

$$\sigma_\theta \approx \sigma_r \sqrt{1 + \frac{r}{2\omega} \frac{\partial \omega}{\partial r}} \tag{69}$$

This result is in agreement with theory. The minimum velocity dispersion required to stabilize all axisymmetric disturbances (ref. 18)

$$\sigma_{r,min} = 3.36 \frac{G\sigma}{\kappa}$$

is plotted in figure 68 for various times during the evolution of the system. The values of σ and κ are calculated from the parameters of the system at the given times.

The variation of

$$Q = \frac{\sigma_r}{\sigma_{r,min}}$$

with r is plotted in figure 69. The value of Q appears to settle down to about 1.7. This rather large value of Q would, of course, suppress any further instabilities which could result in spiral structure. The diffuse, rather structureless appearance of the system shown in figure 61 at $t = 6.8\tau_r$ is to be expected because of the large value of Q. Toomre (ref. 18) calculates the longest unstable wavelength in the absense of velocity dispersion as

$$\lambda_c = \frac{4\pi^2 \sigma G}{\kappa^2}$$

A plot of λ_c as a function of radius for various times during the evolution of the system is presented in figure 70. It can be seen that in the central part of the system the longest unstable wavelength becomes very small. This result is in agreement with the results shown in figure 61, where only very small-scale structure is visible in the central part of the system.

The evolution of a disk galaxy with a fixed central field corresponding to equation (64) and with 50 000 disk stars containing 10 percent of the total mass of the system is shown in figure 71. The initial density distribution is given by equation (28). The disk is initially cold and balanced with a radius of 15 kpc and there are 100 time steps per rotation at 10 kpc. The evolution of the system is similar to that shown in figure 61. At first, a multiarm spiral structure appears in the outer regions of the disk. As the evolution proceeds, the increase in the velocity dispersion causes any structure to become quite diffuse. Four star orbits from the stellar system in figure 71 and the deviations of these orbits from circular orbits are given in figure 72 and figure 73, respectively. The oscillations shown in figure 73 occur at the epicyclic frequency. The variation of the velocity dispersion with radius for this stellar system is presented in figure 74. For $r = 0$ to about 5 kpc, the dynamics is dominated by the fixed central field and the velocity dispersion remains quite low in this region. After three rotations there is little further increase in the velocity dispersion. The variation $Q = \dfrac{\sigma_r}{\sigma_{r,min}}$ with r for this system is shown in figure 75. After three rotations, Q is well above 1 for radii larger than about 5 kpc.

The four systems investigated (figs. 56, 58, 61, and 71) had very little initial central condensation of the disk stars. To determine the effect of increasing the central mass density, the evolution of a disk of stars with an initial Gaussian mass density was studied (fig. 76). The 50 000 disk stars contain 20 percent of the total mass of the galaxy. There is now much more fine scale structure in the central portion of the disk when compared with structure in the other four systems. However, this structure is difficult to detect in figure 76. A better indication of the fine scale structure can be obtained from the evolution of the same system in V_x, V_y space (fig. 77). The individual orbits of four stars in the system are shown in figure 78. The corresponding deviations of the star motion from circular orbits is shown in figure 79. The oscillations occur at the epicyclic frequency which remains practically unchanged during the evolution as can be seen from figure 80. The variation of the velocity dispersion with r is given in figure 81. The increased central star density has the effect of increasing the velocity dispersion in the central region of the disk. After about two rotations the velocity dispersion increases

very little in the outer regions of the disk. Because in the central part of the disk the fixed field is still large compared with the self-consistent field, the velocity dispersion in that region takes longer to reach a larger value. The variation of Q with r for this disk of stars is shown in figure 82. From the low value of Q for $r \leqq 5$ kpc and from the increased central density (compared with the previous 4 systems), one could expect the fine scale structure which persisted in the central part of the disk. The density in the center of the disk did increase by about 30 percent during the evolution shown in figures 56 to 62.

Also investigated was a disk of stars with the same initial conditions as those for the system in figure 76, except that the mass of the 50 000 disk stars was increased to 50 percent of the total mass of the system. The evolution of that system is shown in figure 83. The disk is initially violently unstable but quickly approaches a rather steady state with a much increased central density. By $t = 1.75\tau_r$, the density at the center of the disk has increased by a factor of 6. The variation of the velocity dispersion with r is shown in figure 84. The large central density of disk stars now causes a rapid increase in the velocity dispersion in the central region of the disk. At $t = 1.75\tau_r$, the value of Q is about 2 for the region $0 \leqq r \leqq 13$ and it increases to about 4 for larger radii. The value of Q equal to about 4 indicates that after less than two rotations the system has essentially reached a rather hot steady state. The variation of the radial gravitational field with r is shown in figure 85. As the central mass density of the disk stars increases, the gravitational field due to the disk stars increases sharply near the center of the disk.

CONCLUDING REMARKS

A computer model for isolated disk galaxies has been described in detail. The model was tested by varying the discretization parameters. The evolution of the system was affected very little for the range of parameters used. The evolution of a cold balanced disk was calculated and the disk was found to be violently unstable; this result was in agreement with theoretical predictions. Adding increasing amounts of velocity dispersion to the uniformly rotating disk had the effect of increasing the smallest size of the star condensations that were formed. A velocity dispersion equal to about 27 percent of the circular velocity at the edge of the cold balanced disk stabilized the disk against breakup and any local condensations. These results are in general agreement with the theoretical predictions of Toomre. However, the disks were found to be unstable against long-wavelength nonaxisymmetric disturbances and after only about two rotations the disks assumed a bar-shaped structure. Similar results are obtained for disks with a Gaussian density distribution and with a velocity dispersion equal to or even greater than

the "stabilizing" velocity dispersion calculated by Toomre. A disk with an initial exponential density distribution and with Toomre's stabilizing velocity dispersion displayed the least violent evolution even though it also took on a bar shape. One interesting result of the calculations is that the final density distribution for the disk galaxies investigated can be closely approximated by an exponential distribution irrespective of the initial conditions. This result is in agreement with observational evidence which indicates that the luminosity distribution of many spiral galaxies can be approximated by an exponential distribution. To study the evolution of spiral structure, the model was modified by adding a fixed central force similar to that of the Schmidt model of the galaxy. The fixed force represents the halo population of stars and the central core of the Galaxy. For most of the systems with the fixed central force which were investigated, a spiral structure quickly appeared but became quite diffuse after about six rotations. Also, the velocity dispersion of the disk stars increased to a value that was approximately 50 to 100 percent larger than the value of about 30 km/sec for stars in the solar neighborhood.

Langley Research Center,
    National Aeronautics and Space Administration,
        Hampton, Va., April 13, 1970.

COMPUTER PROGRAM FOR OBTAINING GRAVITATIONAL

POTENTIAL OF ISOLATED DISK GALAXIES

The following listing is a FORTRAN version of the subroutine GETPHI which is used to obtain the gravitational potential for isolated disk galaxies.

```
      SUBROUTINE GETPHI
      COMMON Z(1025),Y(1025),RHO(128,128),I2A,ITEST,     S
      DIMENSION G(65,65)
      IF(ITEST.EQ.0) GO TO 40
      I2B=I2A-1
      N=2**I2A
      NO2=N/2
      M=N+1
      N21=NO2+1
      NP2=N+2
      NGSQ=N21*N21
      IC=NO2/2+1
      RNI=1./(N*N)
      S2=S*S
      DO 1 J=1,N21
      DO 1 I=1,N21
      IF(I.EQ.1.AND.J.EQ.1) GO TO 1
      R2=(I-1.)*(I-1.)+(J-1.)*(J-1.)
      R=SQRT(R2)
      SS=SQRT(1.+S2/R2)
      G(I,J)= RNI*(2./S)*((R/S)*(1.-SS)+ALOG(S/R+SS))
    1 CONTINUE
      G(1,1)=G(1,2)
      CALL GETSET(2,I2B)
      DO 3 J=1,N21
      DO 4 I=1,N21
    4 Z(I)=G(I,J)
      CALL FTRANS(2,I2B)
      DO 10 I=1,N21
   10 G(I,J)=Y(I)
    3 CONTINUE
      DO 2 I=1,N21
      DO 19 J=1,N21
   19 Z(J)=G(I,J)
      CALL FTRANS(2,I2B)
      DO 22 J=1,N21
   22 G(I,J)=Y(J)
    2 CONTINUE
   40 CONTINUE
      CALL GETSET(3,I2A)
      DO 7 J=1,N
```

```
      DO 8 I=1,N
  8 Z(I)=RHO(I,J)
      CALL FTRANS(3,I2A)
      DO 9 I=1,N
  9 RHO(I,J)=Y(I)
  7 CONTINUE
      DO 25 I=1,N
      DO 26 J=1,N
 26 Z(J)=RHO(I,J)
      CALL FTRANS(3,I2A)
      DO 27 J=1,N
 27 RHO(I,J)=Y(J)
 25 CONTINUE
      DO 11 J=2,NO2
      DO 11 I=2,NO2
      I1=I+NO2
      J1=J+NO2
      RHO(I,J)=RHO(I,J)*G(I,J)
      RHO(I1,J)=RHO(I1,J)*G(I,J)
      RHO(I,J1)=RHO(I,J1)*G(I,J)
      RHO(I1,J1)=RHO(I1,J1)*G(I,J)
 11 CONTINUE
      DO 37 I=2,NO2
      RHO(I+NO2,1)=RHO(I+NO2,1)*G(I,1)
      RHO(I+NO2,N21)=RHO(I+NO2,N21)*G(I,N21)
      RHO(I,1)=RHO(I,1)*G(I,1)
 37 RHO(I,N21)=RHO(I,N21)*G(I,N21)
      DO 38 J=2,NO2
      RHO(1,J)=RHO(1,J)*G(1,J)
      RHO(1,J+NO2)=RHO(1,J+NO2)*G(1,J)
      RHO(N21,J)=RHO(N21,J)*G(N21,J)
 38 RHO(N21,J+NO2)=RHO(N21,J+NO2)*G(N21,J)
      RHO(1,1)=RHO(1,1)*G(1,1)
      RHO(N21,1)=RHO(N21,1)*G(N21,1)
      RHO(1,N21)=RHO(1,N21)*G(1,N21)
      RHO(N21,N21)=RHO(N21,N21)*G(N21,N21)
      CALL GETSET(4,I2A)
      DO 14 J=1,N
      DO 12 I=1,N
 12 Z(I)=RHO(I,J)
      CALL FTRANS(4,I2A)
      DO 13 I=1,N
 13 RHO(I,J)=Y(I)
 14 CONTINUE
      DO 28 I=1,N
      DO 29 J=1,N
 29 Z(J)=RHO(I,J)
      CALL FTRANS(4,I2A)
      DO 30 J=1,N
 30 RHO(I,J)=Y(J)
 28 CONTINUE
      ITEST=0
      RETURN
      END
```

The interaction potential $G(I,J)$ calculated in the listing is for finite-length mass rods as given by equation (24). The common variable S defines the length of the mass rods. The variable I2A defines the size of the rectangular array $RHO(I,J)$ used in the potential calculations. When the subroutine GETPHI is called, $RHO(I,J)$ contains the mass density and GETPHI places the values of the corresponding gravitational potential in $RHO(I,J)$. The subroutine FTRANS(I,I2B) has been written by R. Hockney (ref. 58) and it performs a finite Fourier analysis or synthesis on the common input array Z and puts the result in the common output array Y. The subroutine performs a cosine analysis or synthesis for $I = 2$, a periodic analysis for $I = 3$, and a periodic synthesis for $I = 4$. The subroutine GETSET(I,I2B) initializes FTRANS and is called every time the arguments of FTRANS(I,I2B) are changed.

REFERENCES

1. De Vaucouleurs, G.: Classification of Galaxies by Form, Luminosity, and Color. Problems of Extra-Galactic Research, G. C. McVittie, ed., Macmillan Co., c.1962, pp. 3-21.

2. Lin, C. C.: The Dynamics of Disk-Shaped Galaxies. Annual Review of Astronomy and Astrophysics, Vol. 5, Leo Goldberg, David Layzer, and John G. Phillips, eds., Annu. Rev., Inc., 1967, pp. 453-464.

3. De Vaucouleurs, G.: General Physical Properties of External Galaxies. Encycl. Phys., Vol. LIII, Astrophysics IV: Stellar Systems, S. Flügge, ed., Springer-Verlag, 1959, pp. 311-372.

4. Blaauw, Adriaan; and Schmidt, Maarten, eds.: Galactic Structure. Univ. of Chicago Press, c.1965.

5. Van Woerden, Hugo, ed.: Radio Astronomy and the Galactic System. Academic Press, 1967.

6. Oort, J. H.: Radio Data on the Distribution and Motion of Interstellar Gas. The Distribution and Motion of Interstellar Matter in Galaxies, L. Woltjer, ed., W. A. Benjamin, Inc., 1962, pp. 3-22.

7. Carruthers, G. R.: An Upper Limit on the Concentration of Molecular Hydrogen in Interstellar Space. Astrophys. J., vol. 148, no. 3, pt. 2, June 1967, pp. L141-L142.

8. Werner, Michael W.; and Harwit, Martin: Observational Evidence for the Existence of Dense Clouds of Interstellar Molecular Hydrogen. Astrophys. J., vol. 154, no. 3, pt. 1, Dec. 1968, pp. 881-889.

9. Woltjer, L.: Dynamics of Gas and Magnetic Fields; Spiral Structure. Galactic Structure, Adriaan Blaauw and Maarten Schmidt, eds., Univ. of Chicago Press, c.1965, pp. 531-587.

10. Oort, J. H.: Some Topics Concerning the Structure and Evolution of Galaxies. The Structure and Evolution of Galaxies, Interscience Publ., Inc., 1965, pp. 17-29.

11. Woolley, Richard; and Stewart, J. M.: Motion of A Stars Perpendicular to the Galactic Plane — II. Mon. Notic. Roy. Astron. Soc., vol. 136, no. 3, 1967, pp. 329-339.

12. Sandage, Allan: The Hubble Atlas of Galaxies. Publ. 618, Carnegie Inst. of Washington, 1961.

13. Oort, J. H.: Spiral Structure. The Distribution and Motion of Interstellar Matter in Galaxies, L. Woltjer, ed., W. A. Benjamin, Inc., 1962, pp. 234-244.

14. Prendergast, K. H.; and Burbidge, G. R.: The Persistence of Spiral Structure. Astrophys. J., vol. 131, no. 1, Jan. 1960, pp. 243-246.

15. Hunter, C.: Oscillations of Self-Gravitating Disks. Mon. Notic. Roy. Astron. Soc., vol. 129, no. 4, 1965, pp. 321-343.

16. Hunter, C.: The Structure and Stability of Self-Gravitating Disks. Mon. Notic. Roy. Astron. Soc., vol. 126, no. 4, 1963, pp. 299-315.

17. Toomre, Alar: On the Distribution of Matter Within Highly Flattened Galaxies. Astrophys. J., vol. 138, no. 2, 1963, pp. 385-392.

18. Toomre, Alar: On the Gravitational Stability of a Disk of Stars. Astrophys. J., vol. 139, no. 4, May 15, 1964, pp. 1217-1238.

19. Julian, William H.; and Toomre, Alar: Non-Axisymmetric Responses of Differentially Rotating Disks of Stars. Astrophys. J., vol. 146, no. 3, Dec. 1966, pp. 810-830.

20. Lin, C. C.; and Shu, Frank H.: On the Spiral Structure of Disk Galaxies. Astrophys. J., vol. 140, no. 2, Aug. 1964, pp. 646-655.

21. Lin, C. C.; and Shu, Frank H.: On the Spiral Structure of Disk Galaxies, II. Outline of a Theory of Density Waves. Proc. Nat. Acad. Sci. U.S., vol. 55, no. 2, Feb. 1966, pp. 229-234.

22. Lin, C. C.: Stellar Dynamical Theory of Normal Spirals. Relativity Theory and Astrophysics − 2. Galactic Structure, Jürgen Ehlers, ed., Amer. Math. Soc., 1967, pp. 66-97.

23. Lindblad, Bertil: Galactic Dynamics. Encycl. Phys., vol. LIII, Astrophysics IV: Stellar Systems, S. Flügge, ed., Springer-Verlag, 1959, pp. 21-99.

24. Lindblad, Bertil: On the Possibility of a Quasi-Stationary Spiral Structure in Galaxies. Stockholms Observ. Ann., Bd. 22, No. 5, 1963, pp. 3-20.

25. Lindblad, Bertil: On the Theory of Spiral Structure in the Nebulae. Z. Astrophys., Bd. 15, Nr. 2, 1938, pp. 124-136.

26. Vandervoort, Peter O.: Properties of Rapidly Rotating Galaxies. Instabilité Gravitationnelle et Formation des Étoiles, des Galaxies et de Leurs Structures Caractéristiques, Inst. Astrophys. (Belgique), 1967, pp. 209-212.

27. Shu, Frank Hsia-San: The Dynamics and Large-Scale Structure of Spiral Galaxies. Ph. D. Thesis, Harvard Univ., 1968.

28. Wentzel, Donat G.: Magnetic Fields and Spiral Structure. Annual Review of Astronomy and Astrophysics, Vol. I, Leo Goldberg, Armin J. Deutsch, and David Layzer, eds., Annu. Rev., Inc., 1963, pp. 195-218.

29. Chandrasekhar, S.; and Fermi, E.: Problems of Gravitational Stability in the Presence of a Magnetic Field. Astrophys. J., vol. 118, no. 1, July 1953, pp. 116-141.

30. Greyber, Howard D.: On the Steady-State Dynamics of Spiral Galaxies. AFOSR 2958, U.S. Air Force, June 1, 1962.

31. Pasta, John; and Ulam, S.: Heuristic Studies in Problems of Mathematical Physics on High Speed Computing Machines. LA-1557, Los Alamos Sci. Lab., Univ. of California, June 29, 1953.

32. Von Hoerner, Sebastian: Die numerische Integration des n-Körper-Problemes für Sternhaufen I. Z. Astrophys., Bd. 50, Heft 3, 1960, pp. 184-214.

33. Von Hoerner, Sebastian: Die numerische Integration des n-Körper-Problems für Sternhaufen, II. Z. Astrophys., Bd. 57, Heft 2, 1963, pp. 47-82.

34. Aarseth, S. J.: Dynamical Evolution of Clusters of Galaxies, I. Mon. Notic. Roy. Astron. Soc., vol. 126, no. 3, 1963, pp. 223-255.

35. Aarseth, S. J.: Dynamical Evolution of Clusters of Galaxies, II. Mon. Notic. Roy. Astron. Soc., vol. 132, no. 1, 1966, pp. 35-65.

36. Wielen, R.: Dynamical Evolution of Star Cluster Models, I. Nr. 19, Veroeff. Astron. Rechen Inst. (Heidelberg), 1967.

37. Jeans, James H.: Astronomy and Cosmogony. Dover Publ., Inc., c.1961.

38. Chandrasekhar, S.: Principles of Stellar Dynamics. Enlarged ed., Dover Publ., Inc., 1960.

39. Lecar, M.: A One-Dimensional Self-Gravitating Stellar Gas. The Theory of Orbits in the Solar System and in Stellar Systems, George Contopoulos, ed., Academic Press, 1966, pp. 46-48.

40. Lecar, Myron; and Cohen, Leon: Relaxation of a One-Dimensional Self-Gravitating Gas. Symposium on Computer Simulation of Plasma and Many-Body Problems, NASA SP-153, 1967, pp. 299-308.

41. Hohl, Frank; and Feix, Marc R.: Numerical Experiments With a One-Dimensional Model for a Self-Gravitating Star System. Astrophys. J., vol. 147, no. 3, Mar. 1967, pp. 1164-1180.

42. Hohl, Frank; and Feix, M. R.: A Variational Principle for a One-Dimensional Stellar System. Astrophys. J., vol. 151, no. 2, pt. 1, Feb. 1968, pp. 783-788.

43. Hohl, Frank: Theory and Results on Collective and Collisional Effects for a One-Dimensional Self-Gravitating System. NASA TR R-289, 1968.

44. Hohl, Frank; and Campbell, Janet W.: Statistical Mechanics of a Collisionless Self-Gravitating System. Astron. J., vol. 73, no. 7, Sept. 1968, pp. 611-615.

45. Hénon, M.: L'Évolution Initiale d'un Amas Sphérique. Ann. Astrophys., t. 27, no. 2, 1964, pp. 83-91.

46. Hénon, Michel: Collective Motions in a Spherical Star Cluster. Symposium on Computer Simulation of Plasma and Many-Body Problems, NASA SP-153, 1967, pp. 349-364.

47. Hockney, R. W.: Gravitational Experiments With a Cylindrical Galaxy. Astrophys. J., vol. 150, no. 3, Dec. 1967, pp. 797-806.

48. Hohl, Frank: One- and Two-Dimensional Models To Study the Evolution of Stellar Systems. Symposium on Computer Simulation of Plasma and Many-Body Problems, NASA SP-153, 1967, pp. 323-336.

49. Hohl, Frank: Computer Solutions of the Gravitational N-Body Problem. Bull. Astron., ser. 3, vol. III, no. 2, 1968, pp. 227-240.

50. Hohl, Frank: Computer Simulation of a Cylindrical Galaxy. NASA TN D-5200, 1969.

51. Lindblad, Per Olof: The Development of Spiral Structure in a Galaxy Approached by Numerical Computations. Stockholms Observ. Ann., Bd. 21, No. 4, 1960, pp. 3-73.

52. Lindblad, P. O.: Gravitational Resonance Effects in the Central Layer of a Galaxy. The Distribution and Motion of Interstellar Matter in Galaxies, L. Woltjer, ed., W. A. Benjamin, Inc., 1962, pp. 222-233.

53. Miller, R. H.; and Prendergast, K. H.: Stellar Dynamics in a Discrete Phase Space. Astrophys. J., vol. 151, no. 2, Feb. 1968, pp. 699-709.

54. Buneman, O.: Time-Reversible Difference Procedures. J. Comput. Phys., vol. 1, no. 4, June 1967, pp. 517-535.

55. Gentry, R. A.; Harlow, F. H.; and Martin, R. E.: Computer Experiments for Molecular Dynamics Problems. Applications in Hydrodynamics. Vol. 4 of Methods in Computational Physics, Berni Alder, Sidney Fernbach, and Manuel Rotenberg, eds., Academic Press, Inc., 1965, pp. 211-245.

56. Cooley, James W.; and Tukey, John W.: An Algorithm for the Machine Calculation of Complex Fourier Series. Math. Comput., vol. 19, no. 90, Apr. 1965, pp. 297-301.

57. Gentleman, W. M.; and Sande, G.: Fast Fourier Transforms — For Fun and Profit. AFIPS Conference Proceedings, Vol. 29 — Fall Joint Computer Conference, Spartan Books, Inc., 1966, pp. 563-578.

58. Hockney, R. W.: The Potential Calculation. Proceedings of the APS Topical Conference on Numerical Simulation of Plasma, LA-3990 (AEC Contract W-7405-Eng. 36), Los Alamos Sci. Lab., Univ. of California, Sept. 1968, pp. D6-1 – D6-7.

59. Hohl, Frank; and Hockney, R. W.: A Computer Model of Disks of Stars. J. Comput. Phys., vol. 4, no. 3, Oct. 1969, pp. 306-324.

60. Birdsall, C. K.; and Fuss, D.: Cloud-in-Cell Computer Experiments in Two and Three Dimensions. Proceedings of the APS Topical Conference on Numerical Simulation of Plasma, LA-3990 (AEC Contract W-7405-Eng. 36), Los Alamos Sci. Lab., Univ. of California, Sept. 1968, pp. D1-1 – D1-6.

61. Wyse, A. B.; and Mayall, N. U.: Distribution of Mass in the Spiral Nebulae Messier 31 and Messier 33. Astrophys. J., vol. 95, no. 1, Jan. 1942, pp. 24-47.

62. Brandt, John C.: On the Distribution of Mass in Galaxies. I. The Large-Scale Structure of Ordinary Spirals With Applications to M31. Astrophys. J., vol. 131, no. 2, Mar. 1960, pp. 293-303.

63. Ng, E. W.: Self-Consistent Models of Disk Galaxies. Astrophys. J., vol. 150, no. 3, Dec. 1967, pp. 787-796.

64. Abramowitz, Milton; and Stegun, Irene A., eds.: Handbook of Mathematical Functions. Dover Publ., Inc., 1965.

65. Lynden-Bell, D.: Statistical Mechanics of Violent Relaxation in Stellar Systems. Mon. Notic. Roy. Astron. Soc., vol. 136, no. 1, 1967, pp. 101-121.

66. Hunter, C.; and Toomre, Alar: Dynamics of the Bending of the Galaxy. Astrophys. J., vol. 155, no. 3, Mar. 1969, pp. 747-776.
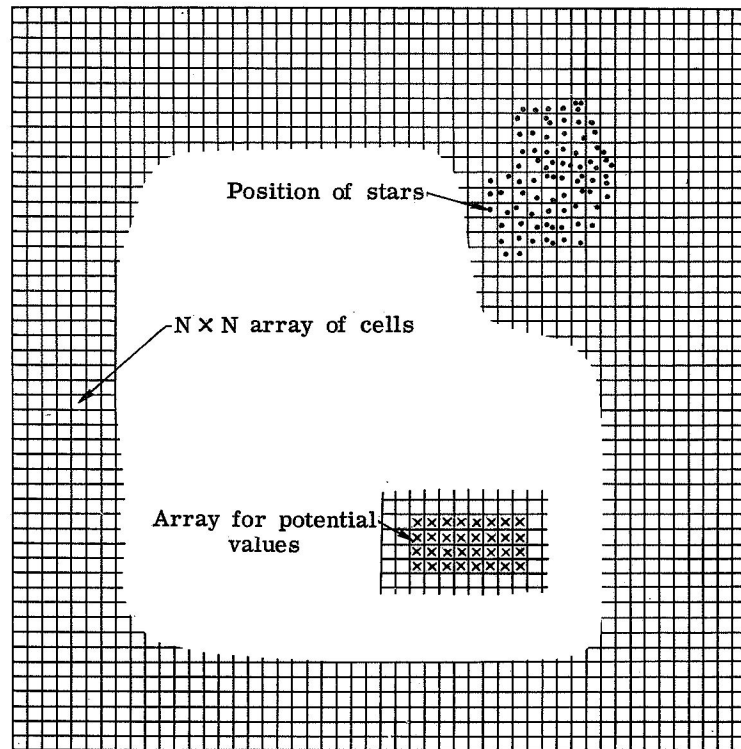
Figure 1.- Computer model illustrating the N × N array of cells used in calculating the gravitational potential.
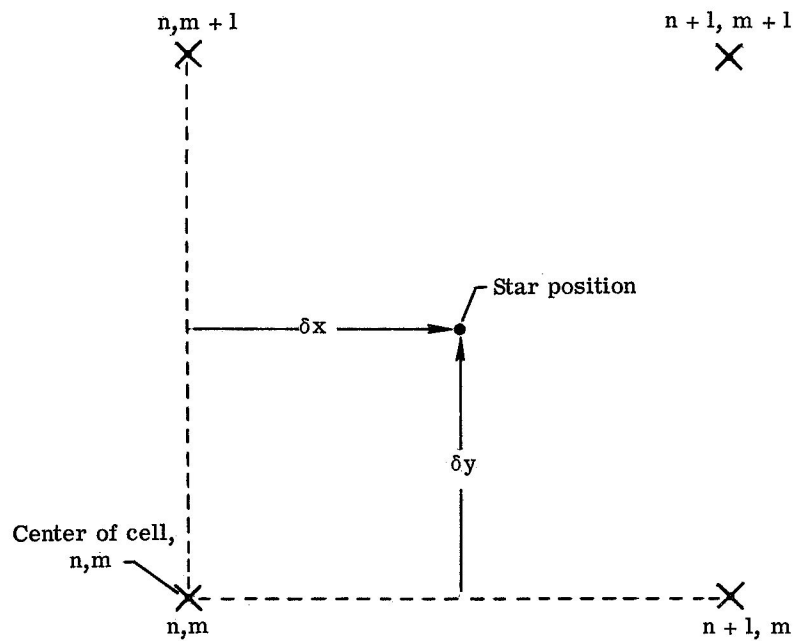
Figure 2.- Parameters used for bilinear interpolation of the gravitational field.
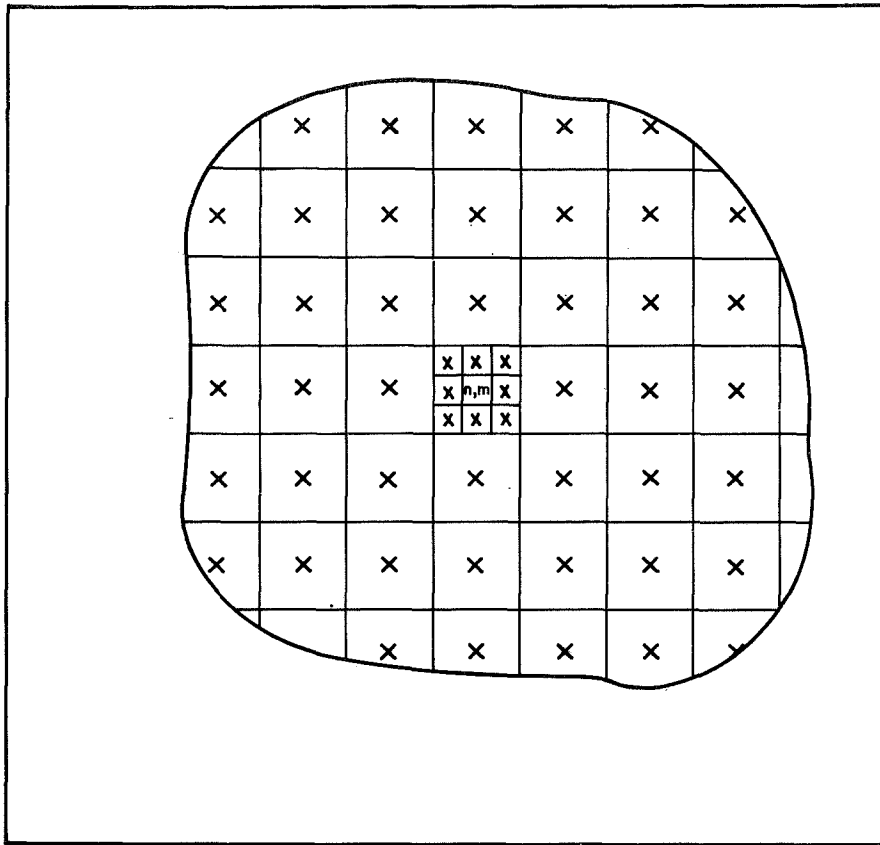
Figure 3.- Illustration of the array of cells used for calculating the gravitational potential by the summation method.
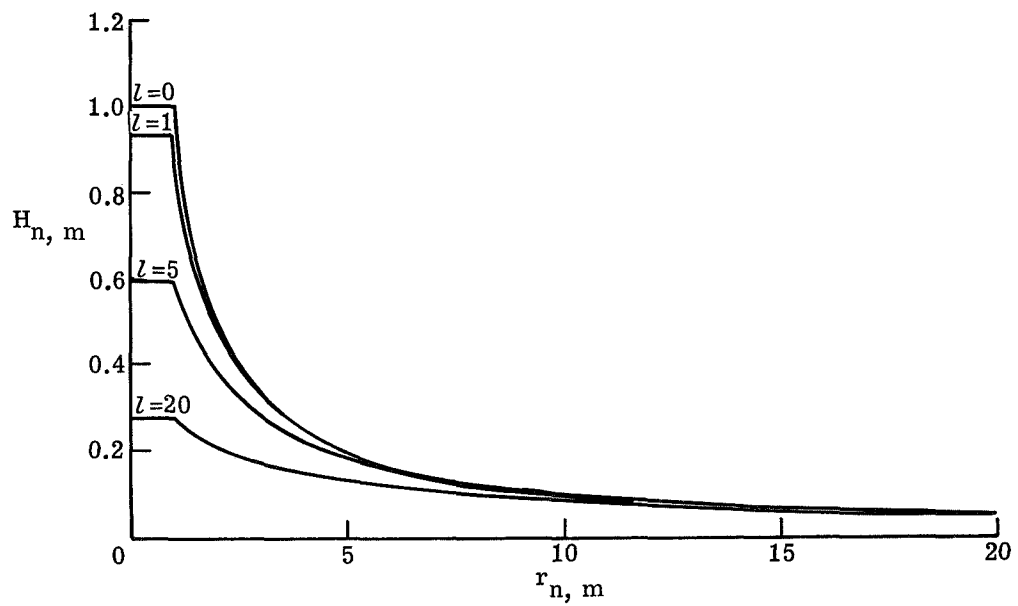
Figure 4.- Two-body interaction potential of mass rods for various rod lengths l.
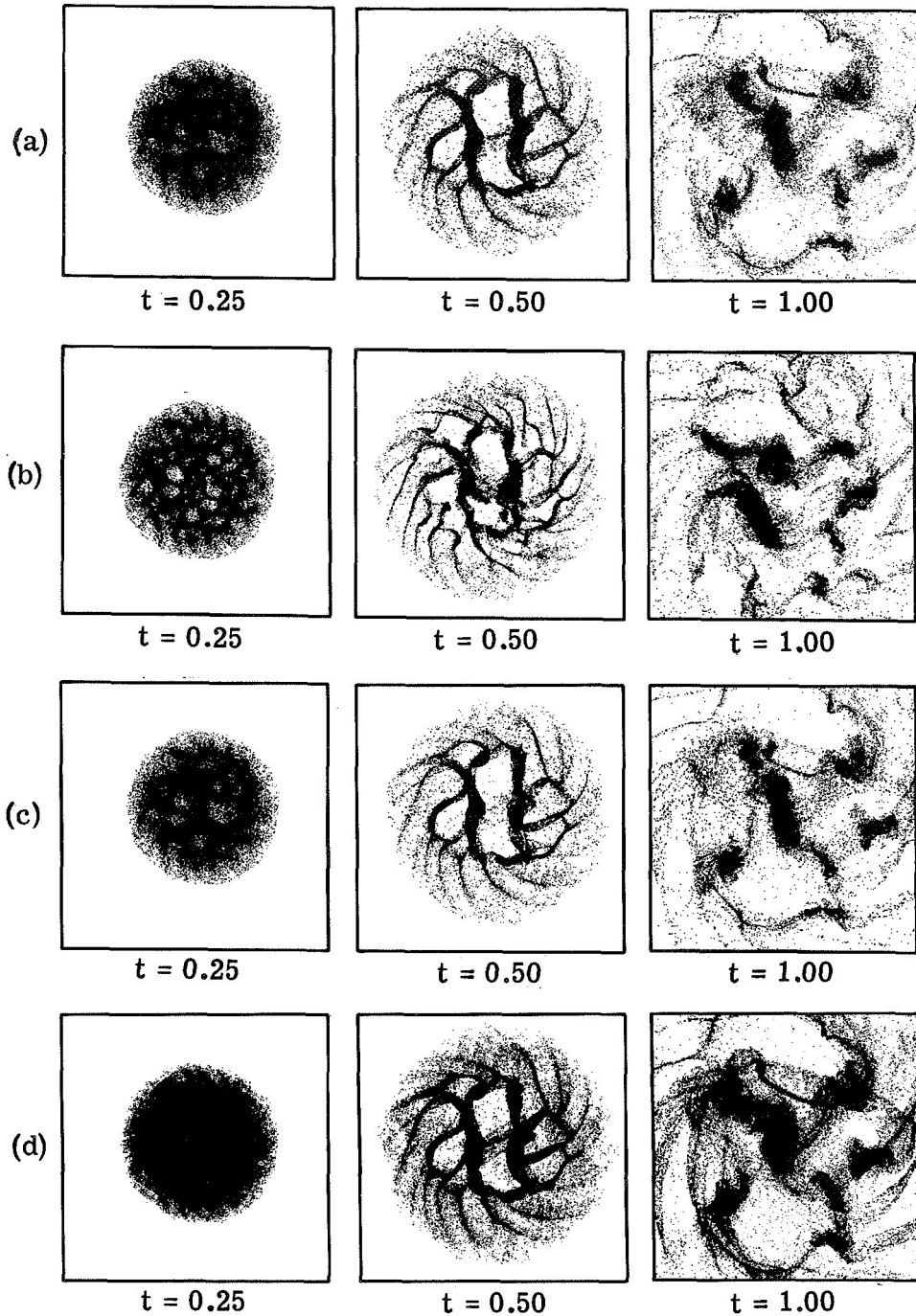
(a) Cold disk containing 50000 stars; 200 time steps per rotation; potential calculated by Fourier method on a 64×64 active array of cells.

(b) Cold disk containing 50000 stars; 200 time steps per rotation; potential calculated by summation method on a 64×64 active array of cells.

(c) Cold disk containing 50000 stars; 400 time steps per rotation; potential calculated by Fourier method on a 64×64 active array of cells.

(d) Cold disk containing 200000 stars; 200 time steps per rotation; potential calculated by Fourier method on a 64×64 active array of cells.

Figure 5.- Effect of varying the model discretization parameters on the evolution of a cold disk of stars. (Time in rotational periods given by eq. (52).)
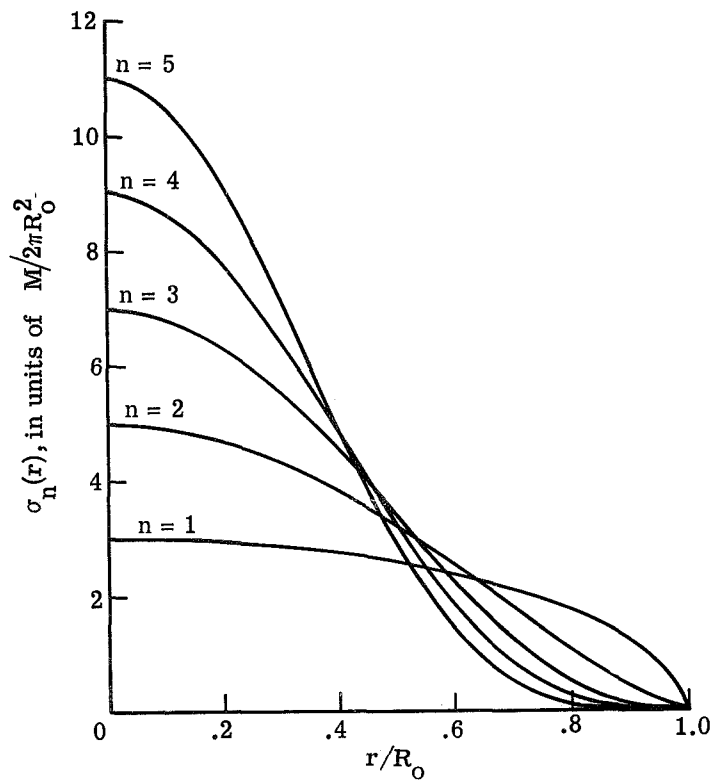
Figure 6.- Variation of surface density obtained from

$$\sigma_n(r) = \frac{M}{2\pi R_0^2}(2n + 1)\left(1 - \frac{r^2}{R_0^2}\right)^{n-1/2} \quad \text{for various}$$

values of n.
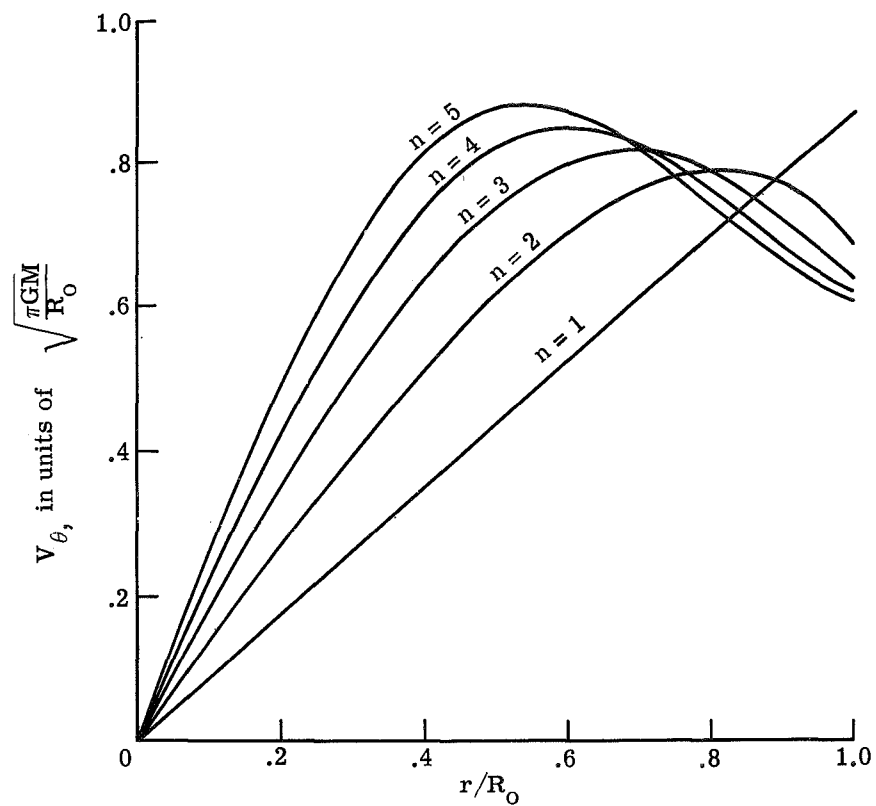
Figure 7.- Variation of rotational velocity V_θ corresponding to density distributions in figure 6.
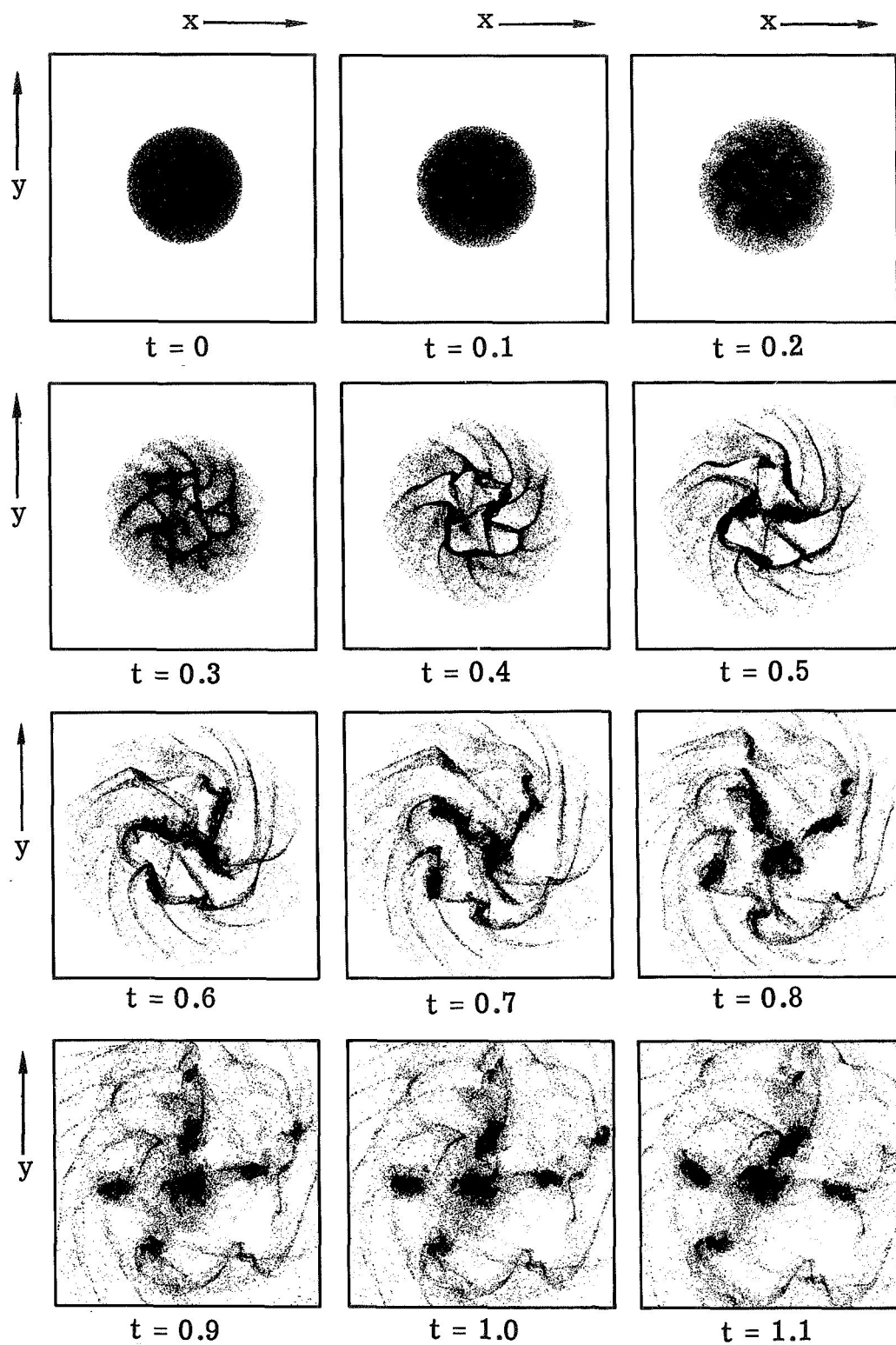
Figure 8.- Evolution of an initially balanced uniformly rotating cold disk of 50000 stars. (Time in rotational periods of the cold disk.)

54
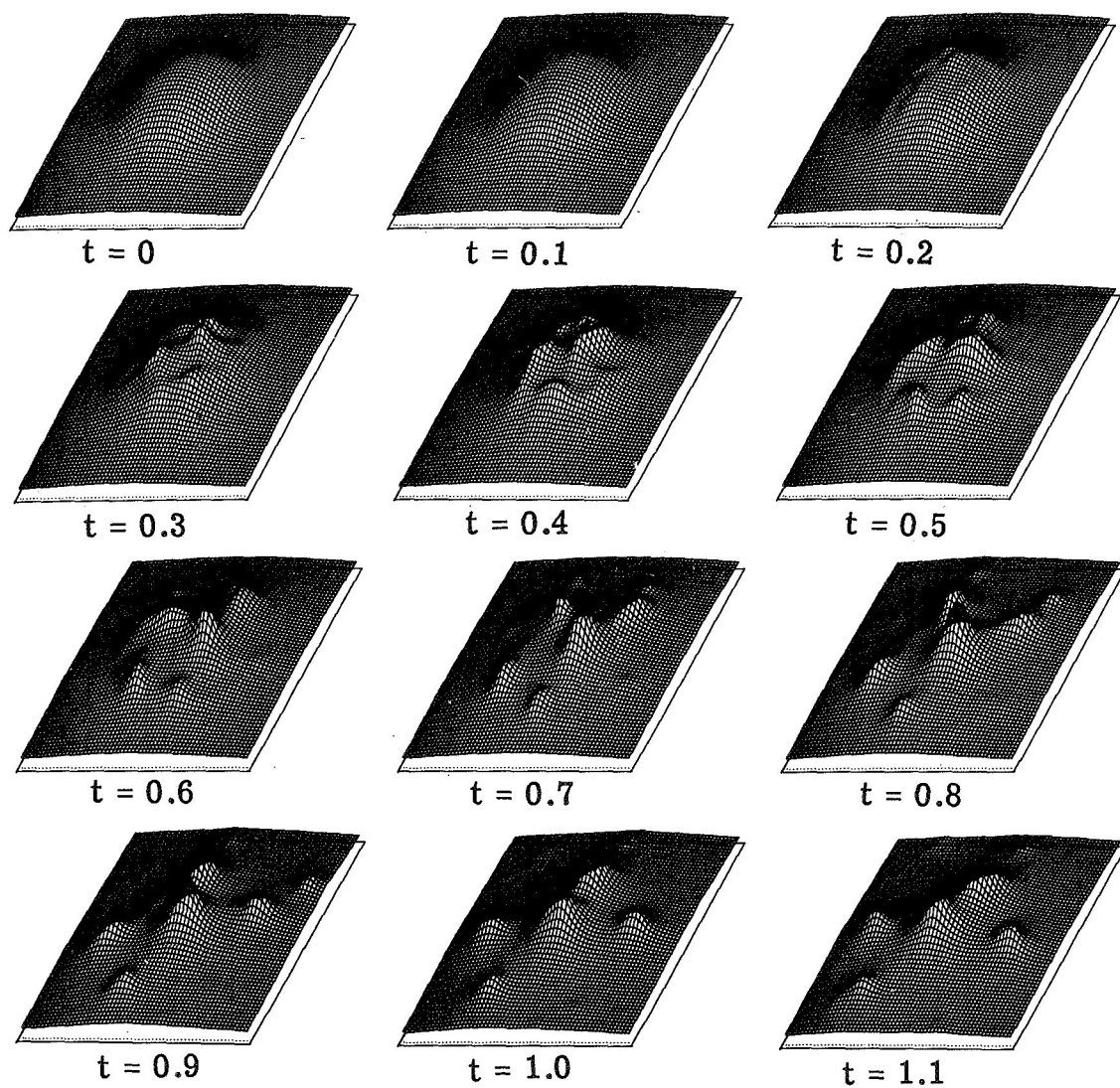
Figure 9.- Evolution of the gravitational potential for the stellar system in figure 8. (Time in rotational periods of the cold disk.)
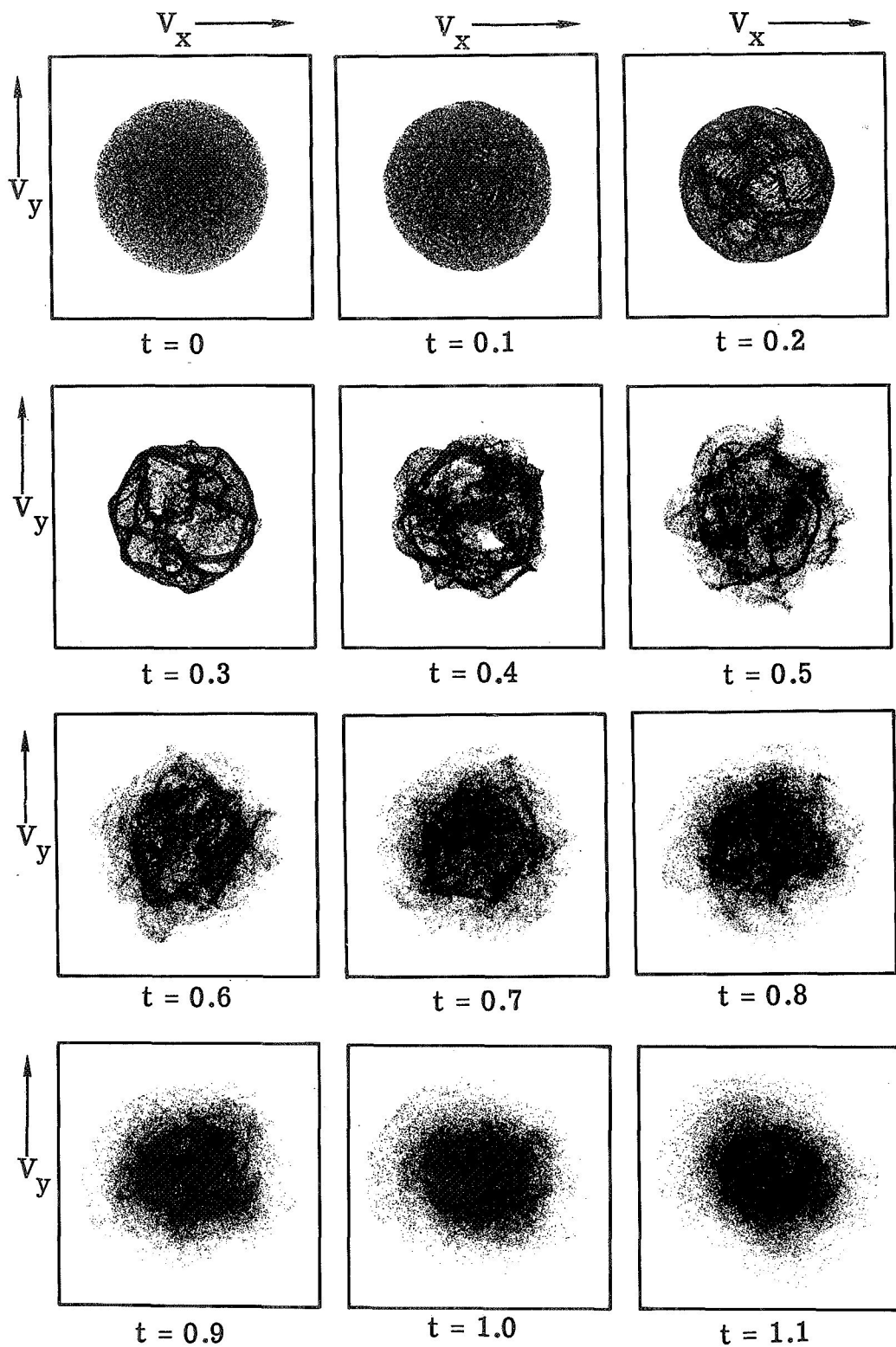
Figure 10.- Evolution of the stellar system in figure 8 in V_x, V_y space. (Time in rotational periods of the cold disk.)
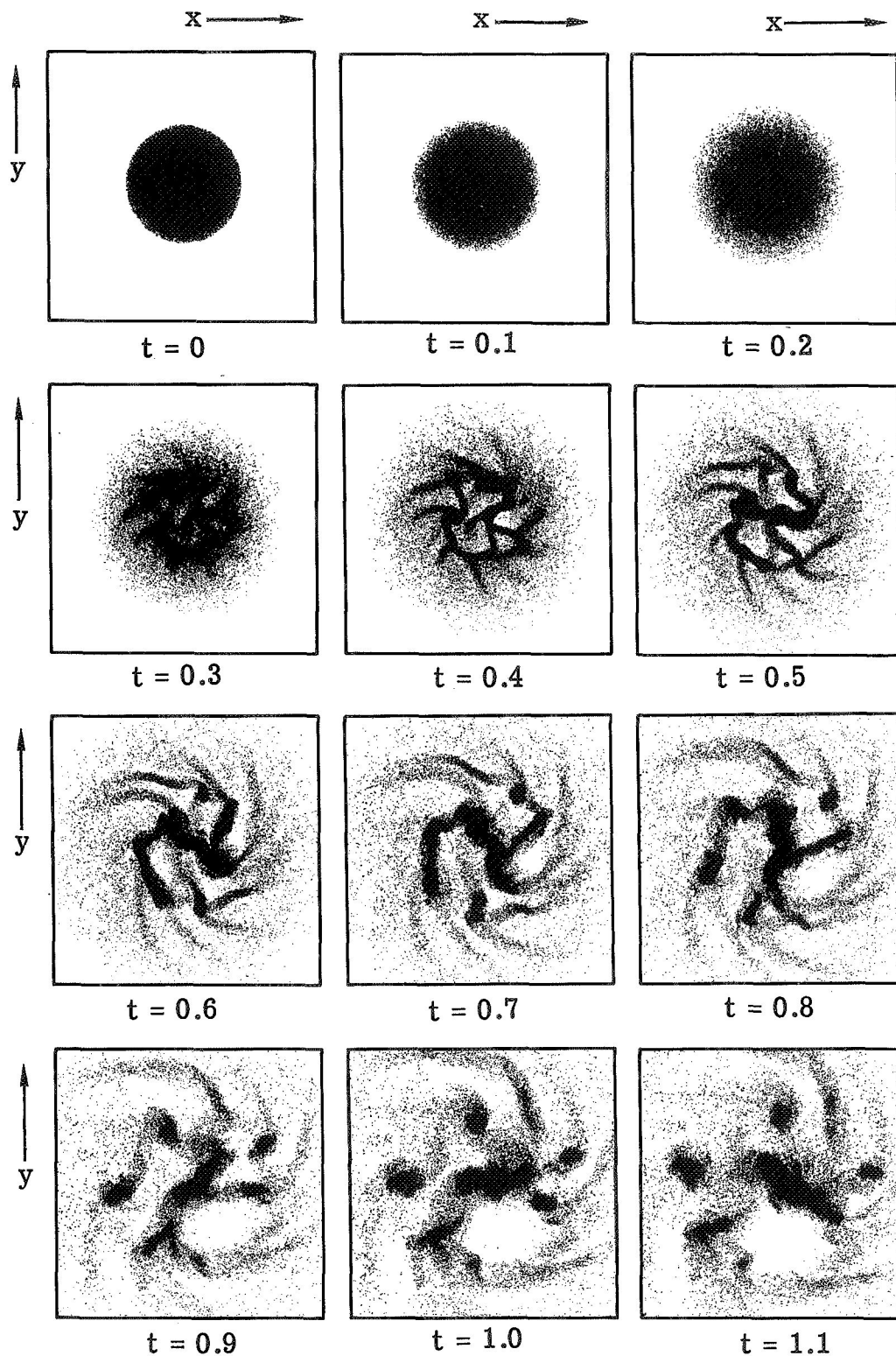
Figure 11.- Evolution of a disk of stars with a constant initial velocity dispersion equal to 6.8 percent of the circular velocity at the edge of the cold balanced disk. (Time in rotational periods of the cold disk.)
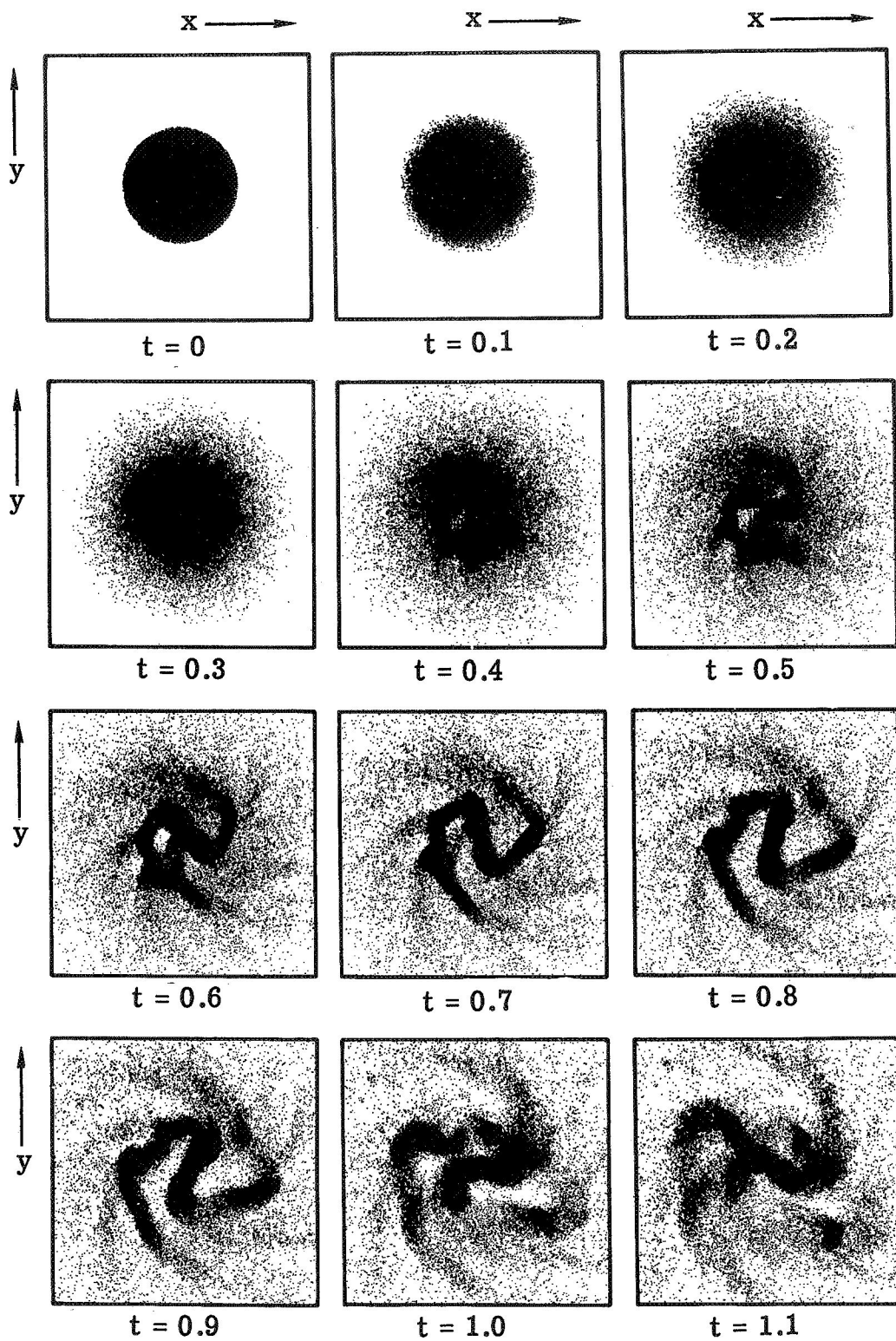
Figure 12.- Evolution of a disk of stars with a constant initial velocity dispersion equal to 13.6 percent of the circular velocity at the edge of the cold balanced disk. (Time in rotational periods of the cold disk.)
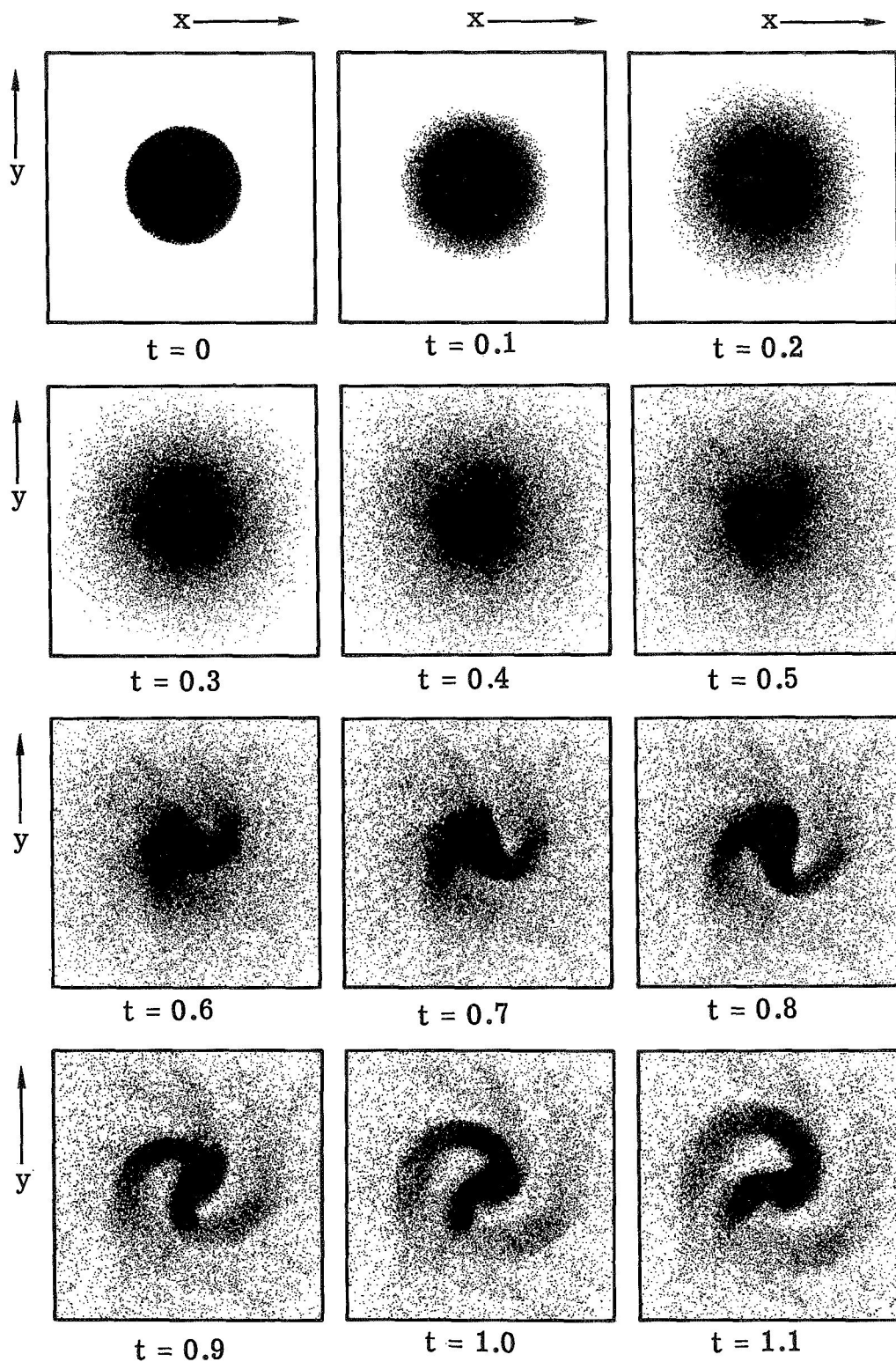
Figure 13.- Evolution of a disk of stars with a constant initial velocity dispersion equal to 20.4 percent of the circular velocity at the edge of the cold balanced disk. (Time in rotational periods of the cold disk.)
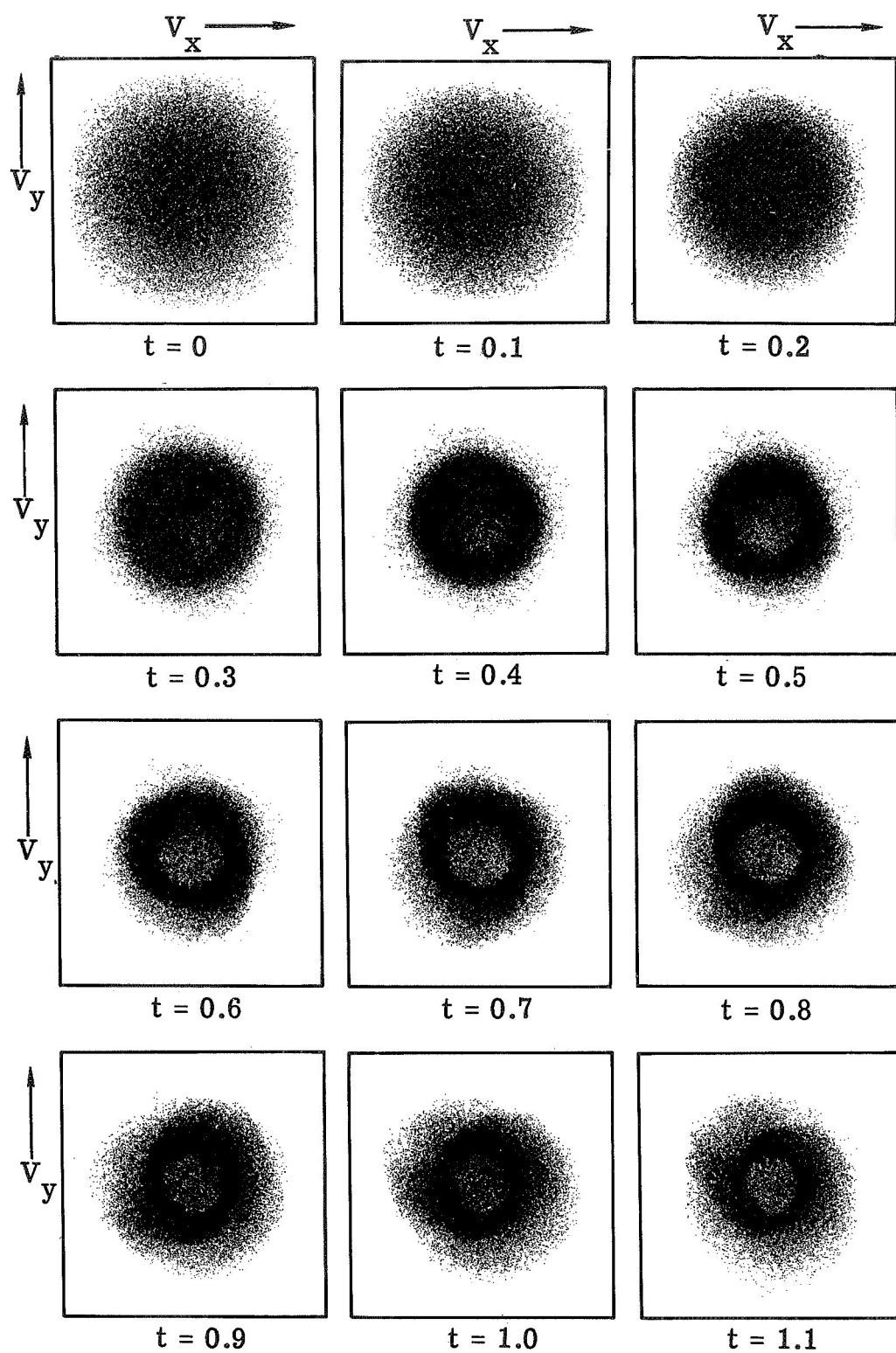
Figure 14.- Evolution of the disk of stars in figure 13 in V_x, V_y. (Time in rotational periods of the cold disk.)
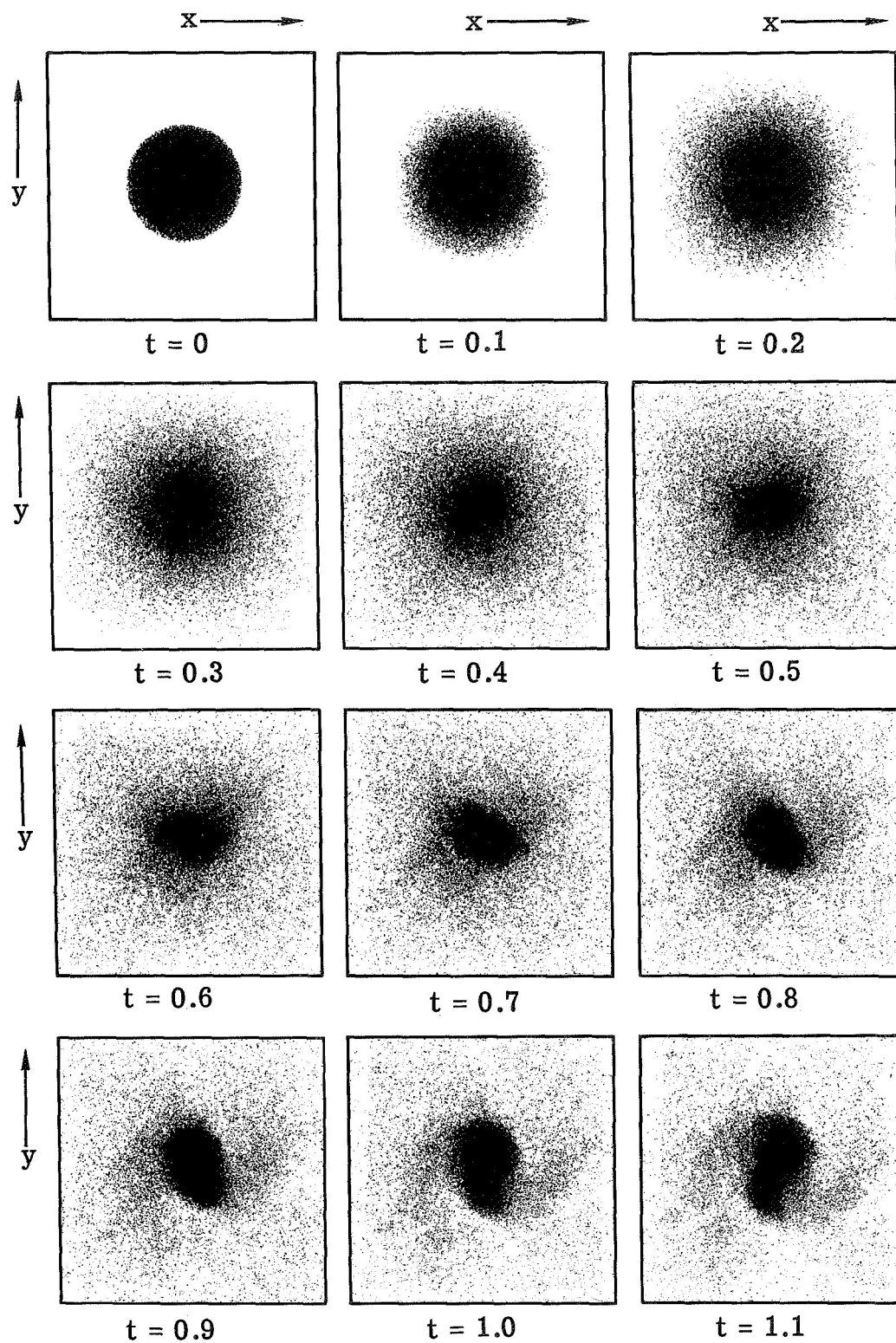
Figure 15.- Evolution of a disk of stars with a constant initial velocity dispersion equal to 27.2 percent of the circular velocity at the edge of the cold balanced disk. (Time in rotational periods of the cold disk.)
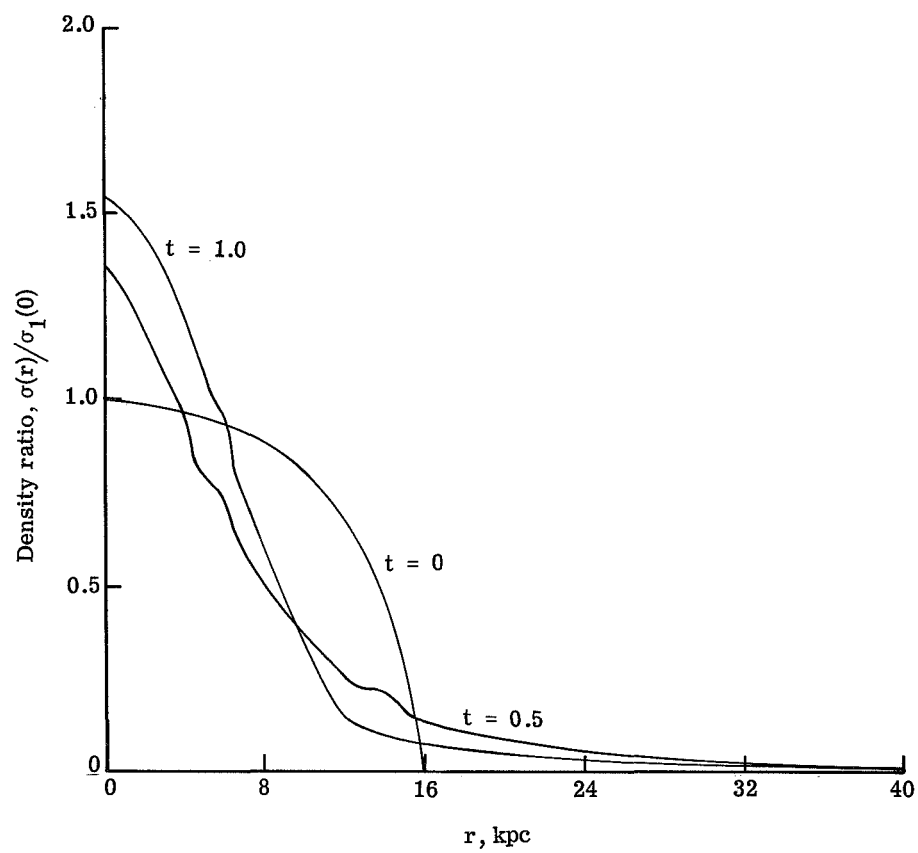
Figure 16.- Azimuthally averaged radial density for the system in figure 15. (Time in rotational periods of the cold disk.)
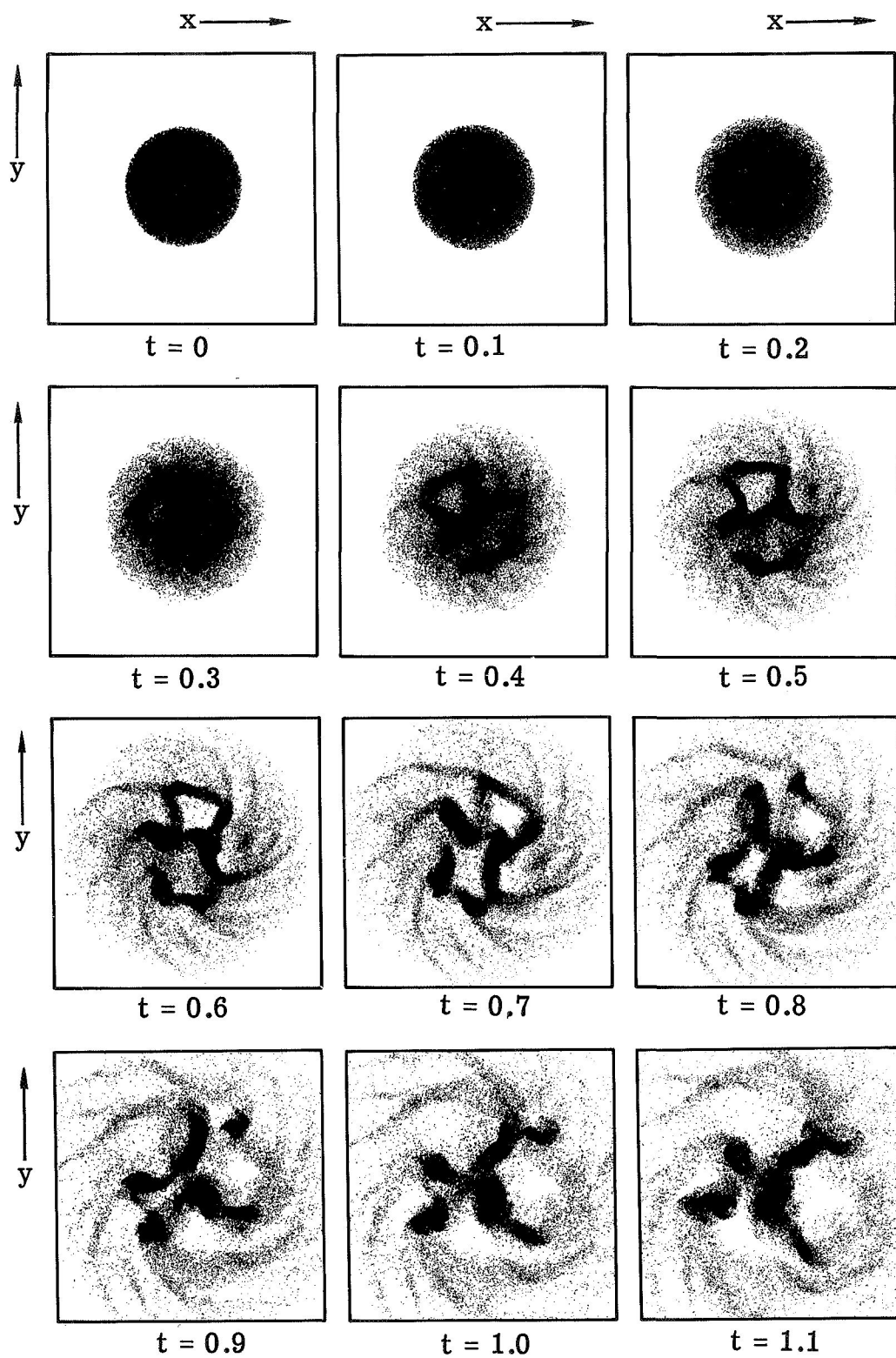
Figure 17.- Evolution of an initially balanced uniformly rotating disk of stars with an initial velocity dispersion equal to $\frac{1}{2}\sigma_{r,min}$. (Time in rotational periods of the cold disk.)
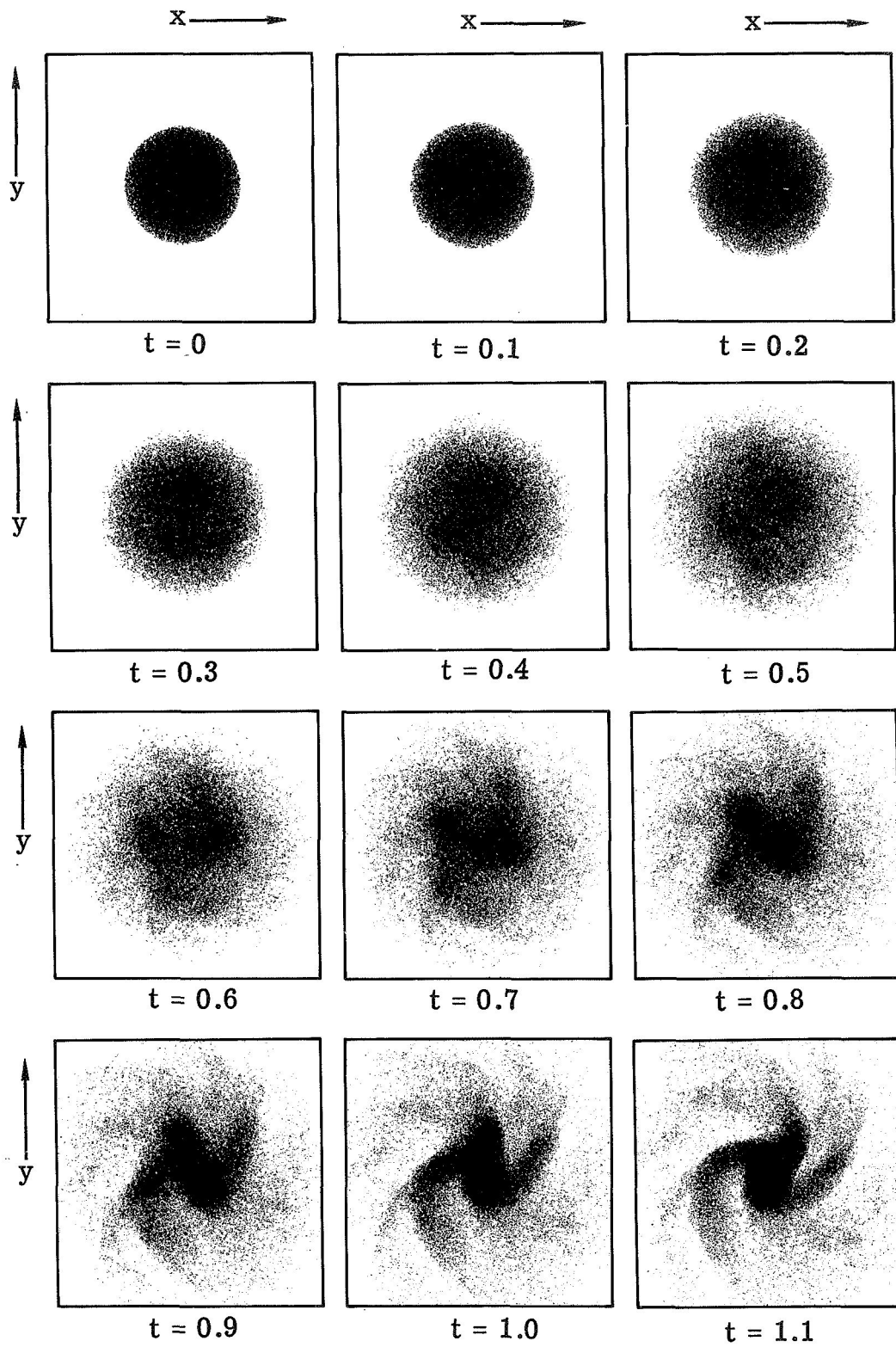
Figure 18.- Evolution of an initially balanced uniformly rotating disk of stars with an initial velocity dispersion equal to $\sigma_{r,min}$. (Time in rotational periods of the cold disk.)
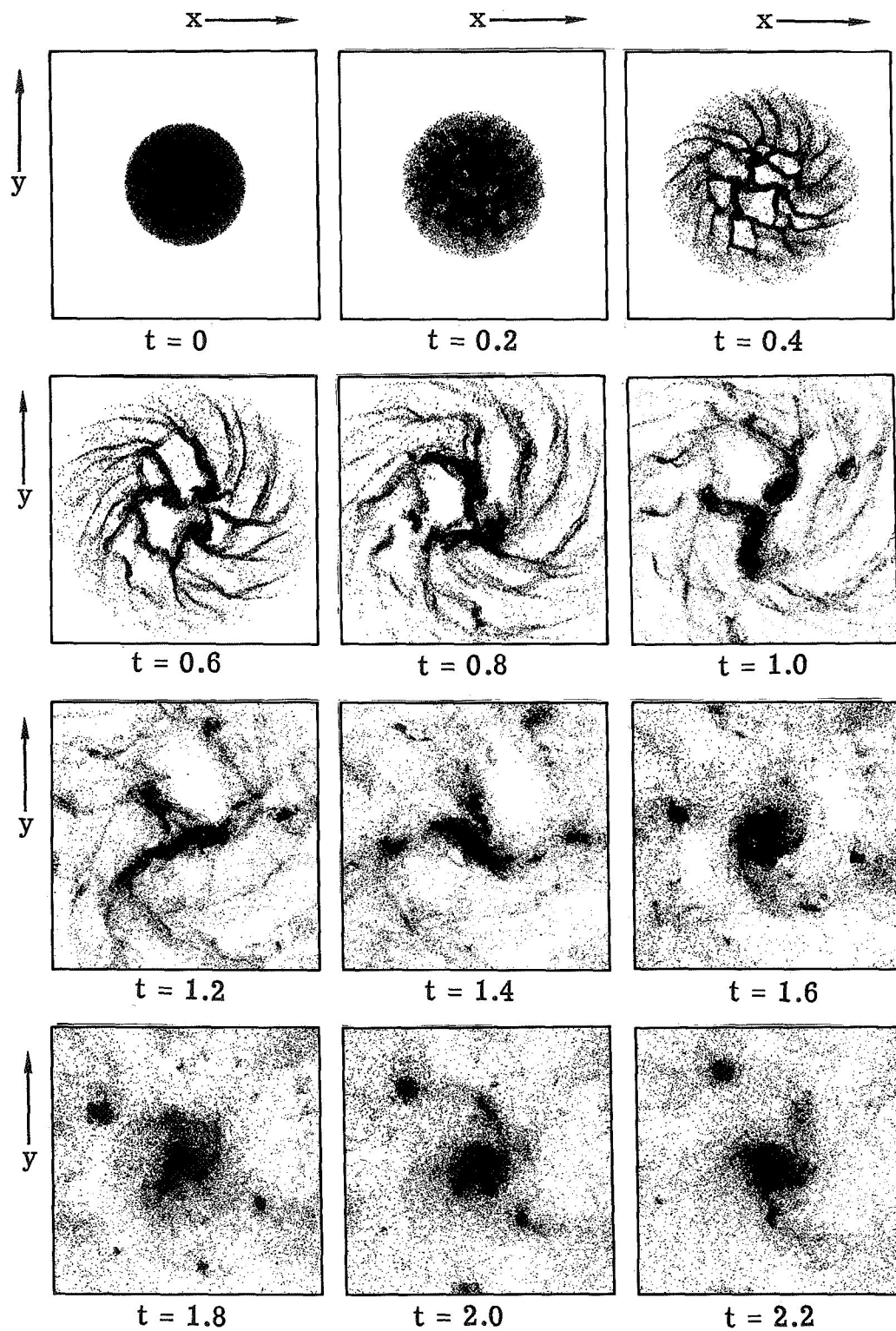
Figure 19.- Evolution of an initially balanced uniformly rotating cold disk of 50 000 stars with gravitational potential obtained by the summation method. (Time in rotational periods of the cold disk.)
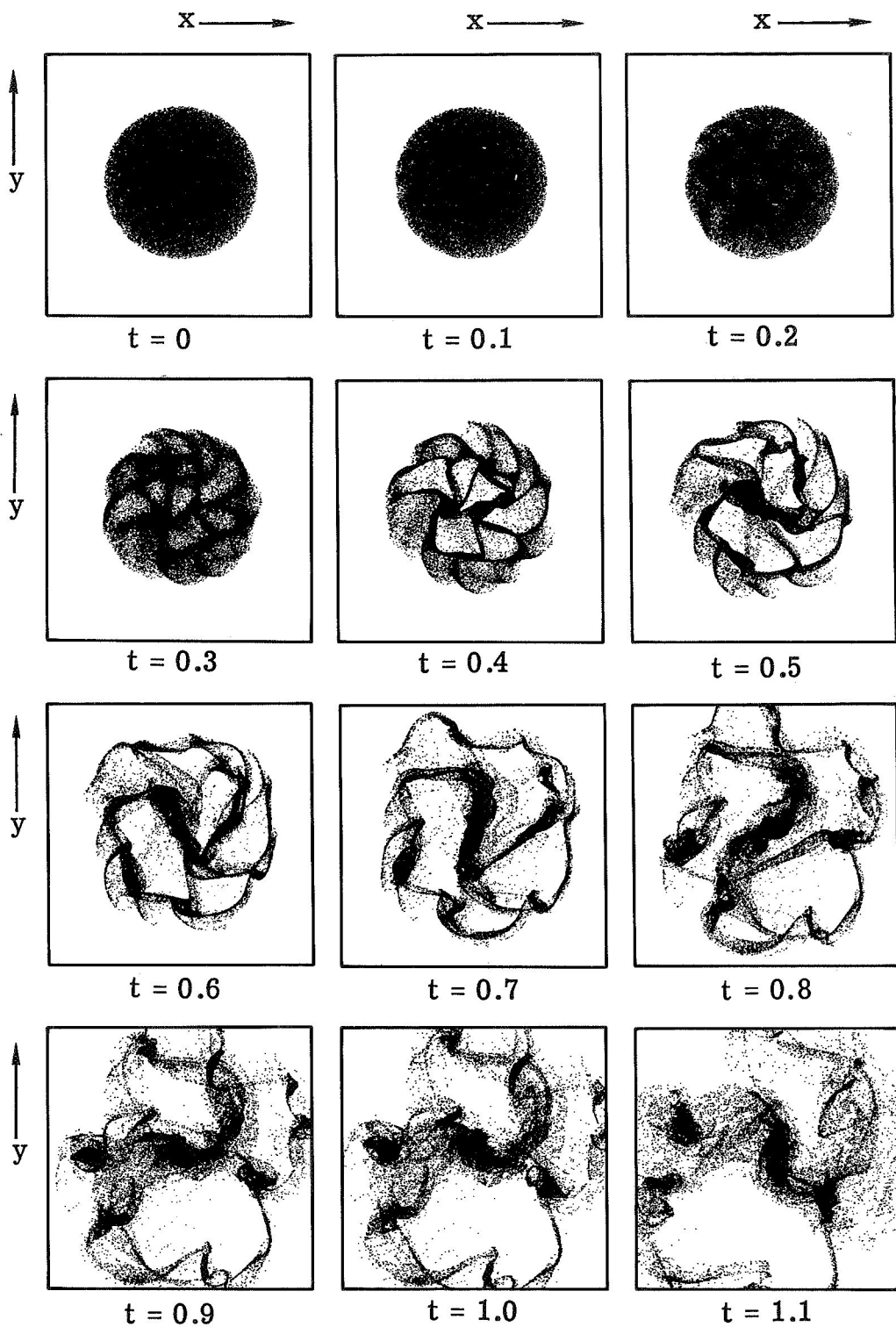
Figure 20.- Evolution of an initially balanced cold disk of finite-length rod stars. Length of each rod is two cell dimensions. (Time in rotational periods of the cold disk.)
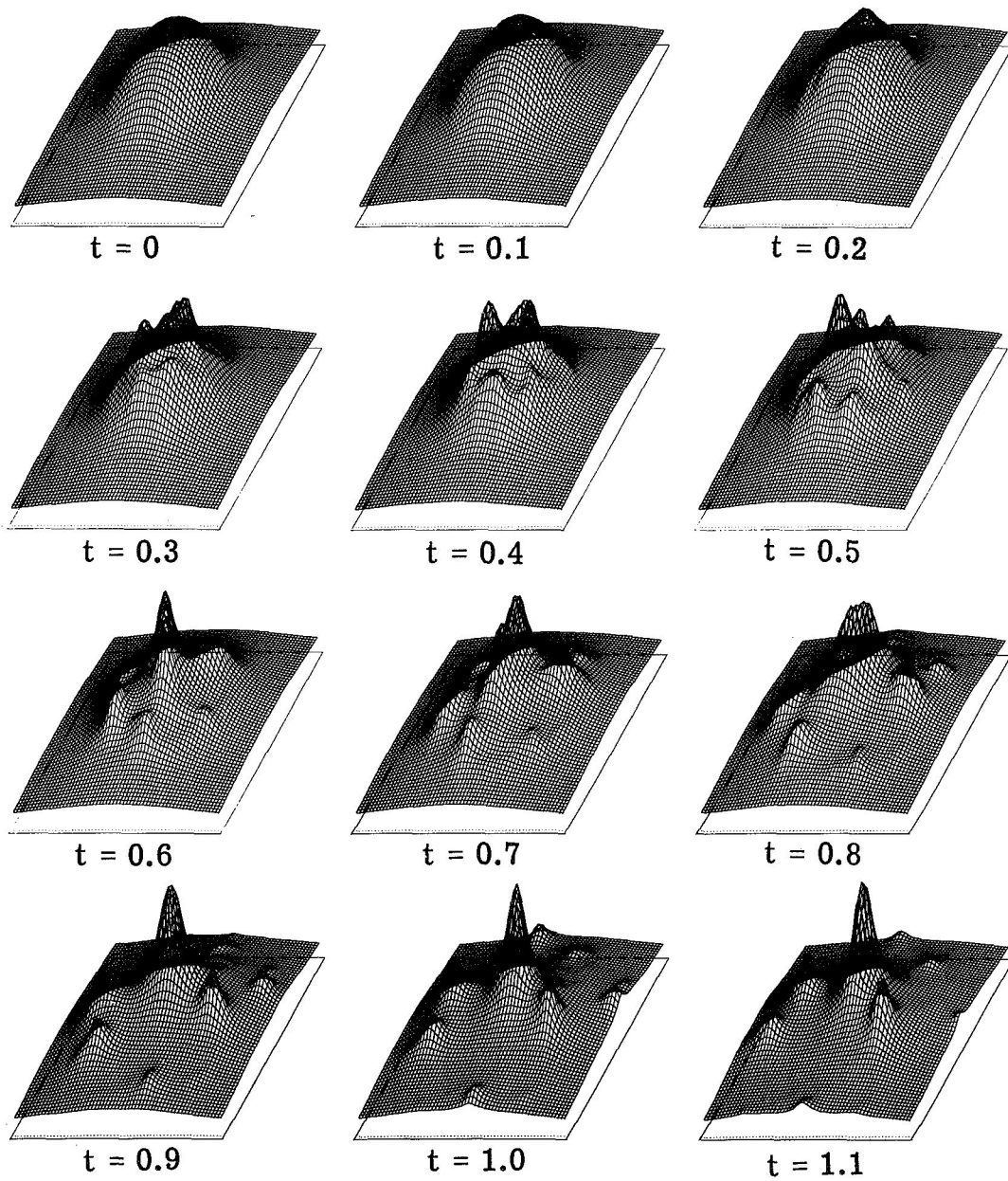
Figure 21.- Evolution of the gravitational potential for the stellar system in figure 20. (Time in rotational periods of the cold disk.)
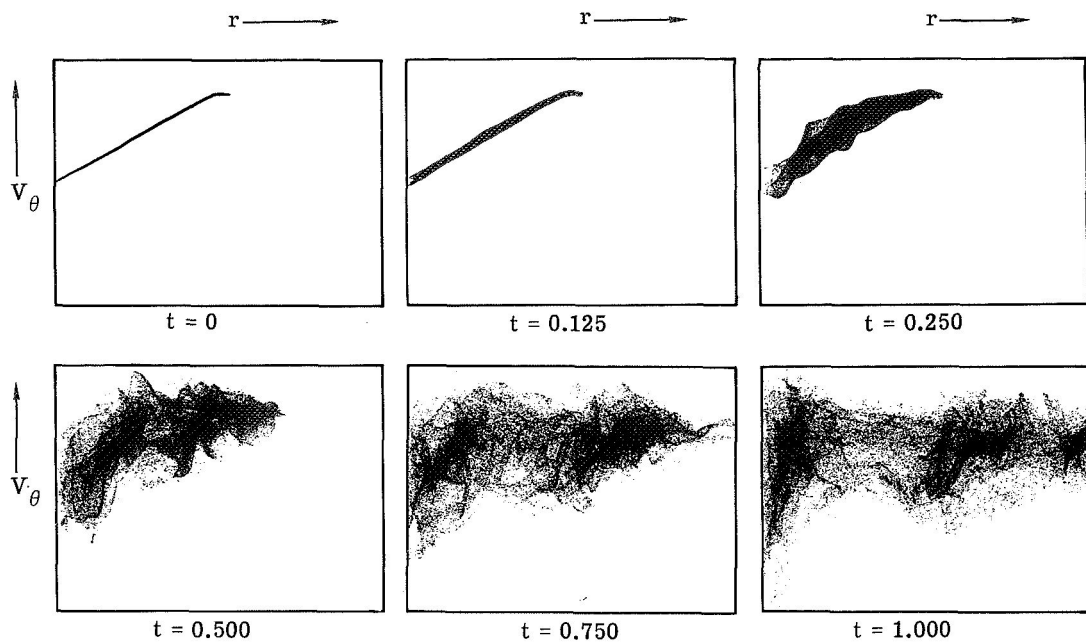
Figure 22.- Evolution of the circular velocities of the stars for the system in figure 20. (Time in rotational periods of the cold disk.)
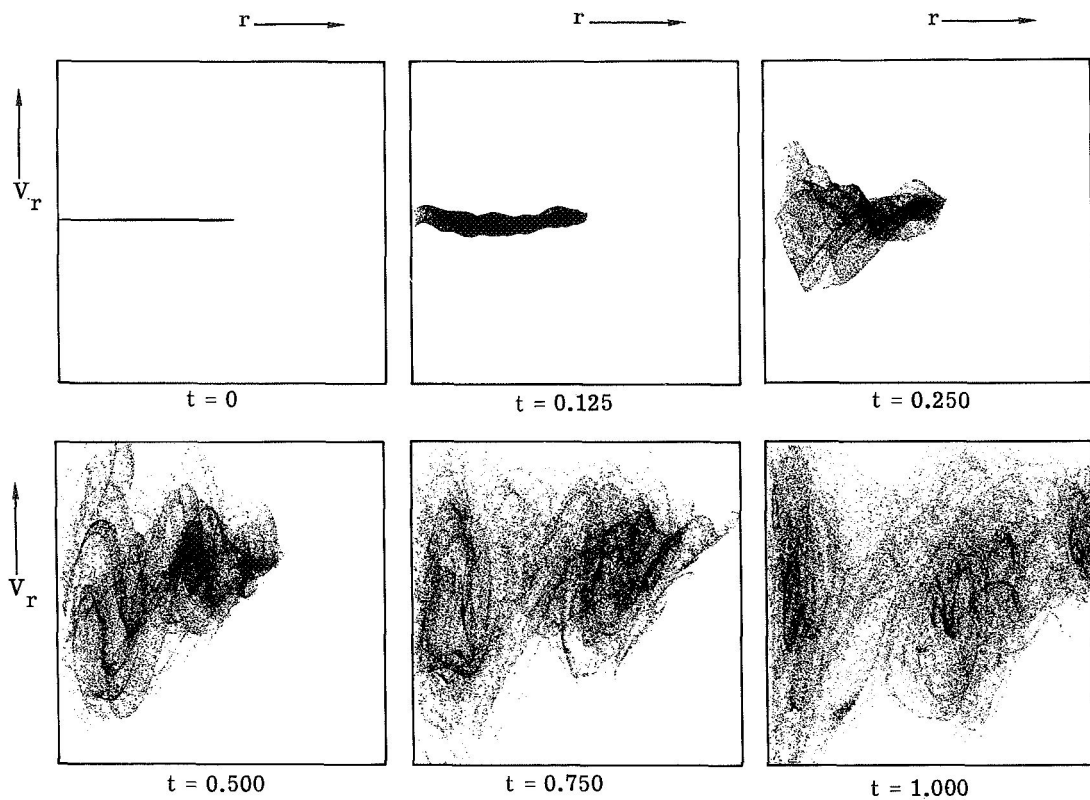
Figure 23.- Evolution of the radial velocities of the stars for the system in figure 20. (Time in rotational periods of the cold disk.)
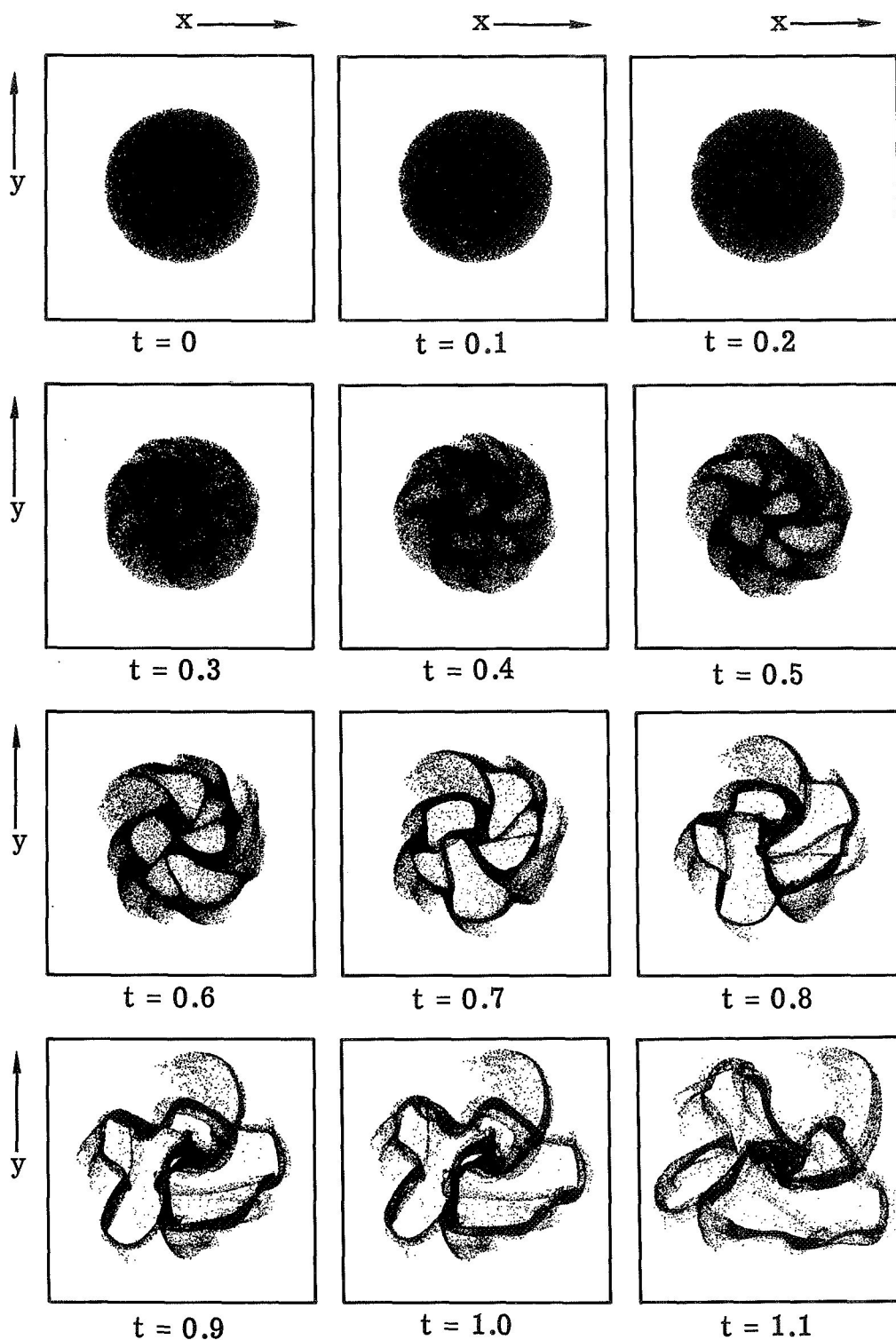
Figure 24.- Evolution of an initially cold balanced disk of finite-length rod stars. Length of each rod is five cell dimensions. (Time in rotational periods of the cold disk.)
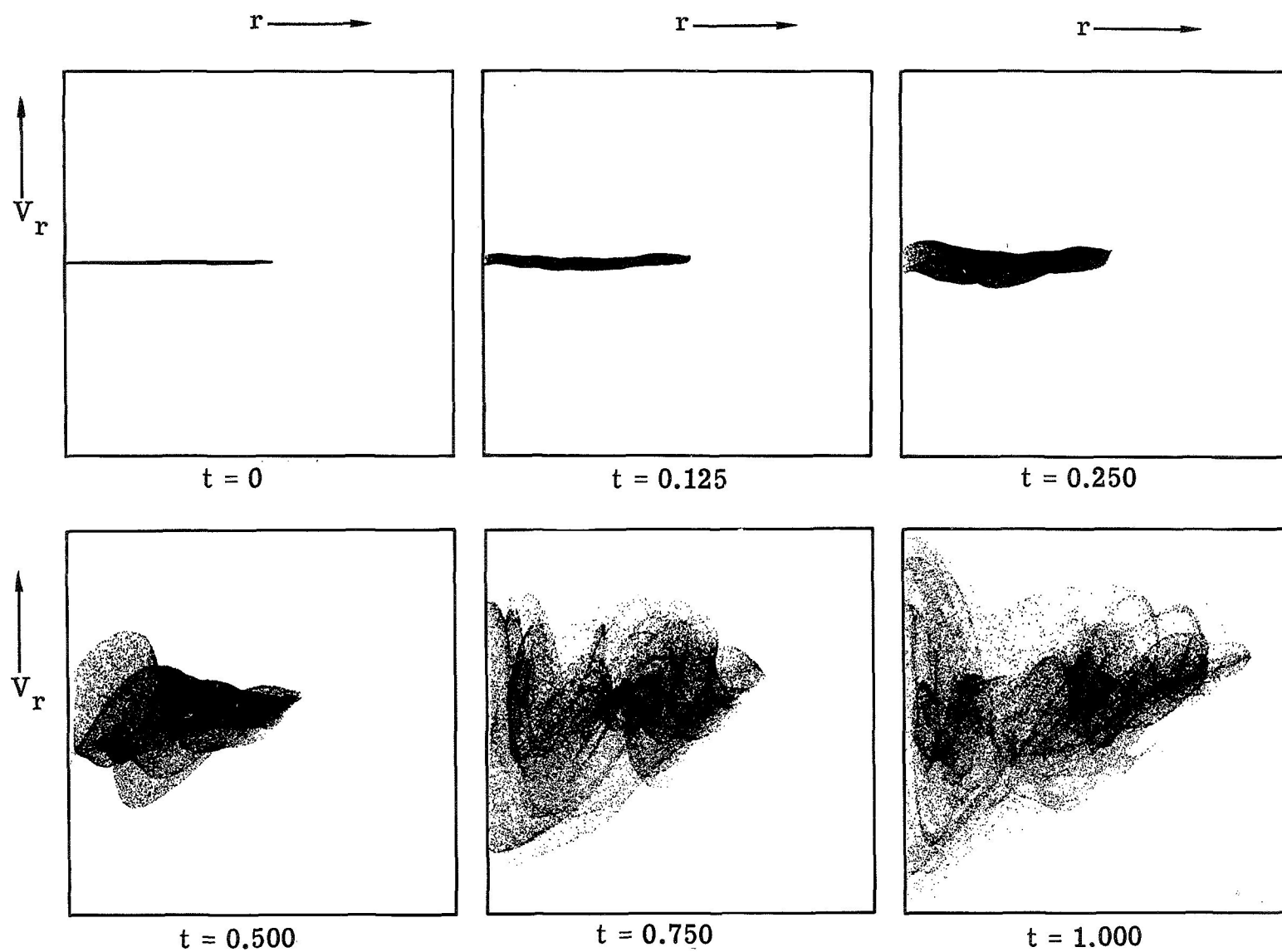
Figure 25.- Evolution of the radial velocities of the stars for the system in figure 24. (Time in rotational periods of the cold disk.)
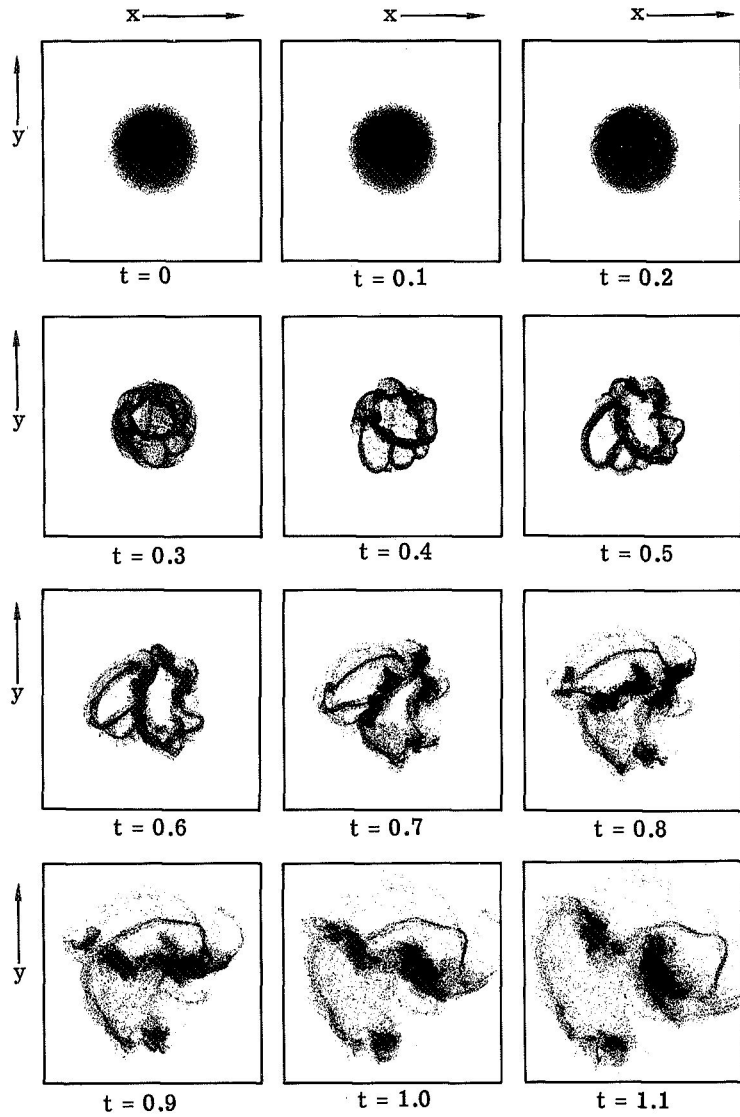
Figure 26.- Evolution of an initially balanced cold disk of stars with a density distribution given by $\sigma_3(r)$. (Time in rotational periods of the cold disk.)
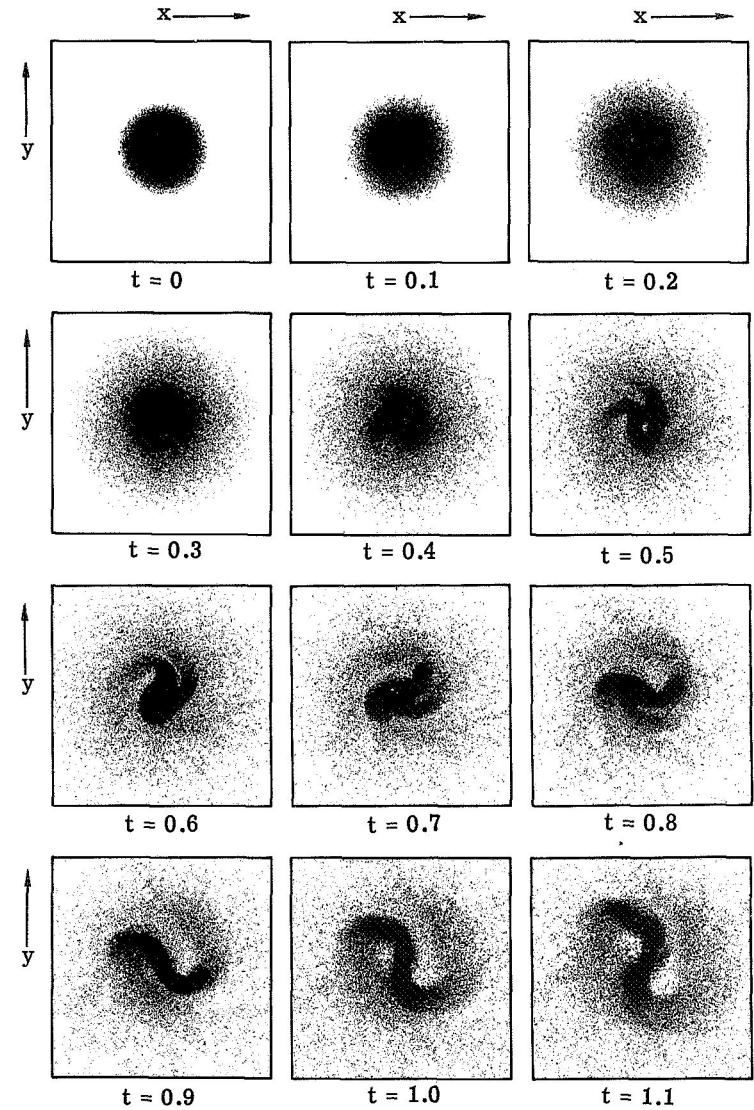
Figure 27.- Evolution of a disk of stars with initial conditions the same as those of the disk in figure 20 except that a uniform velocity dispersion equal to 30 percent of the velocity at the edge of the cold balanced disk has been added. (Time in rotational periods of the cold disk.)
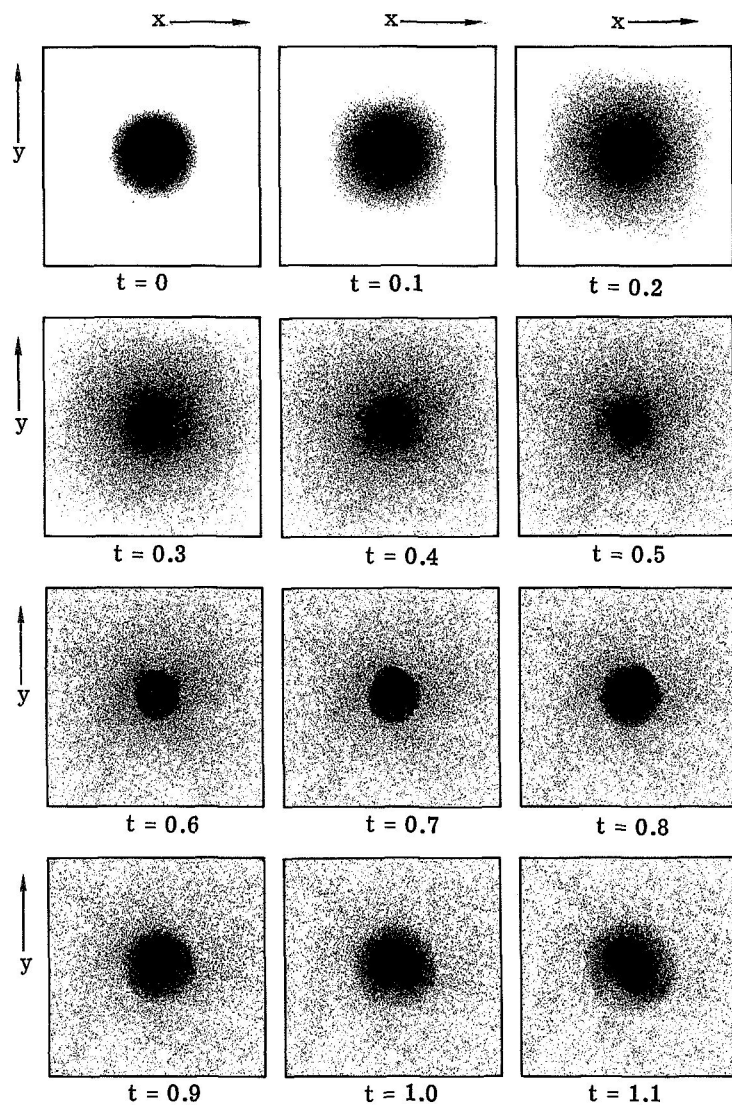
Figure 28.- Evolution of a disk of stars with initial conditions the same as those of the disk in figure 26 except that a uniform velocity dispersion equal to 60 percent of the velocity at the edge of the cold balanced disk has been added. (Time in rotational periods of the cold disk.)
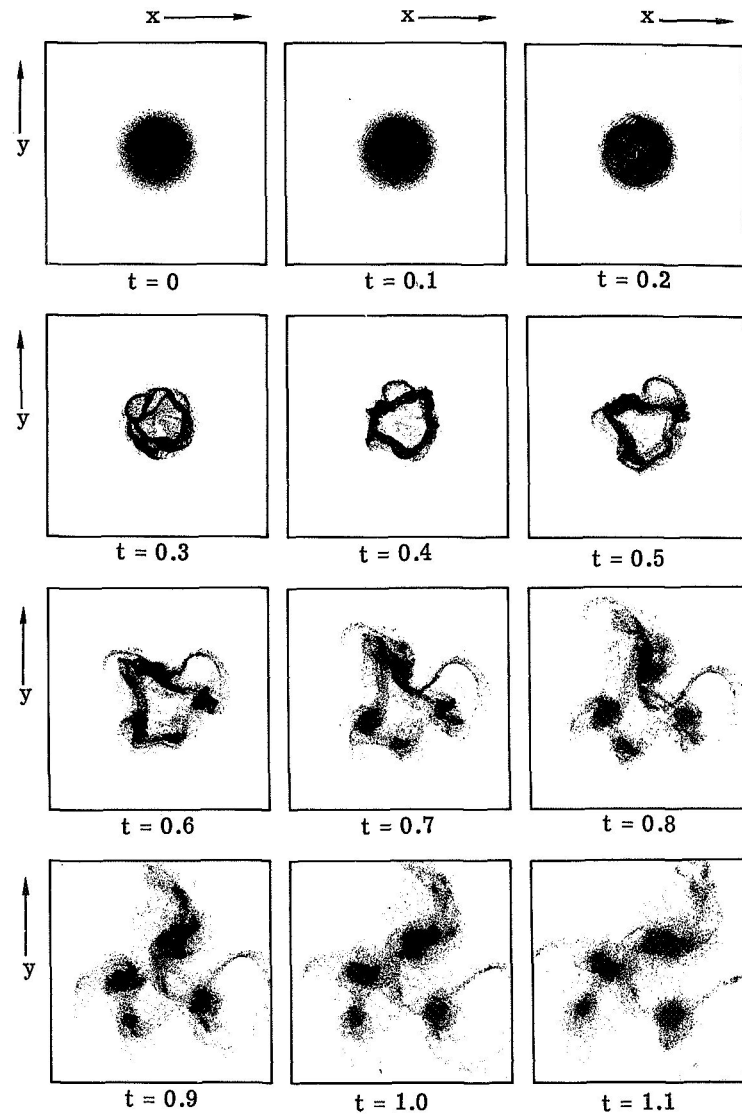
Figure 29.- Evolution of an initially cold balanced disk of stars with a density distribution given by $\sigma_5(r)$. (Time in rotational periods of the cold disk.)
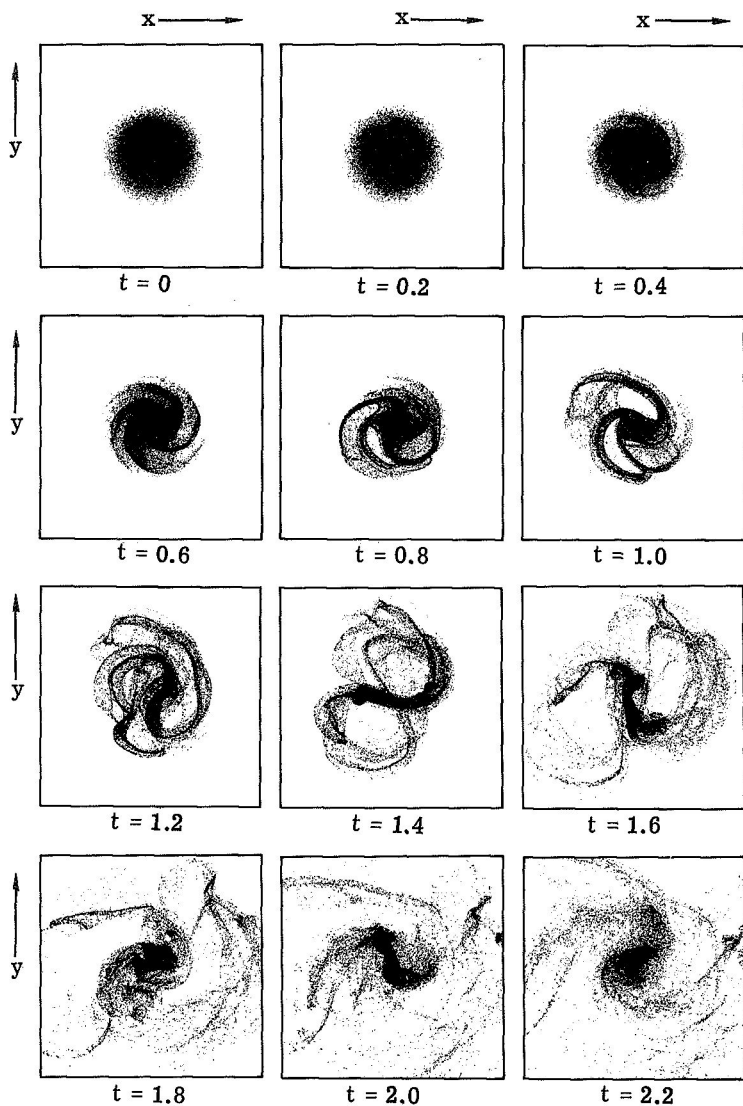
Figure 30.- Evolution of the stellar system displayed in figure 29 except that the point stars are mass rods having a length of five cell dimensions. (Time in rotational periods of the cold disk.)
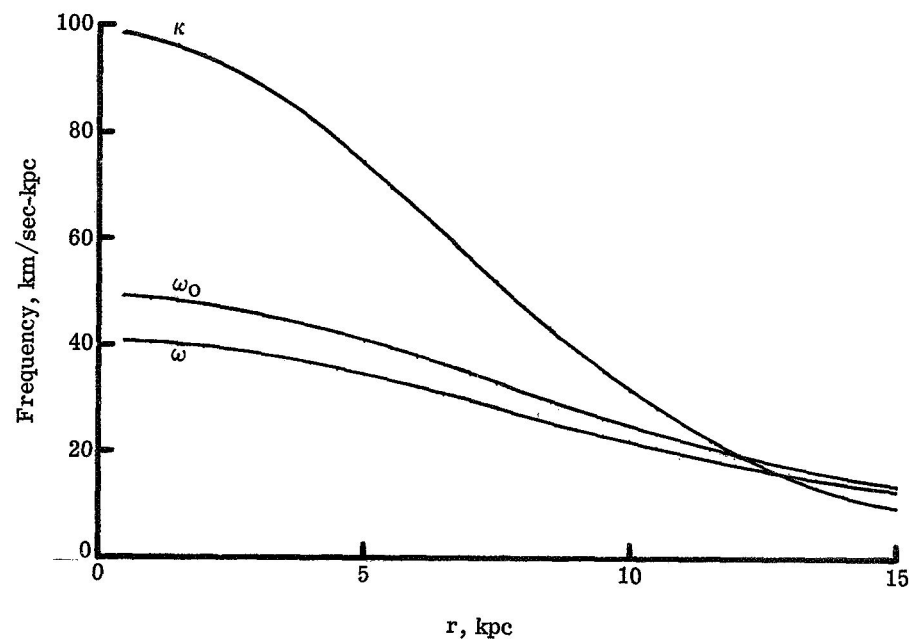
Figure 31.- Variation of ω_0, ω, and κ with r for a disk of stars with a Gaussian mass density.
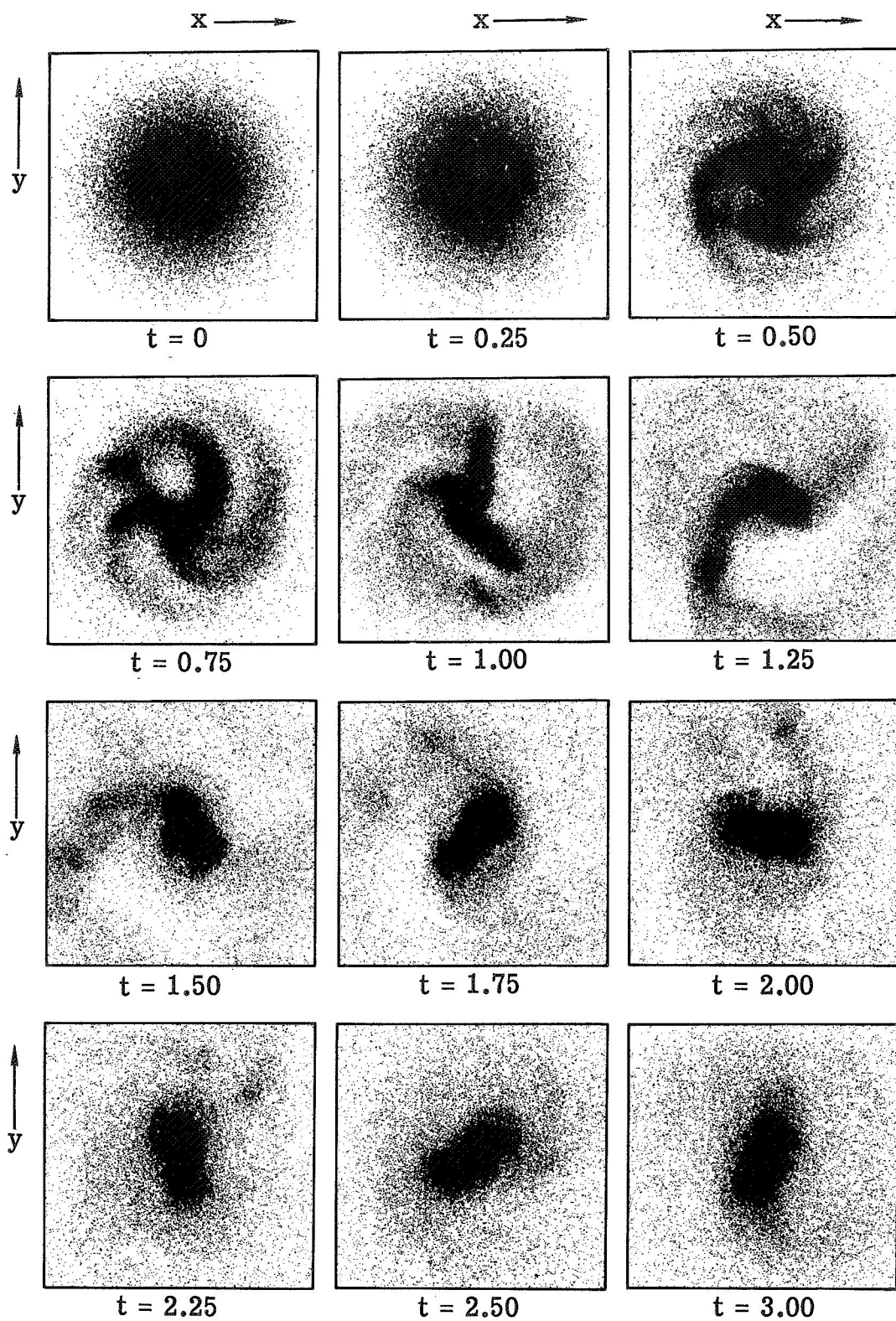
Figure 32.- Evolution of a disk of stars with a Gaussian mass density and with an initial velocity dispersion equal to $\sigma_{r,min}$ and $\sigma_{\theta,min}$ as calculated by Toomre. (Time in rotational periods of the cold balanced Gaussian disk at $r = 10$ kpc.)
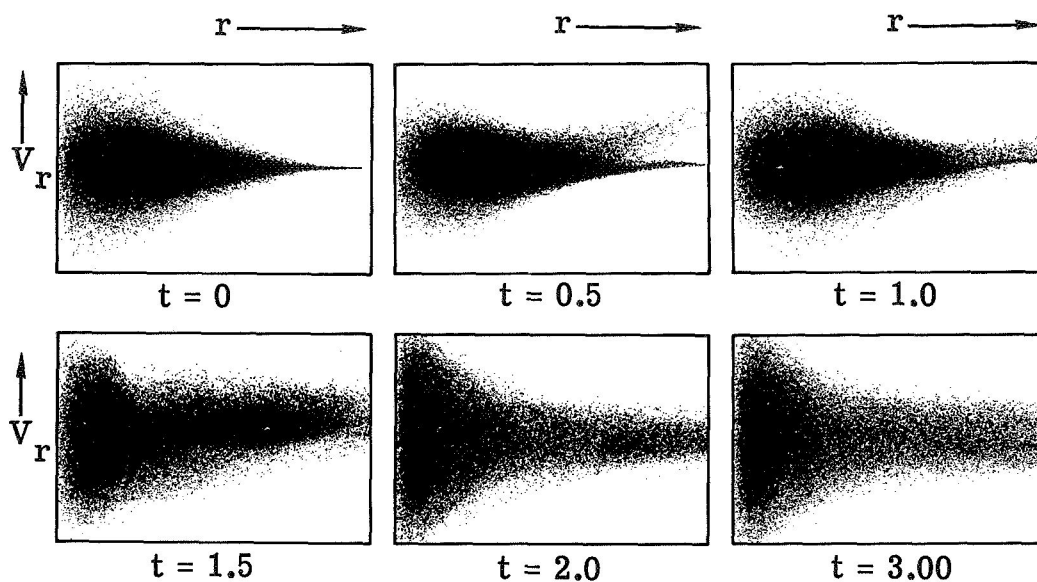
Figure 33.- Evolution of the radial velocities of the stars for the system in figure 32. (Time in rotational periods of the cold balanced Gaussian disk at r = 10 kpc.)
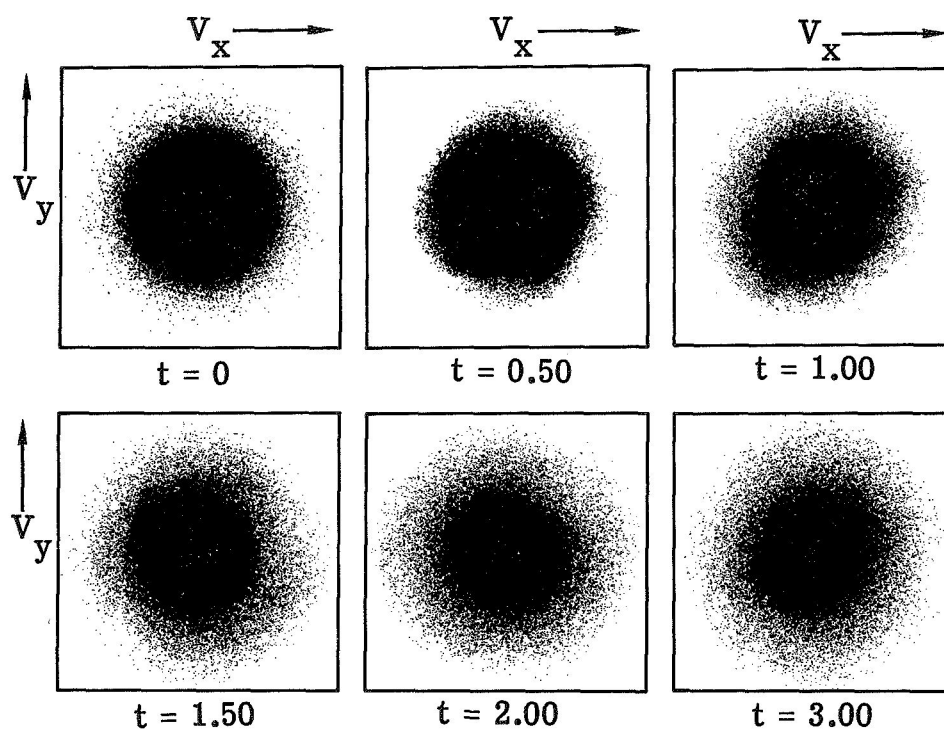
Figure 34.- Evolution of the stellar system in figure 32 in V_x, V_y space. (Time in rotational periods of the cold balanced Gaussian disk at r = 10 kpc.)
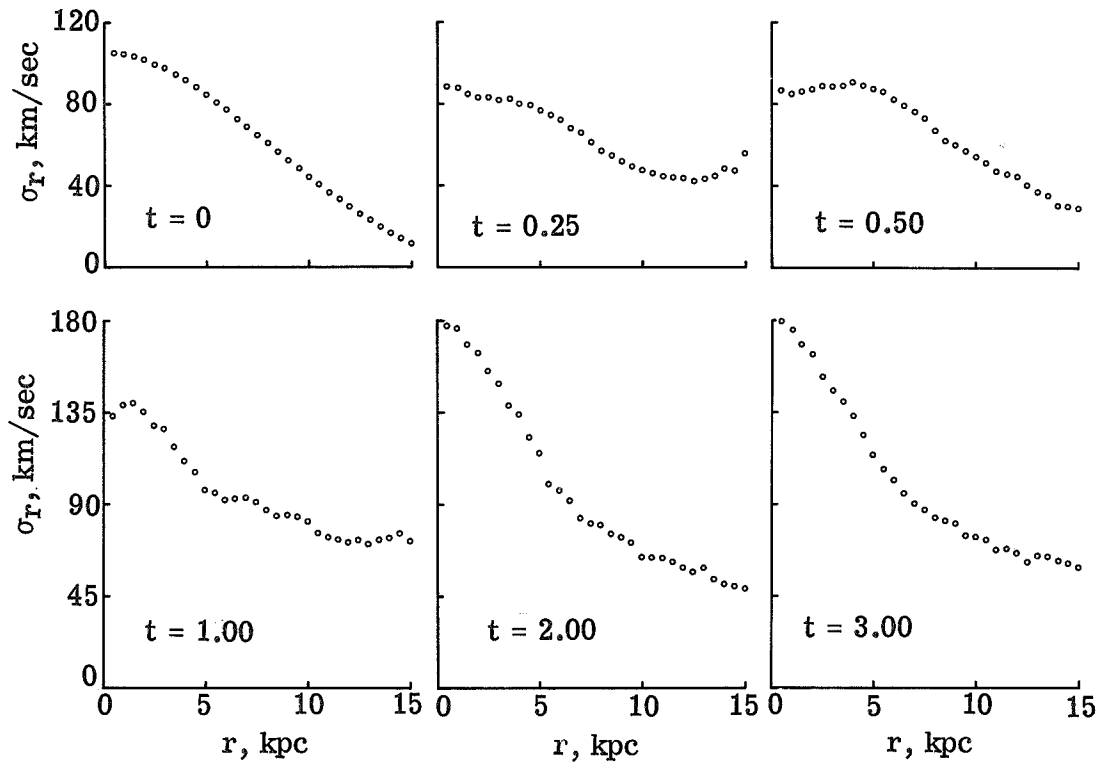
Figure 35.- Variation of radial velocity dispersion with radius for the disk of stars with a Gaussian mass distribution. (Time in rotational periods of the cold balanced Gaussian disk at r = 10 kpc.)
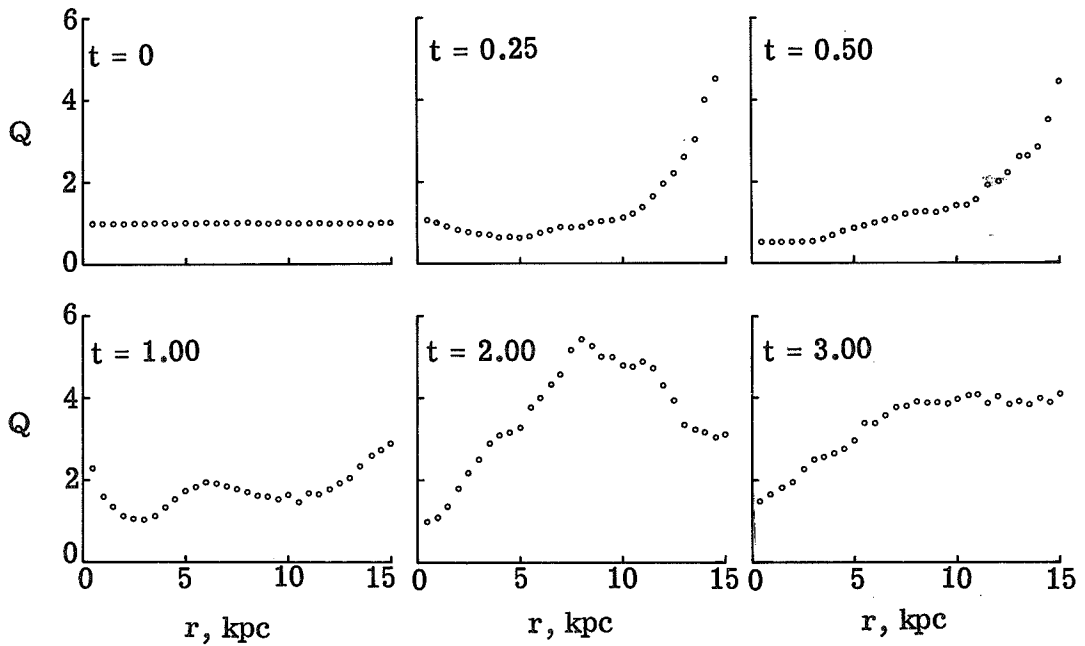
Figure 36.- Variation of Q with radius for the Gaussian disk. (Time in rotational periods of the cold balanced Gaussian disk at r = 10 kpc.)
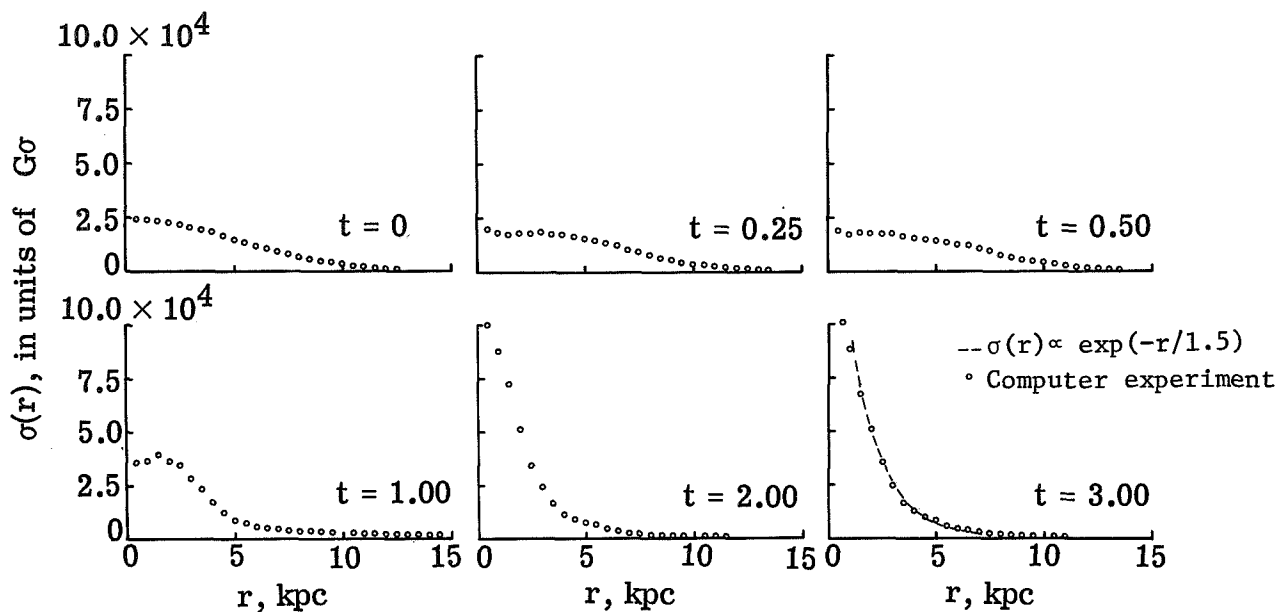
Figure 37.- Variation of mass density with radius for the Gaussian disk. (Time in rotational periods of the cold balanced Gaussian disk at r = 10 kpc.)
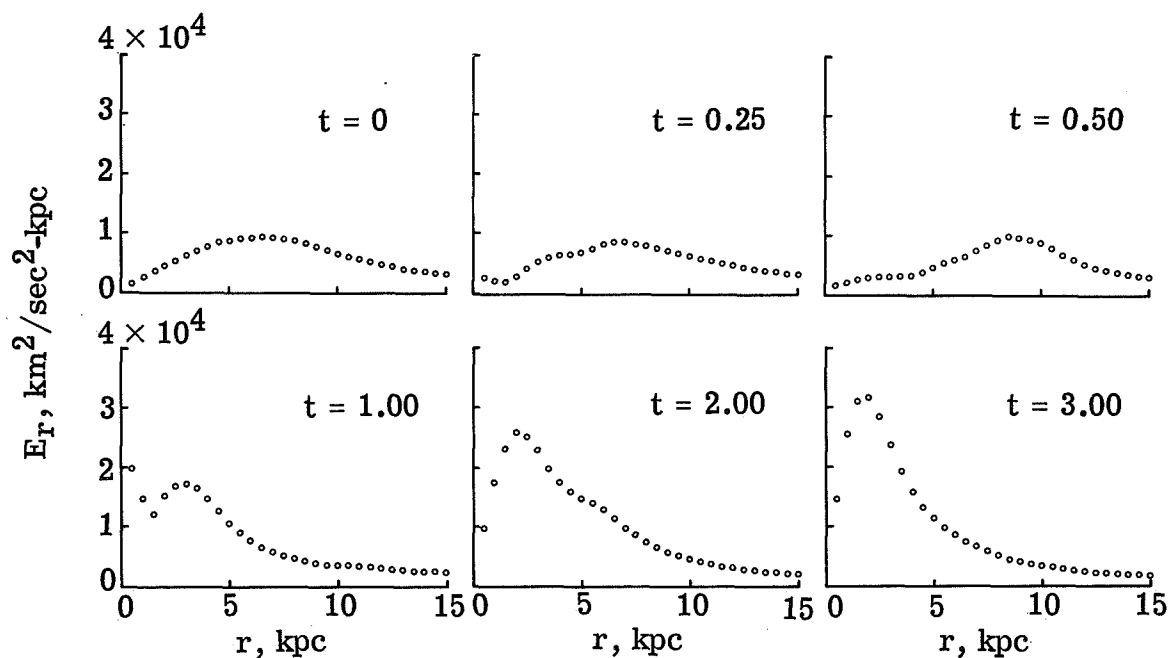
Figure 38.- Variation of the radial gravitational field for the Gaussian disk. (Time in rotational periods of the cold balanced Gaussian disk at r = 10 kpc.)
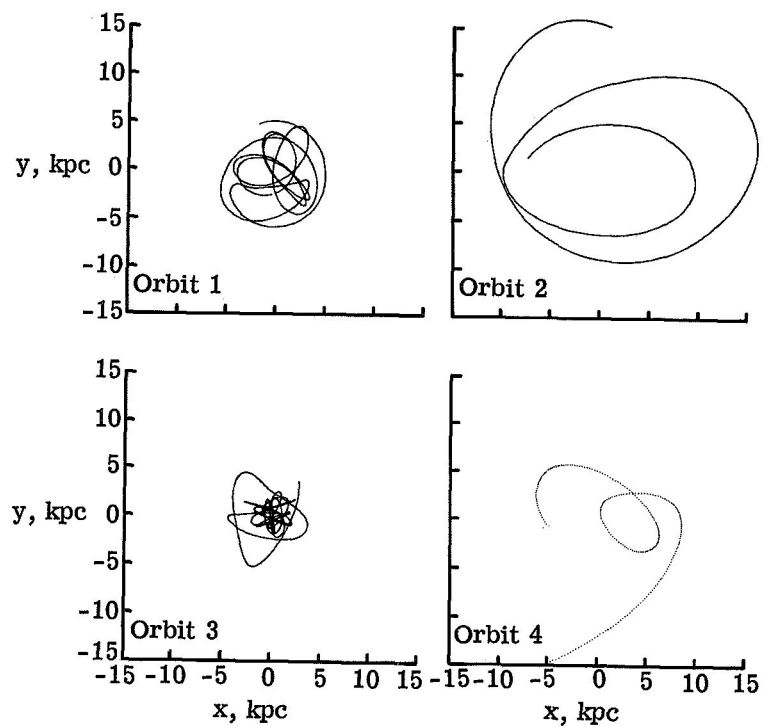
Figure 39.- Four individual star orbits from the disk in figure 32.
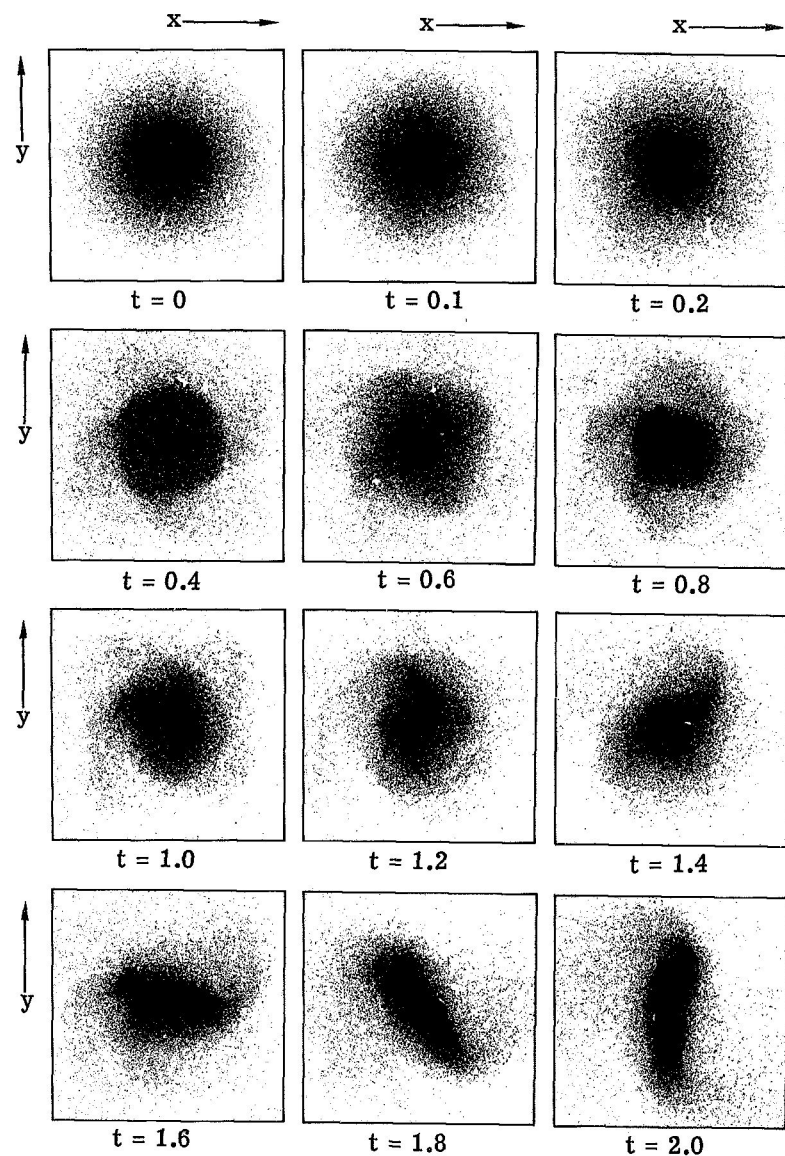
Figure 40.- Evolution of a disk with a Gaussian mass distribution and with an initial velocity dispersion 10 percent larger than $\sigma_{r,min}$. (Time in rotational periods of the cold balanced Gaussian disk at $r = 10$ kpc.)
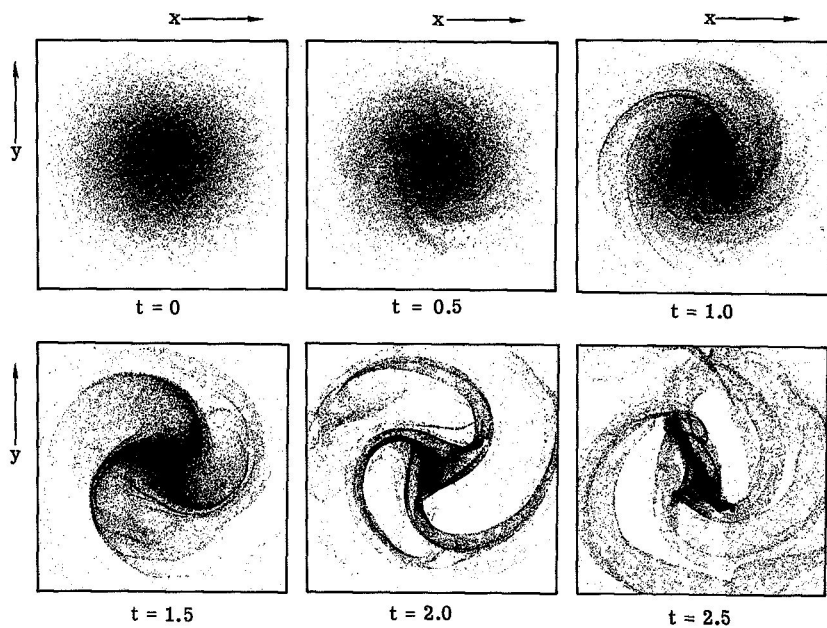
Figure 41.- Evolution of an initially balanced cold Gaussian disk consisting of mass rods each 2 kpc long. (Time in rotational periods of the cold balanced Gaussian disk at r = 10 kpc.)
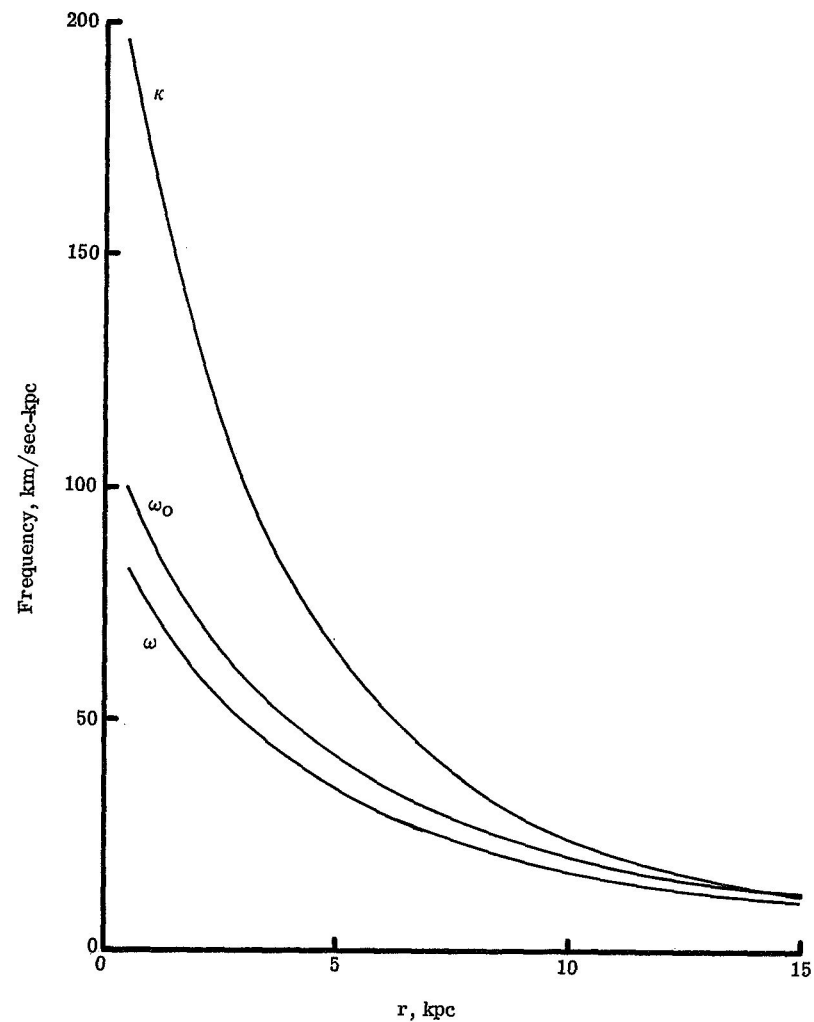
Figure 42.- Variation of ω_0, ω, and κ with radius for a disk of stars with an exponential mass distribution.
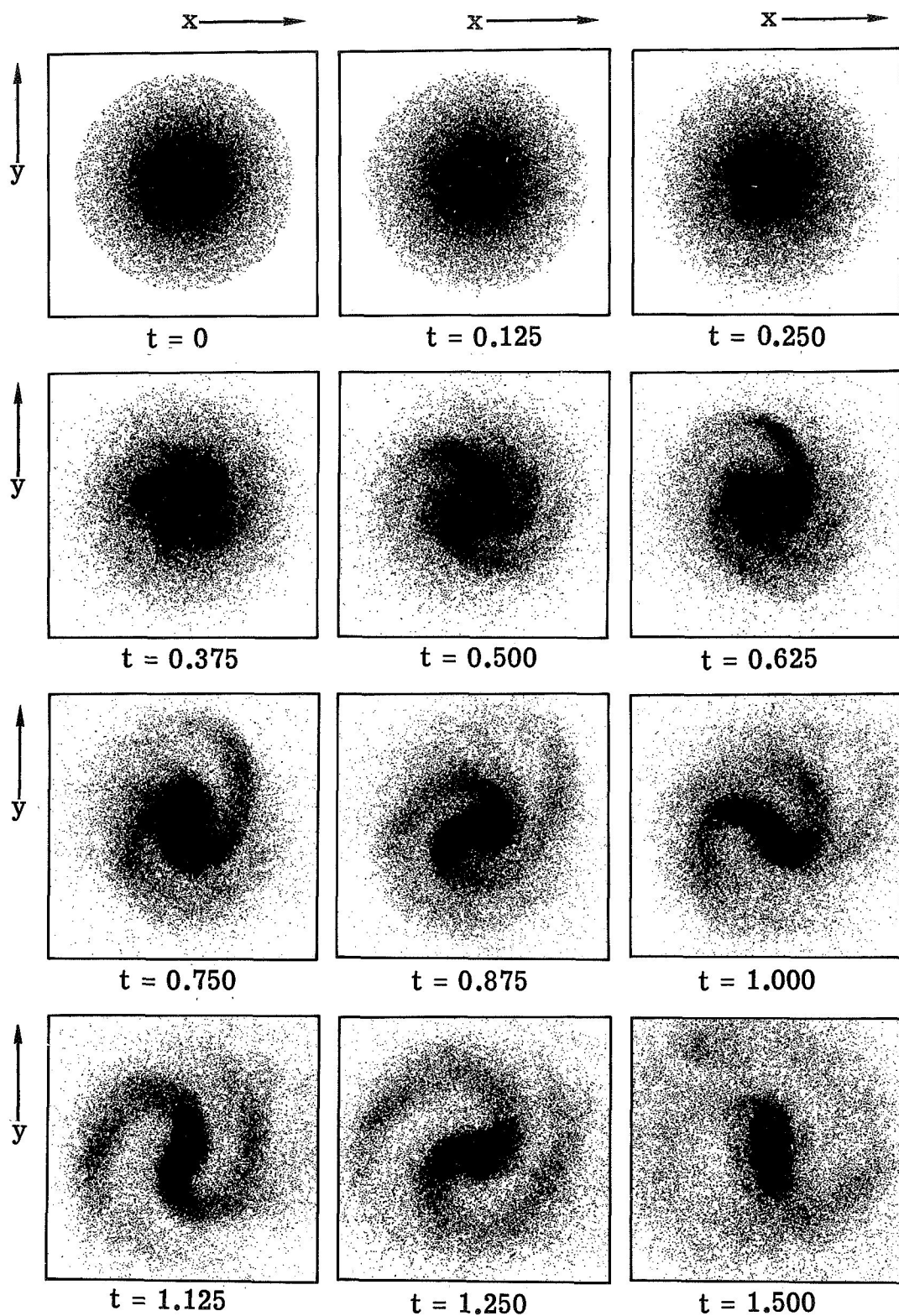
Figure 43.- Evolution of a disk of stars with an initial exponential mass distribution. (Time in rotational periods of the cold exponential disk at r = 10 kpc.)
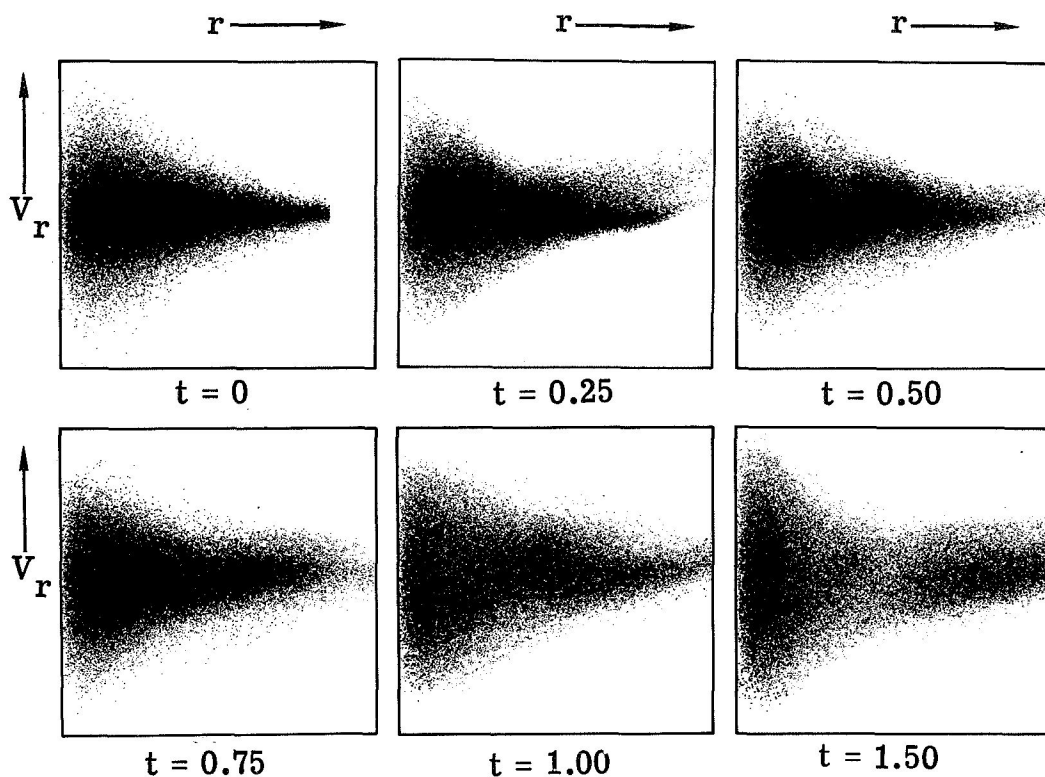
Figure 44.- Evolution of the radial star velocities for the exponential disk. (Time in rotational periods of the cold exponential disk at r = 10 kpc.)
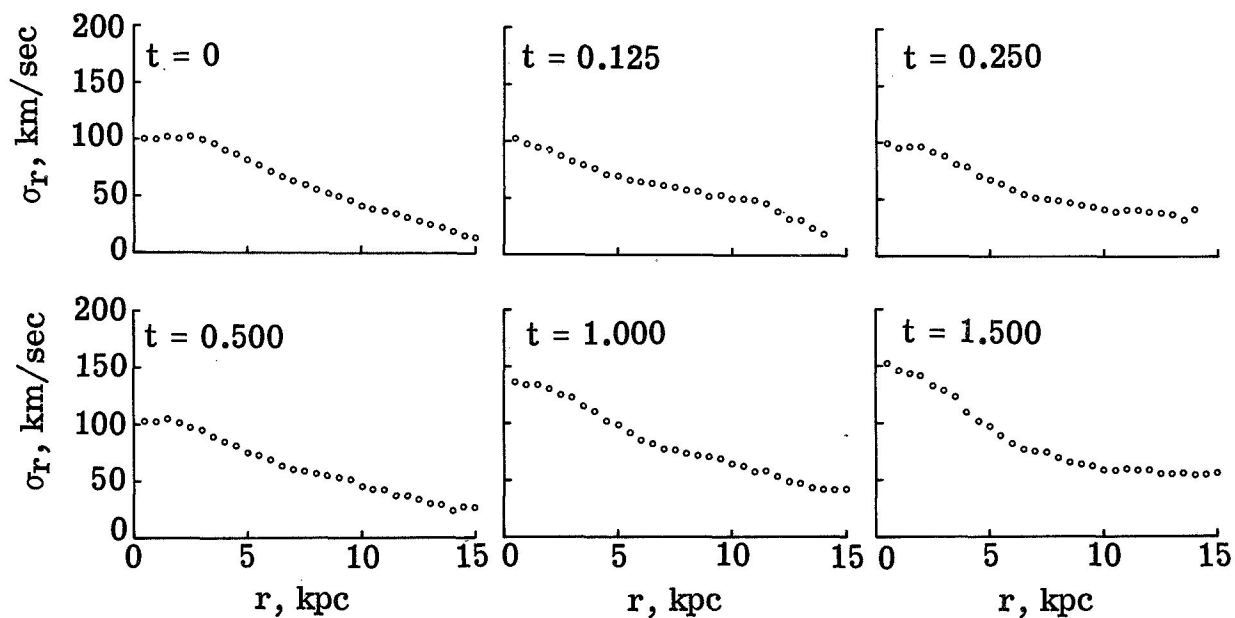
Figure 45.- Variation of radial velocity dispersion with radius for the exponential disk. (Time in rotational periods of the cold exponential disk at r = 10 kpc.)

81
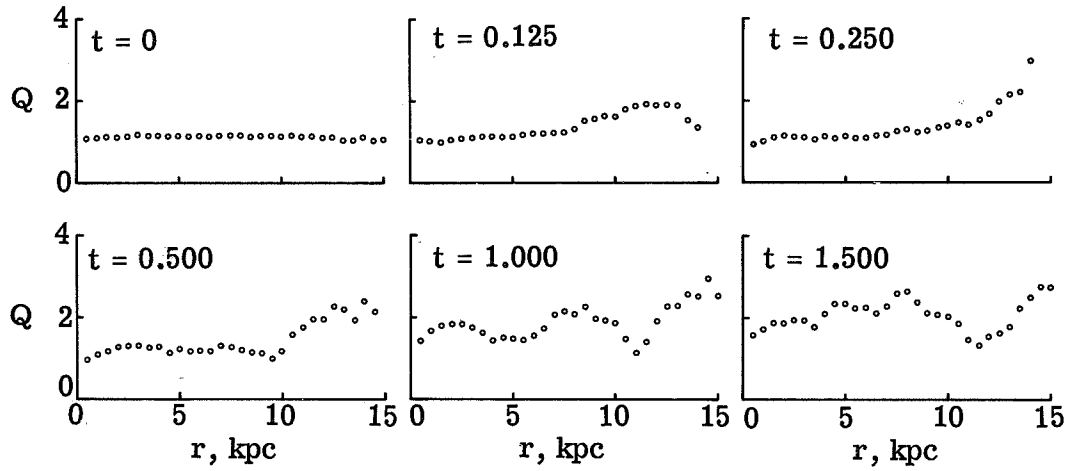
Figure 46.- Variation of $Q = \sigma_r/\sigma_{r,min}$ with radius for the exponential disk. (Time in rotational periods of the cold exponential disk at $r = 10$ kpc.)
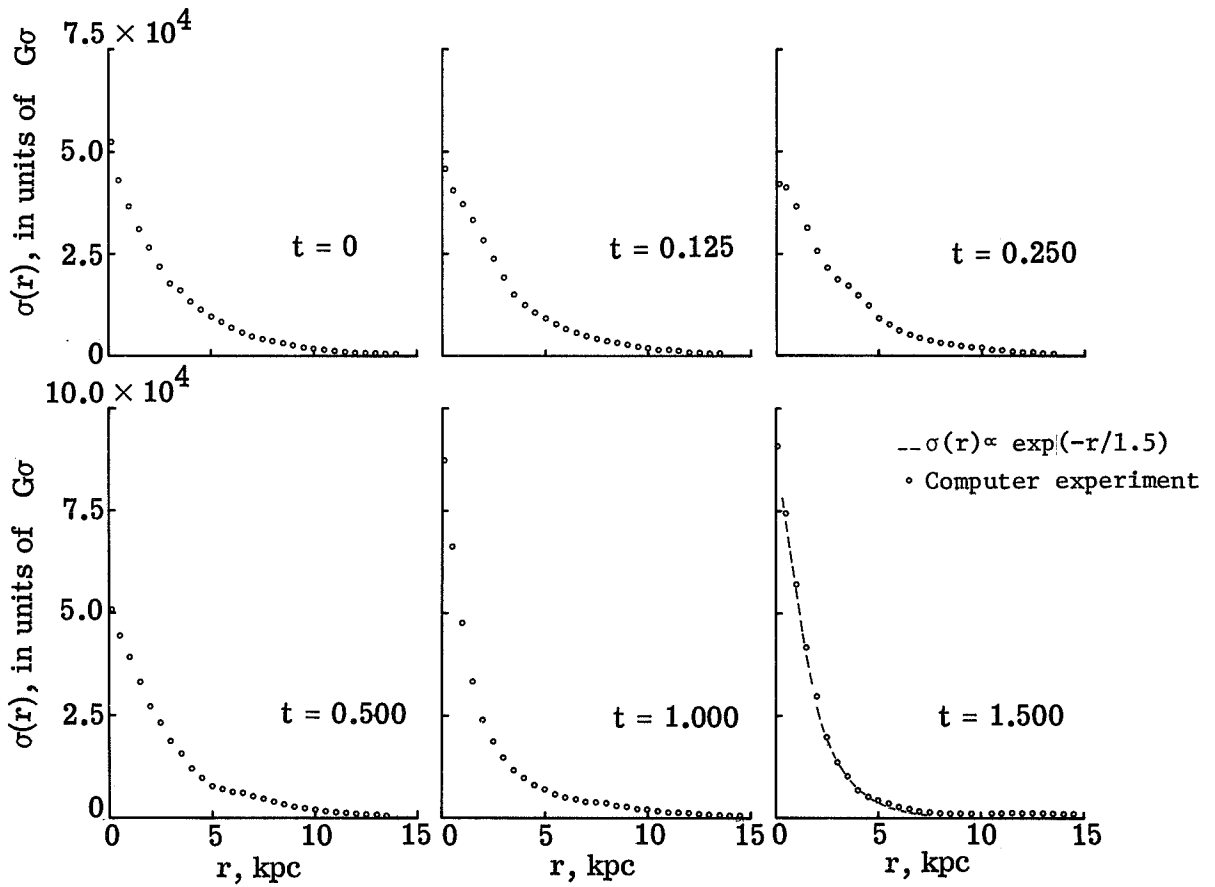
Figure 47.- Variation of mass density with radius for the exponential disk. (Time in rotational periods of the cold exponential disk at $r = 10$ kpc.)
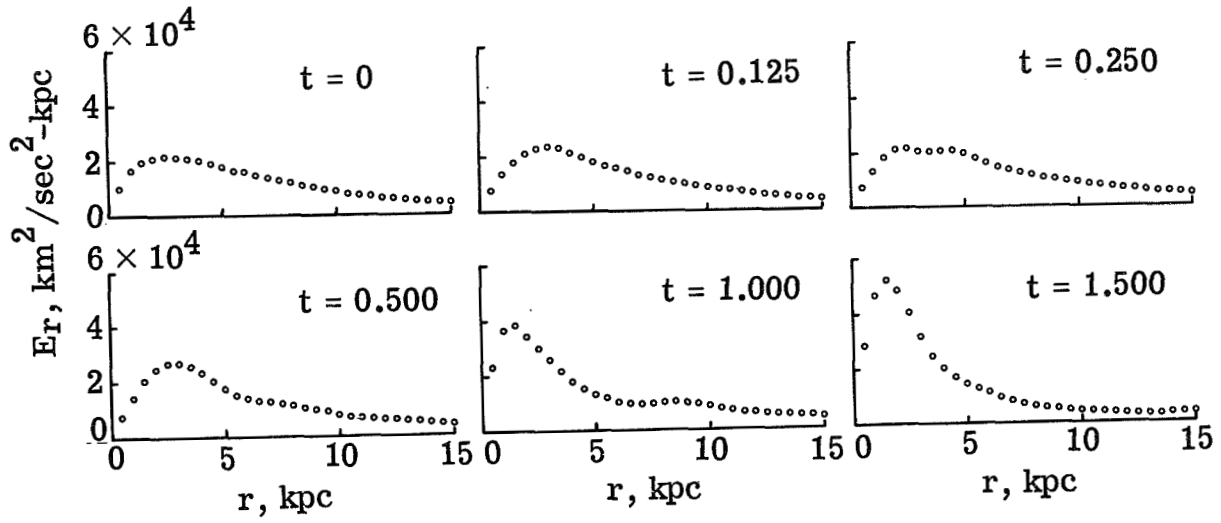
Figure 48.- Variation of the radial component of the gravitational field with radius for the exponential disk. (Time in rotational periods of the cold exponential disk at r = 10 kpc.)
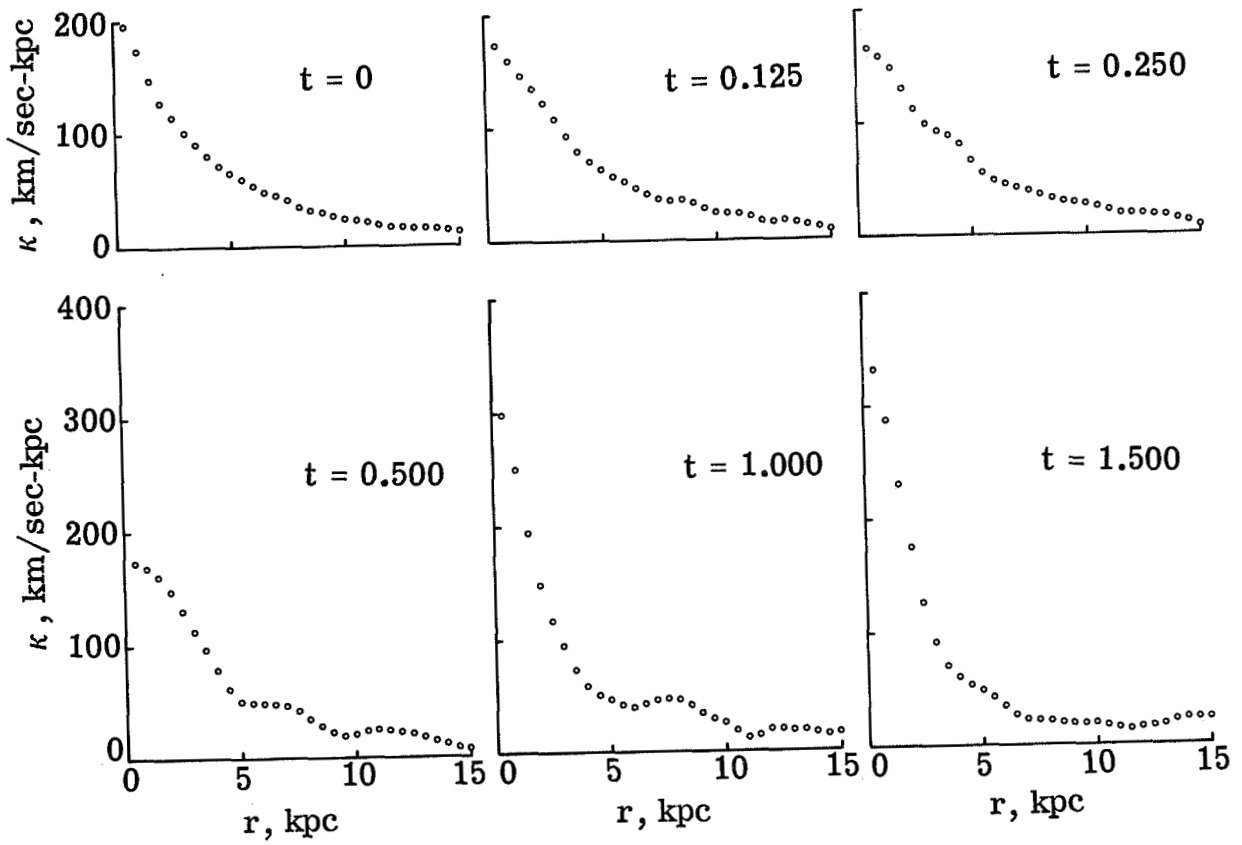
Figure 49.- Variation of the epicyclic frequency with radius for the exponential disk. (Time in rotational periods of the cold exponential disk at r = 10 kpc.)
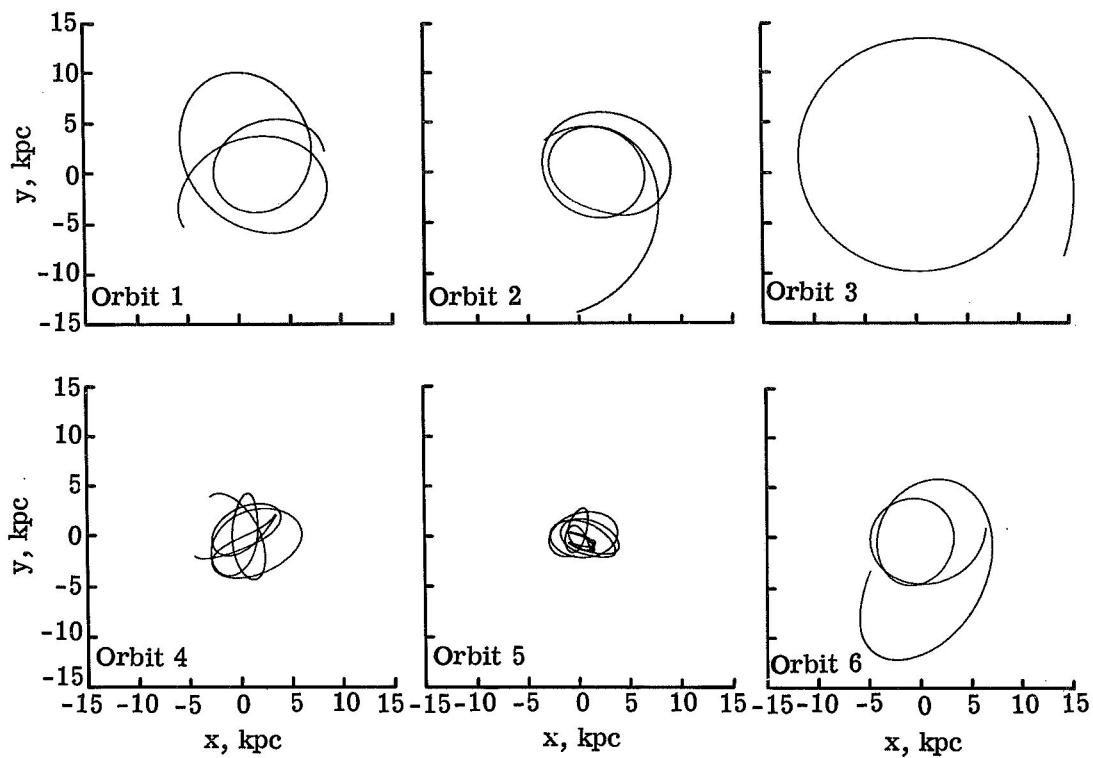
Figure 50.- Six individual star orbits from the disk in figure 43.
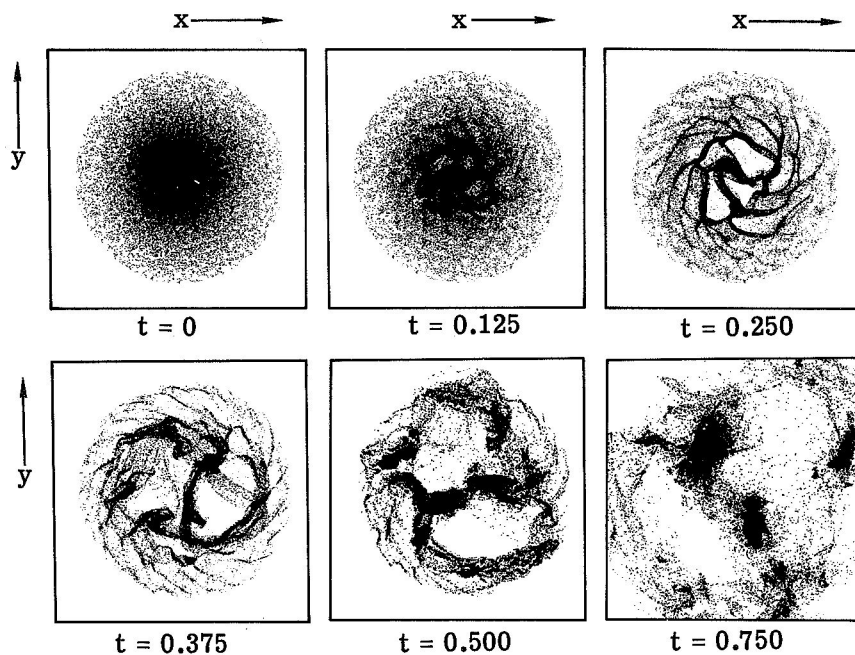
Figure 51.- Evolution of a cold disk of stars with an initial exponential mass distribution. (Time in rotational periods of the cold exponential disk at r = 10 kpc.)
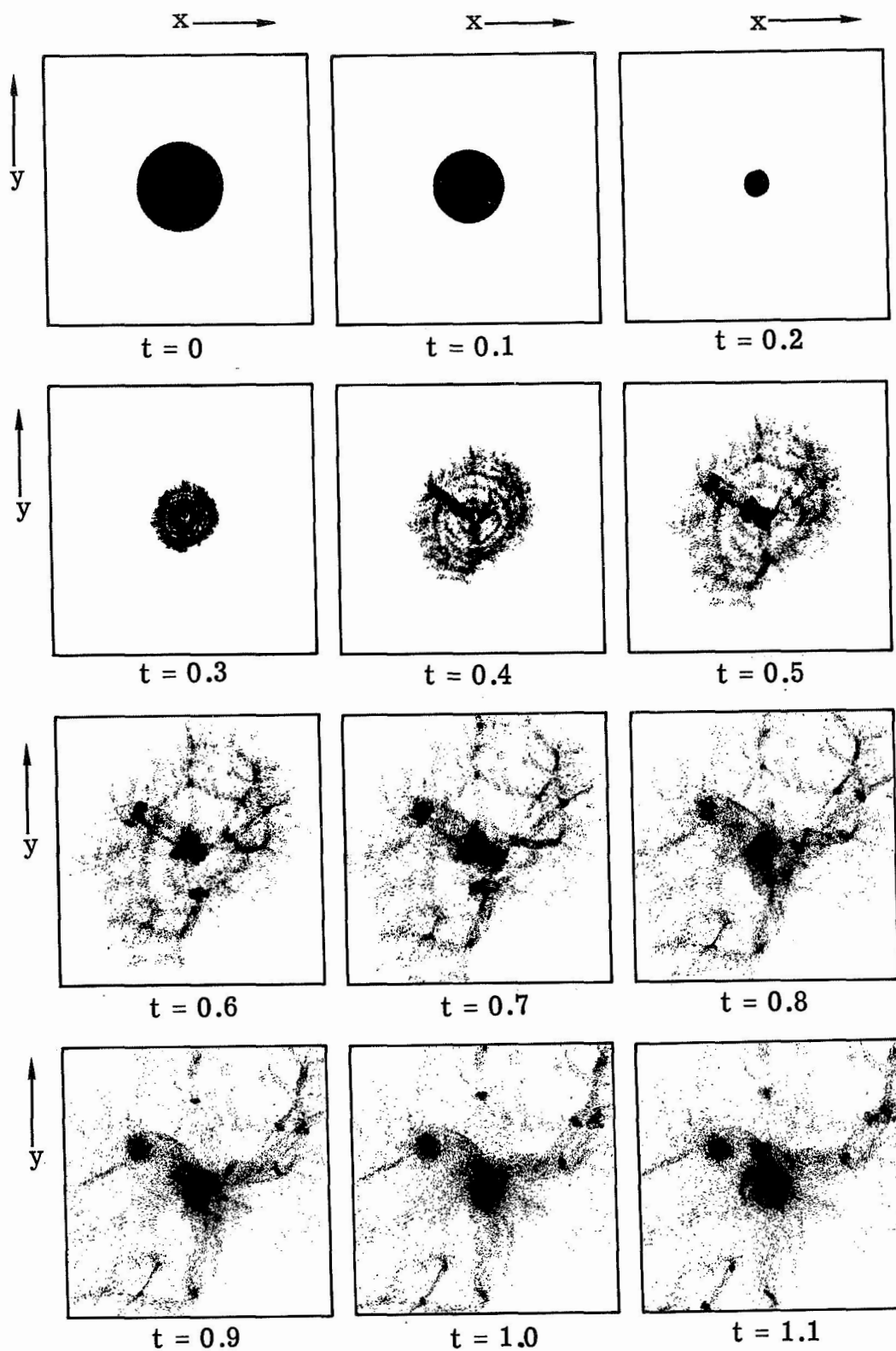
Figure 52.- Collapse and further evolution of an initially nonrotating cold disk of stars. (Time in rotational periods given by eq. (52).)
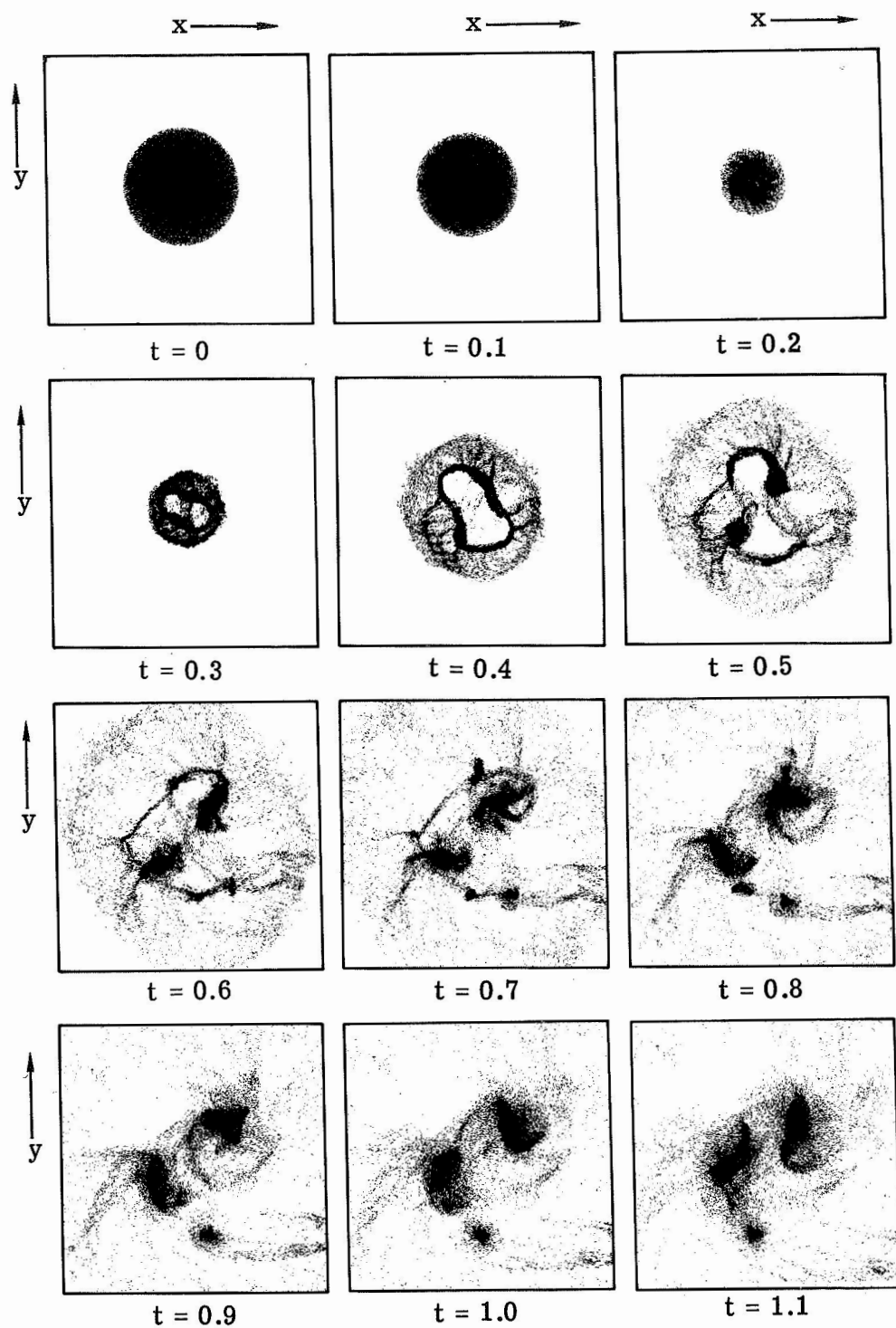
Figure 53.- Evolution of a cold disk of stars with an initial rotation equal to one-half that required to balance the disk. (Time in rotational periods given by eq. (52).)
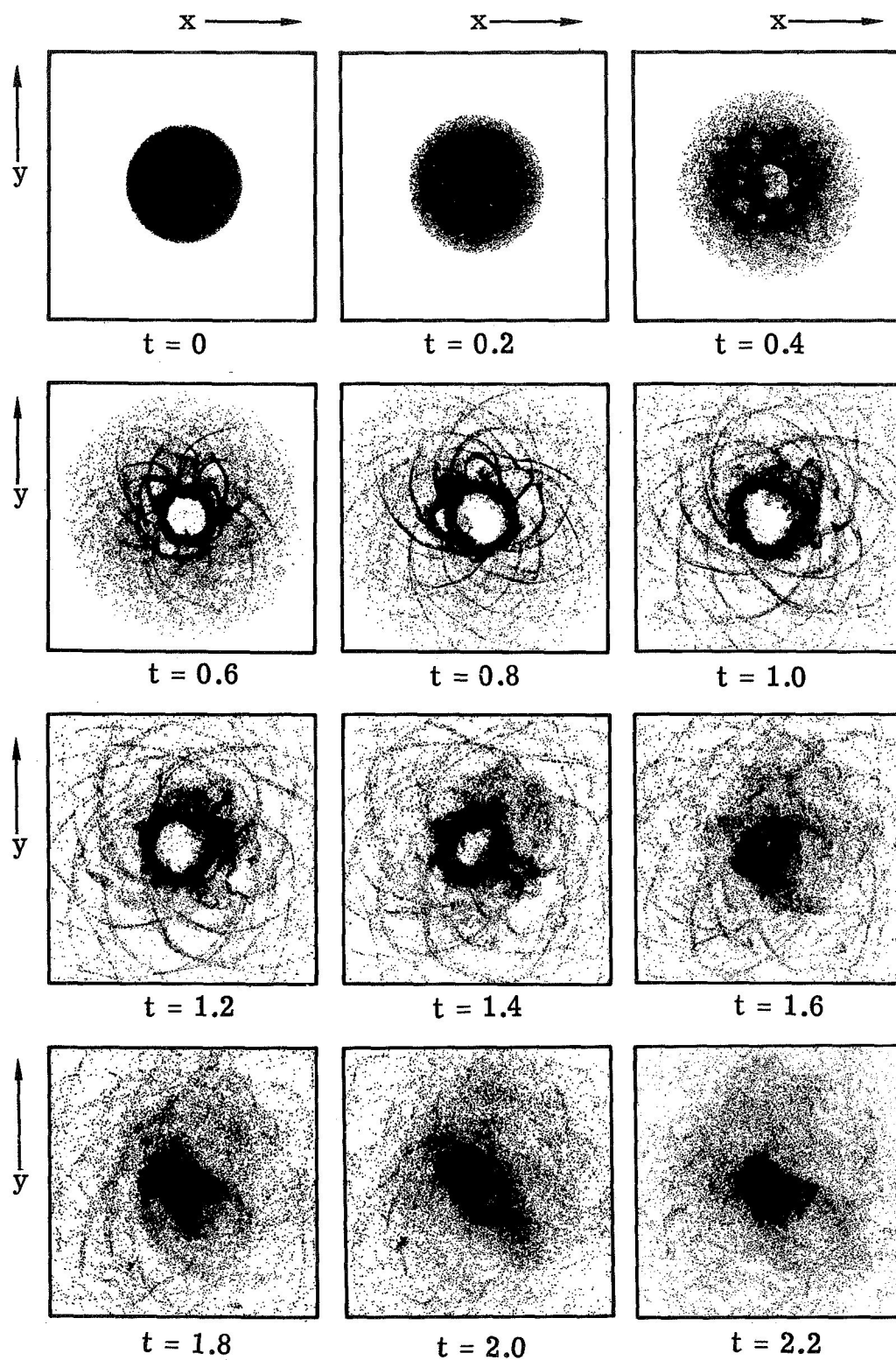
Figure 54.- Evolution of an initially balanced disk of stars with half of the stars rotating clockwise and remaining half counterclockwise. (Time in rotational periods given by eq. (52).)
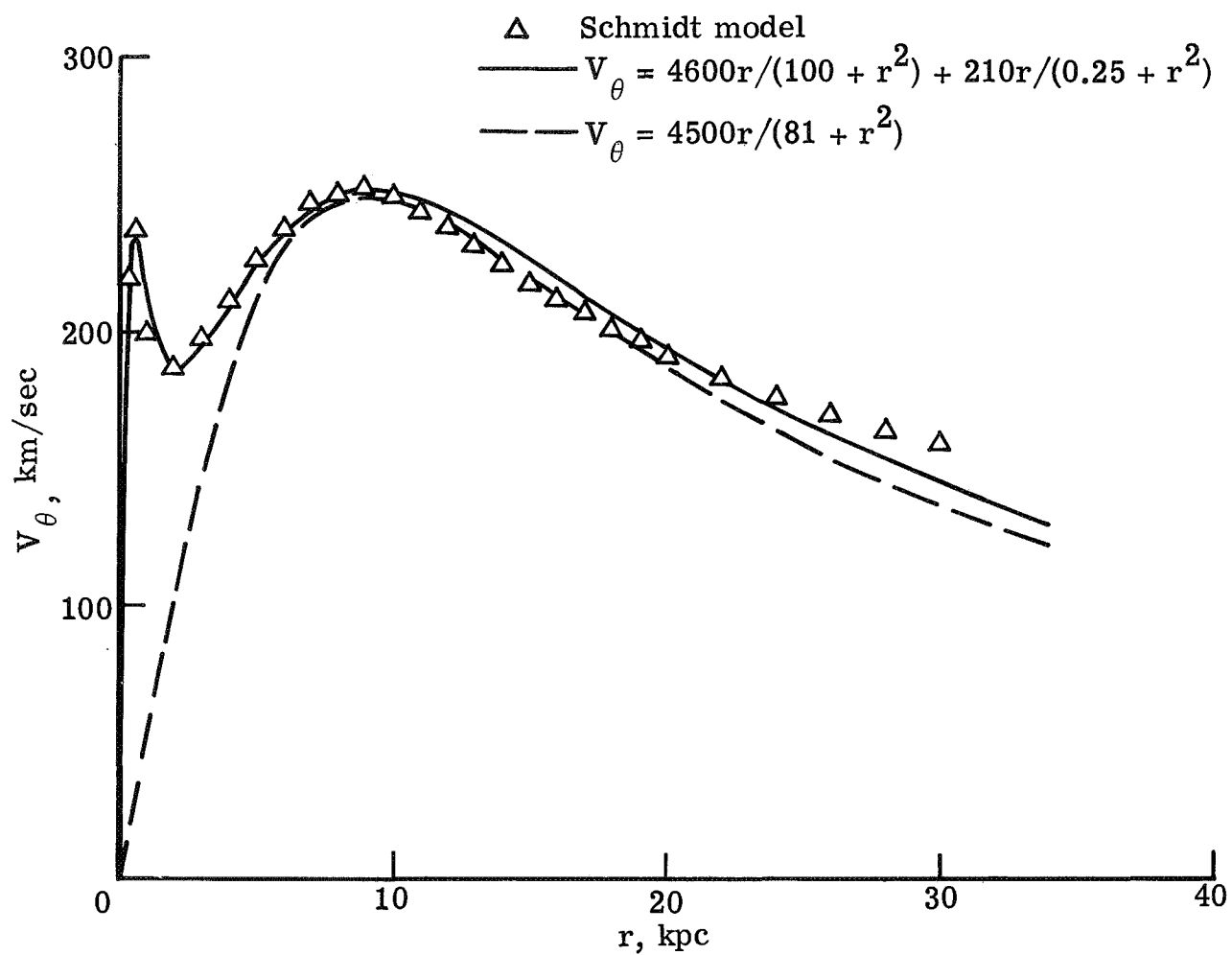
Figure 55.- Comparison of two rotation curves with the Schmidt model of the Galaxy. A fixed gravitational potential corresponding to the two rotation curves is used to study the evolution of spiral structure.
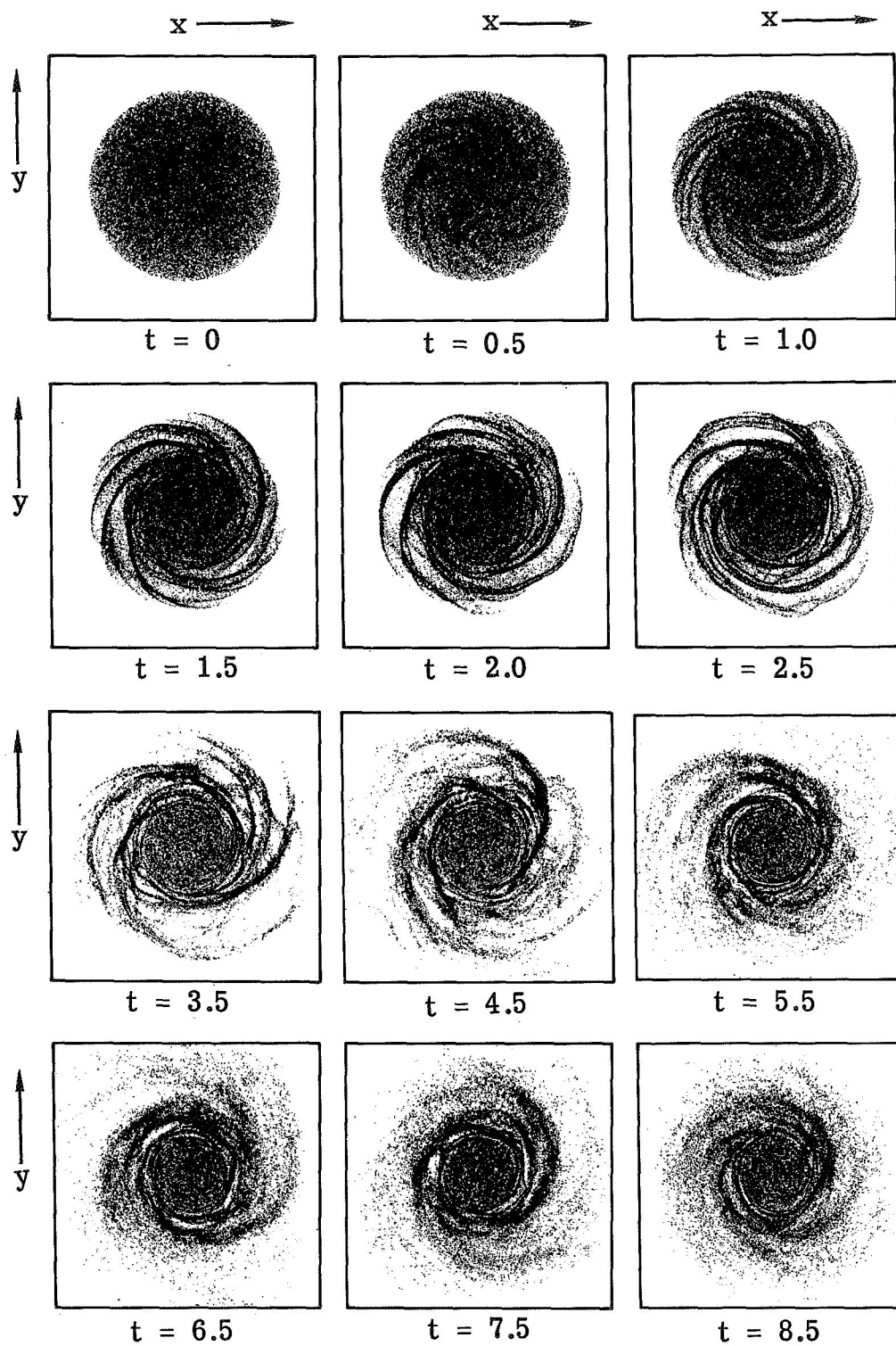
Figure 56.- Evolution of a 50000-star system under influence of a fixed central force corresponding to rotation curve given by equation (64). The disk stars contain 10 percent of total mass of system. (Time in rotational periods of the initial balanced disk at r = 10 kpc.)
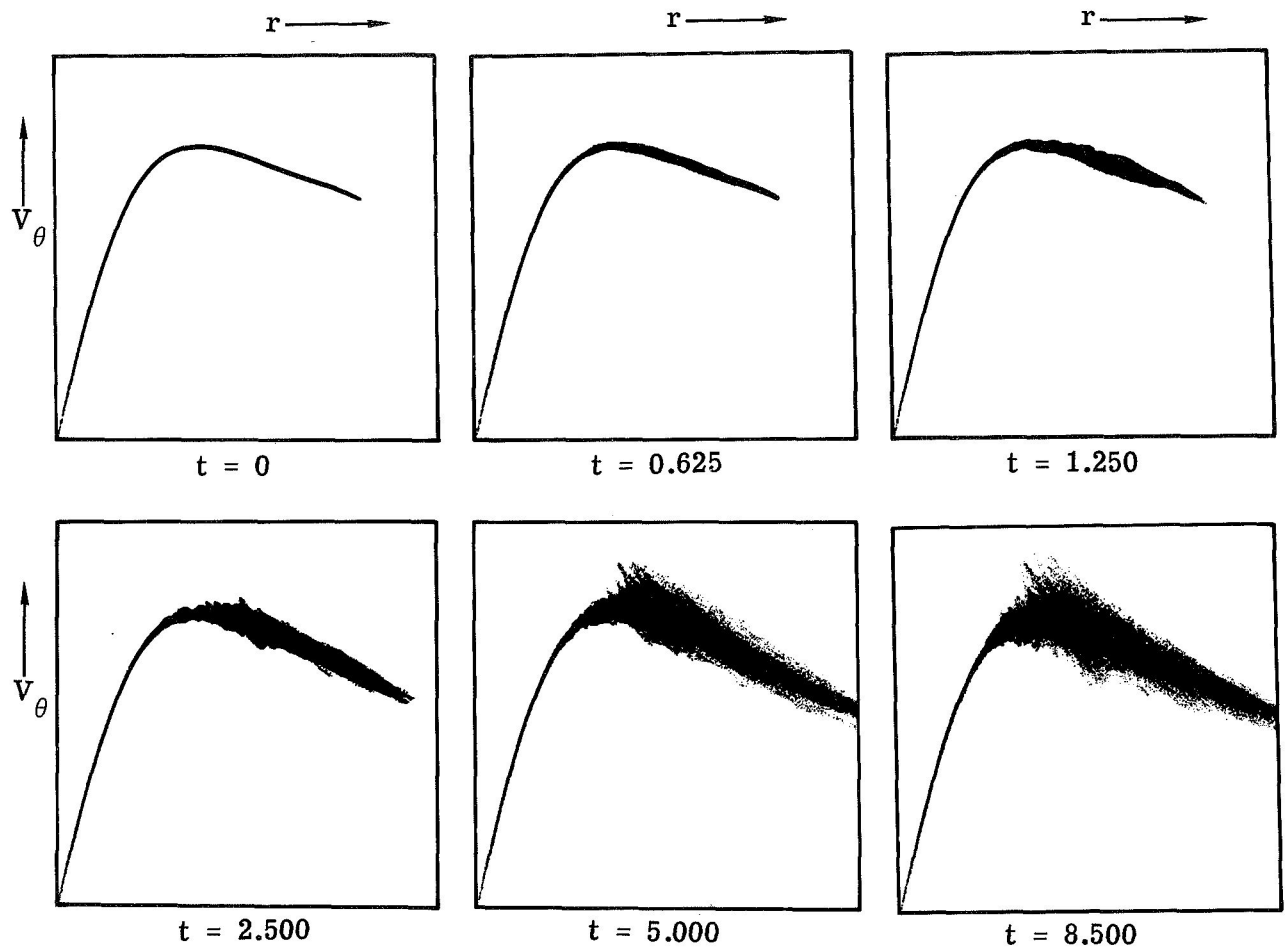
Figure 57.- Evolution of the circular velocities of the stars for the galaxy in figure 56. (Time in rotational periods of the initial balanced disk at r = 10 kpc.)
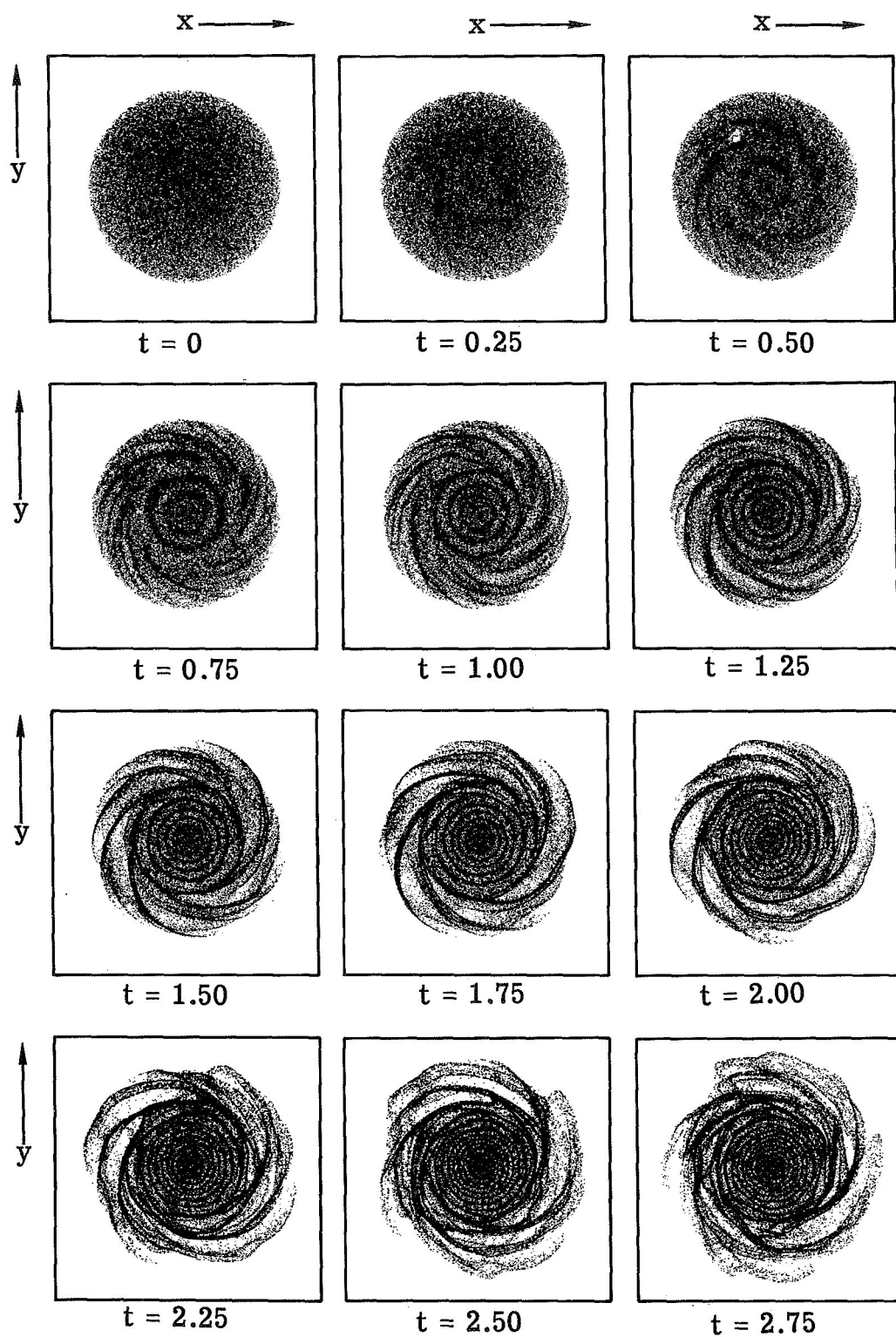
Figure 58.- Evolution of the same stellar system displayed in figure 56 except that the initial star positions have received an initial perturbation which is proportional to the distance of the star from the center of the disk. (Time in rotational periods of the initial balanced disk at r = 10 kpc.)
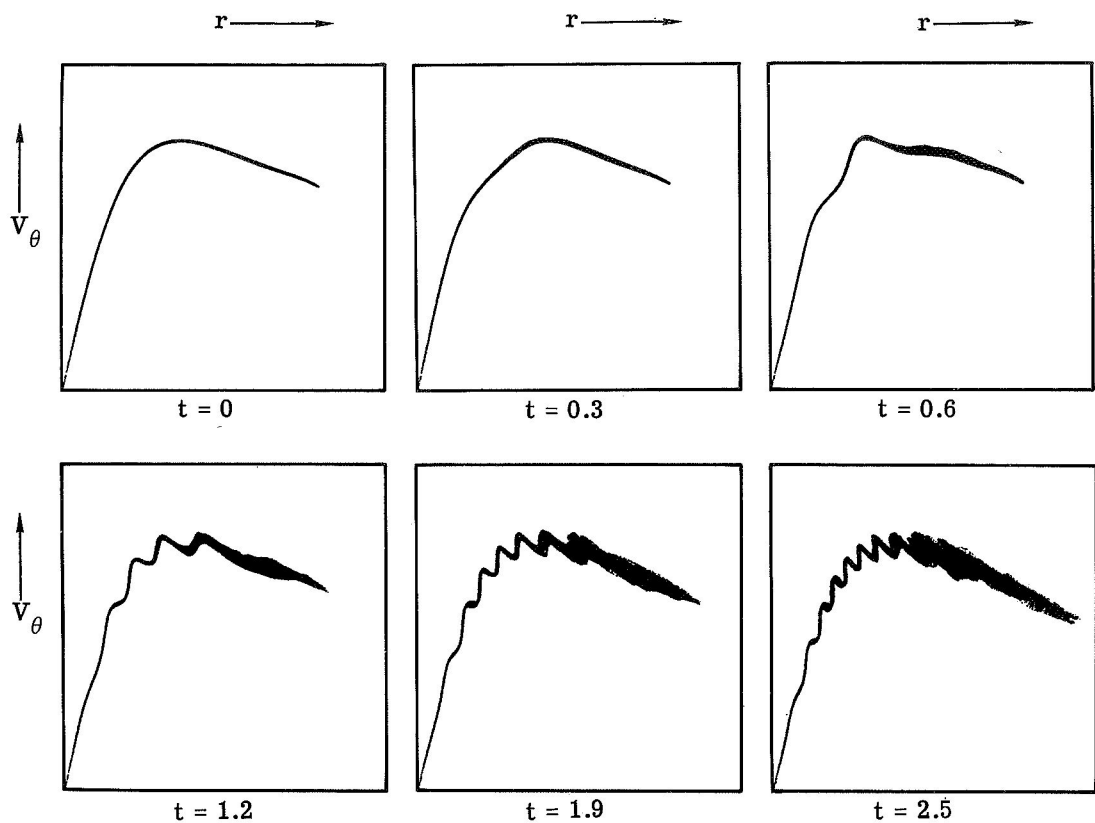
Figure 59.- Evolution of the circular velocities of the stars for the stellar system in figure 58. (Time in rotational periods of the initial balanced disk at r = 10 kpc.)
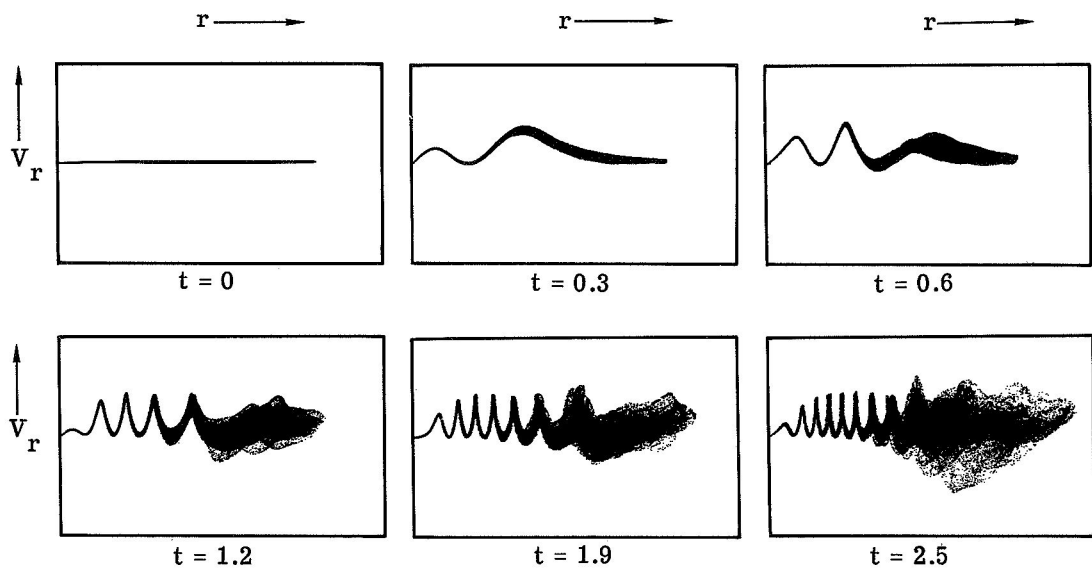
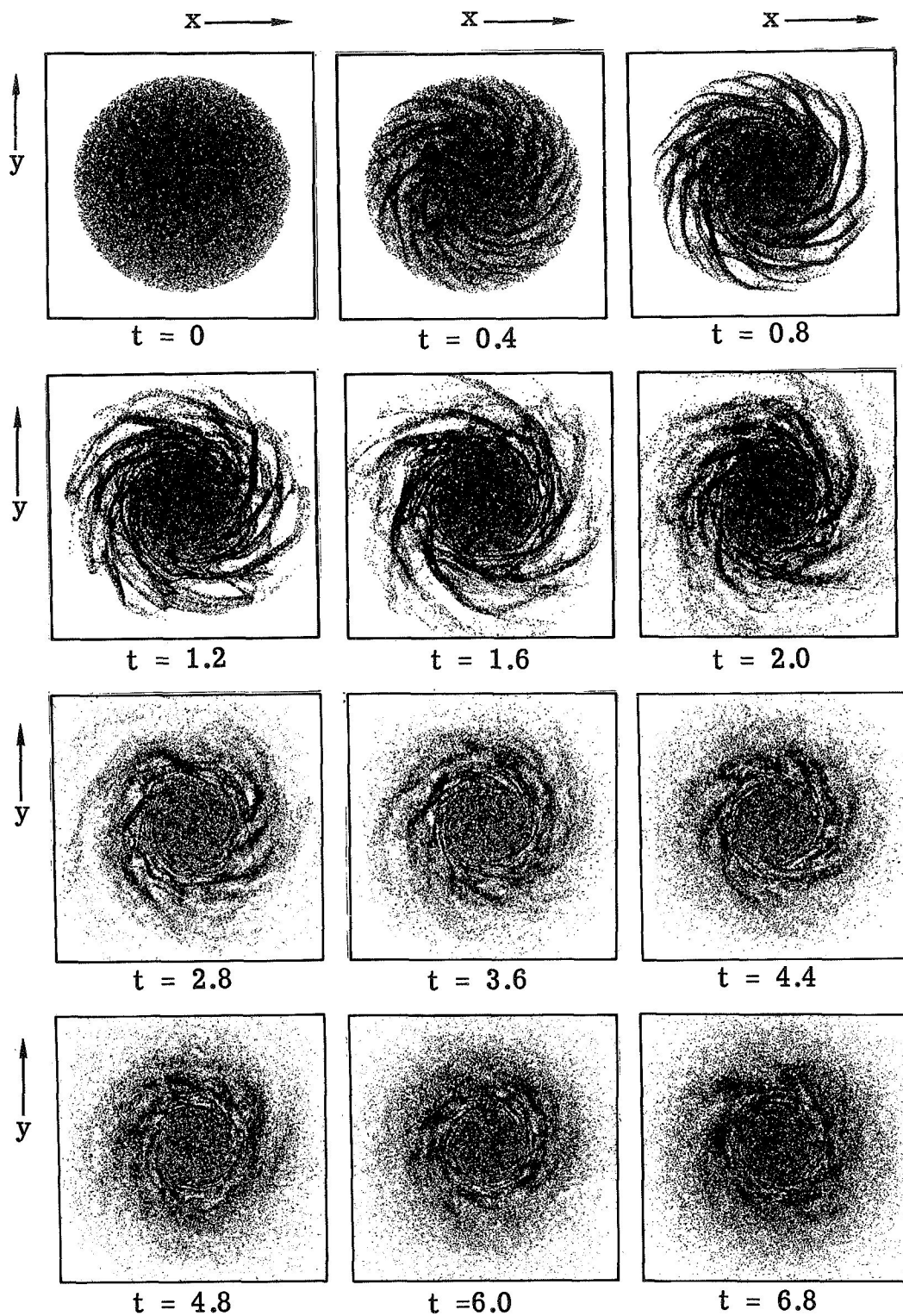Figure 60.- Evolution of the radial velocities of the stars for the stellar system in figure 58. (Time in rotational periods of the initial balanced disk at r = 10 kpc.)
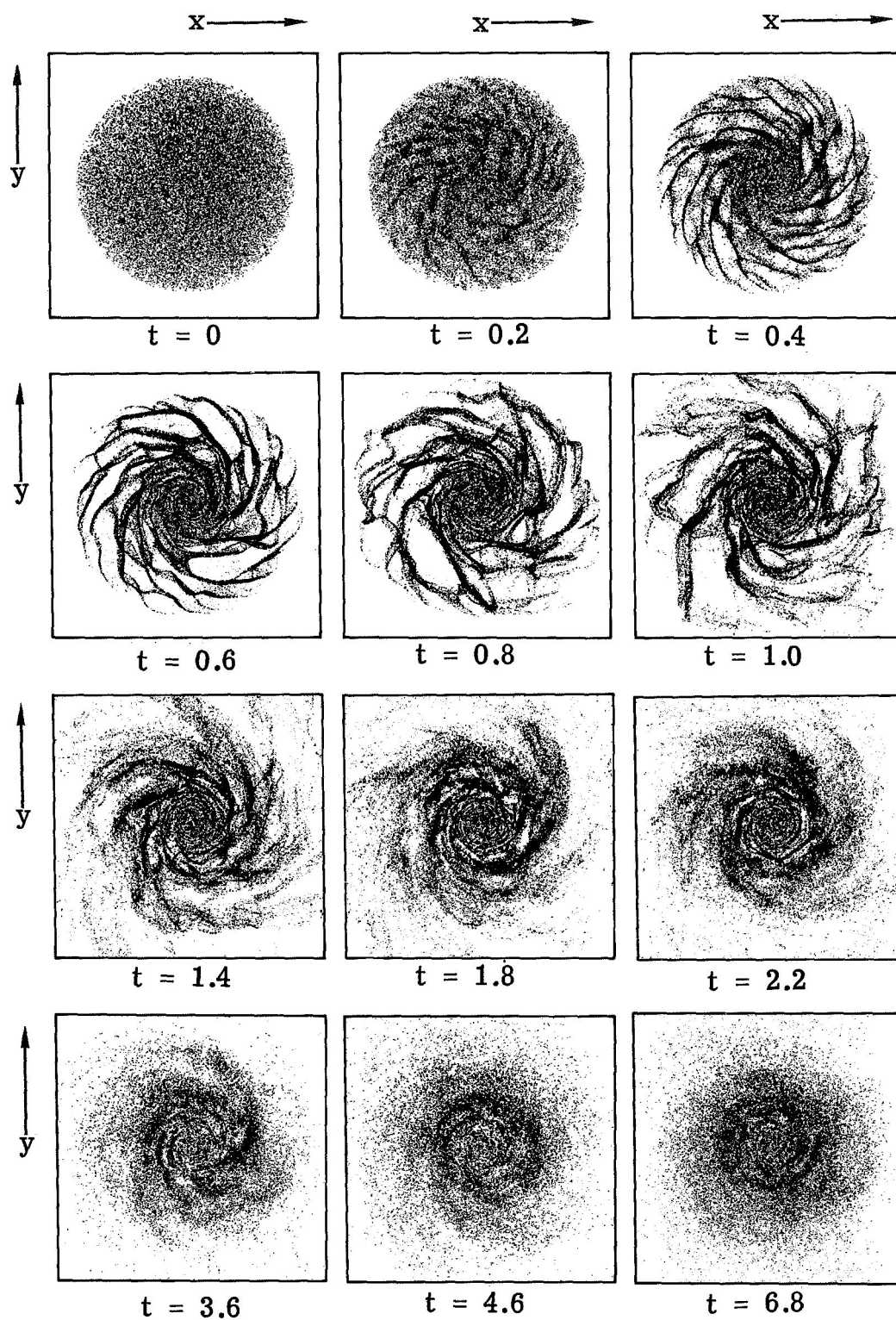
Figure 61.- Evolution of a disk of stars under the influence of a fixed central force corresponding to the rotation curve given by equation (65). The 50000 disk stars contain 20 percent of the total mass of the system. (Time in rotational periods of the initial balanced disk at r = 10 kpc.)
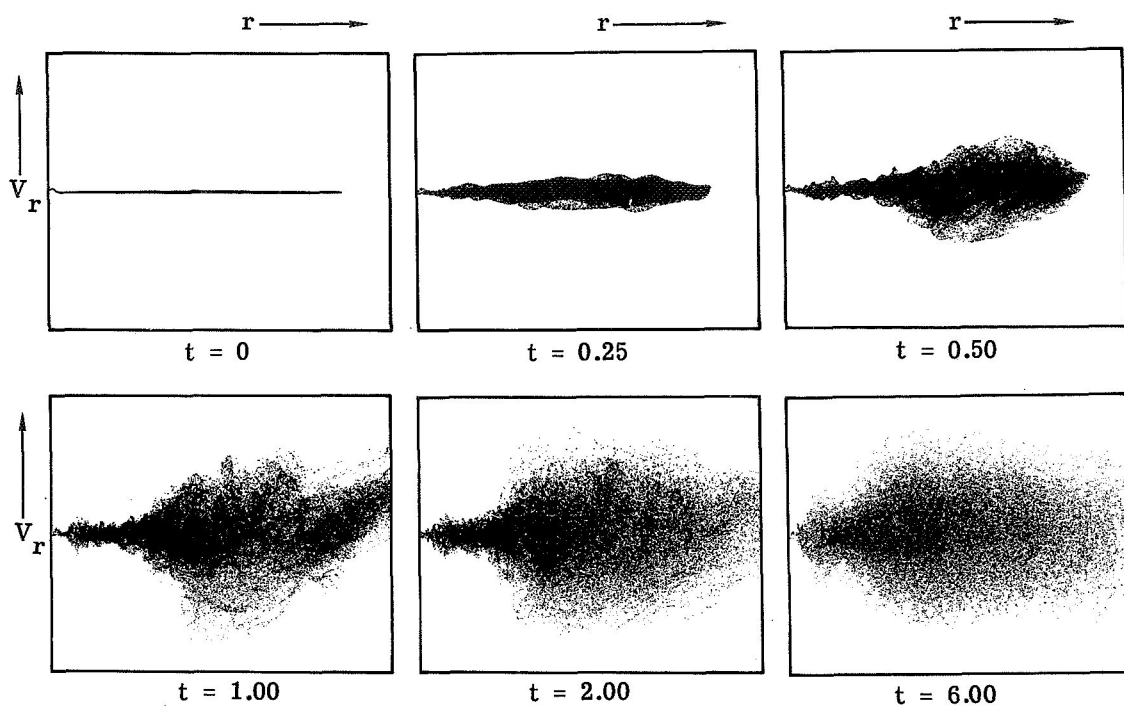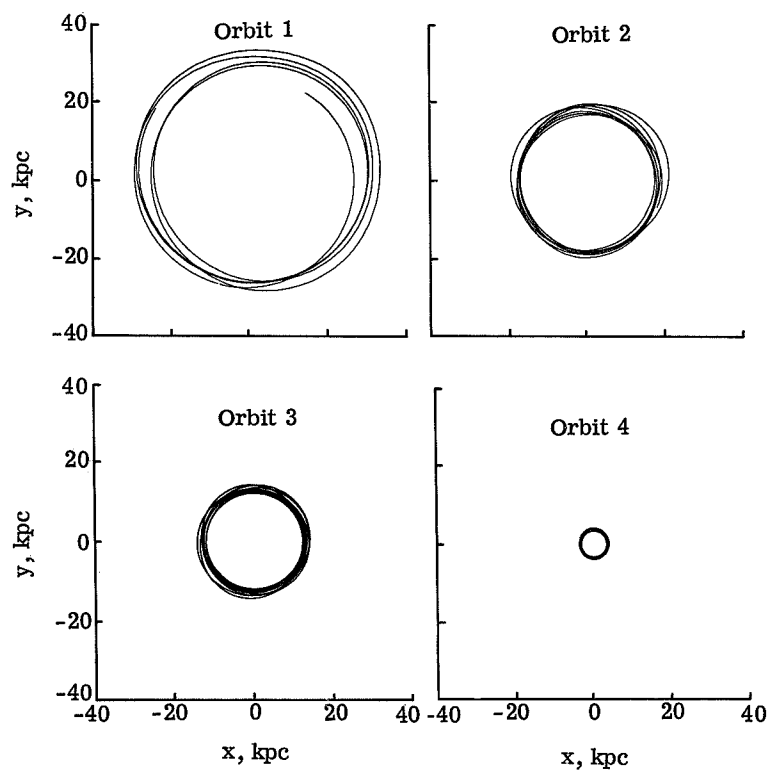
Figure 62.- Evolution of the radial velocities of the stars for the galaxy in figure 61. (Time in rotational periods of the initial balanced disk at r = 10 kpc.)
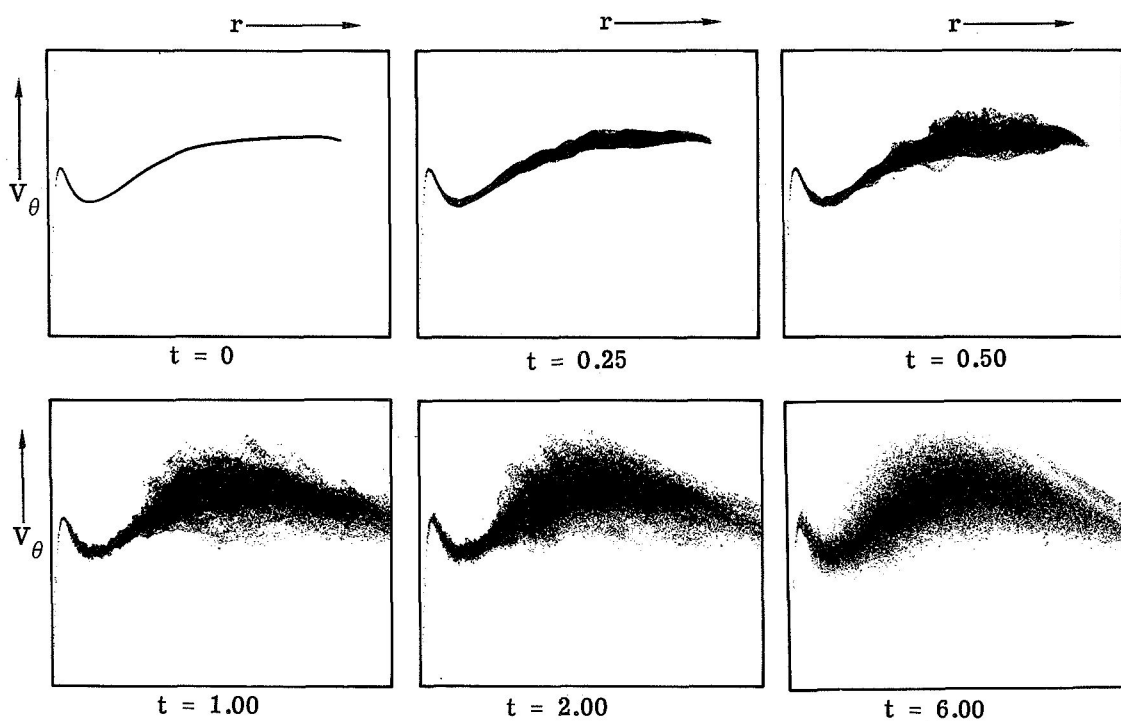
Figure 63.- Evolution of the circular velocity of the stars for the galaxy in figure 61. (Time in rotational periods of the initially balanced disk at r = 10 kpc.)

94
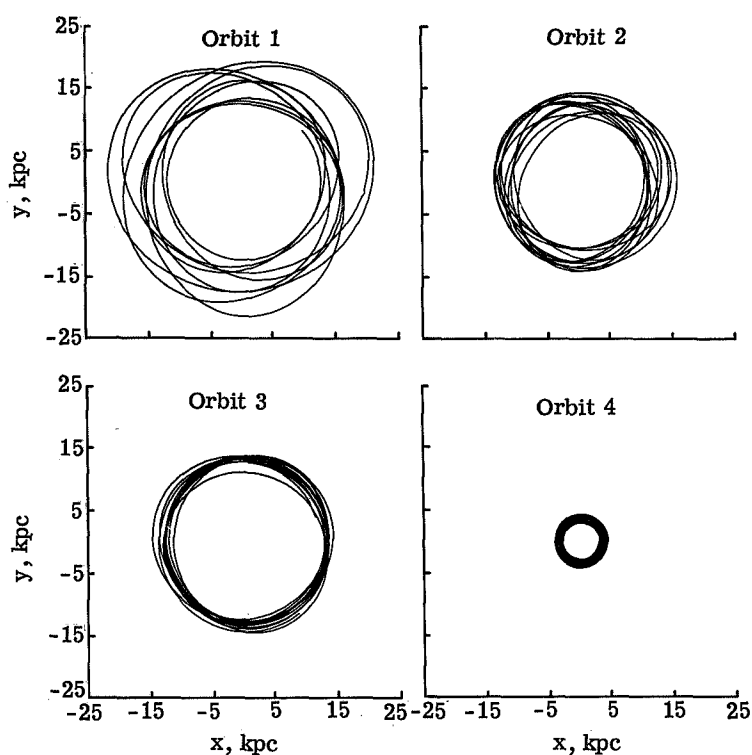
Figure 64.- Four individual star orbits from the galaxy in figure 61.
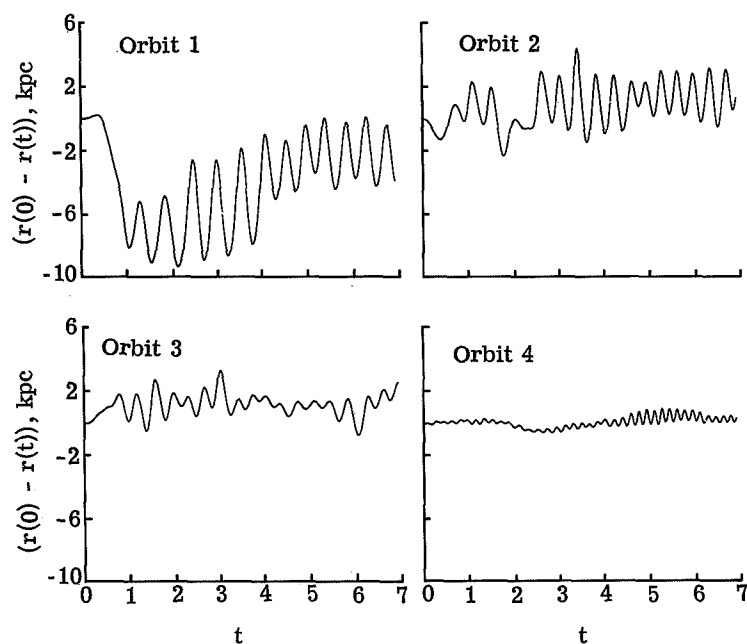
Figure 65.- Deviations of the star orbits in figure 64 from circular orbits displaying the epicyclic motion. (Time in rotational periods of the initial balanced disk at r = 10 kpc.)
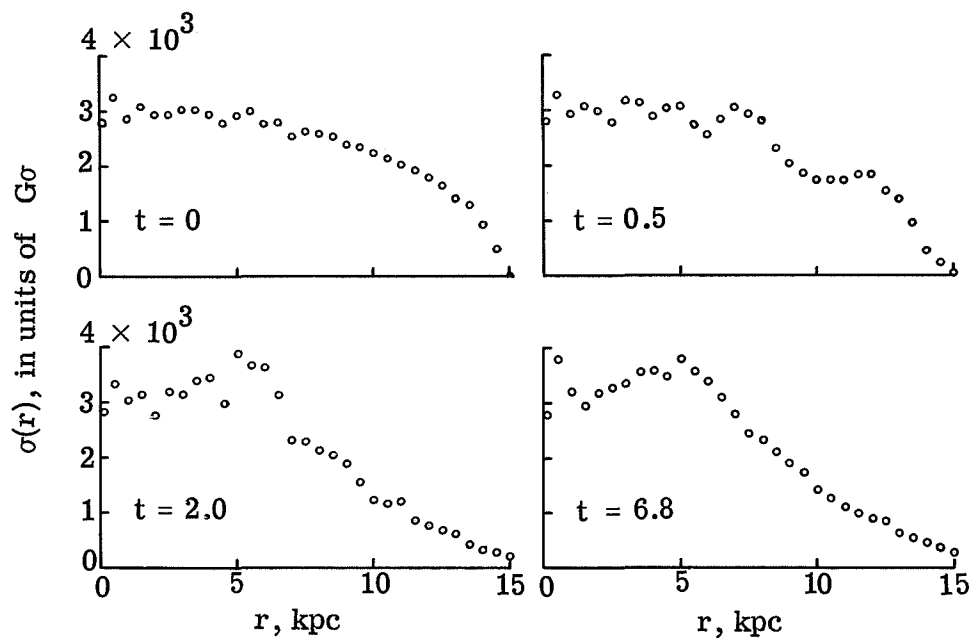
Figure 66.- Variation of the azimuthally averaged mass density of the disk stars with radius for the galaxy in figure 61. (Time in rotational periods of the initial balanced disk at r = 10 kpc.)
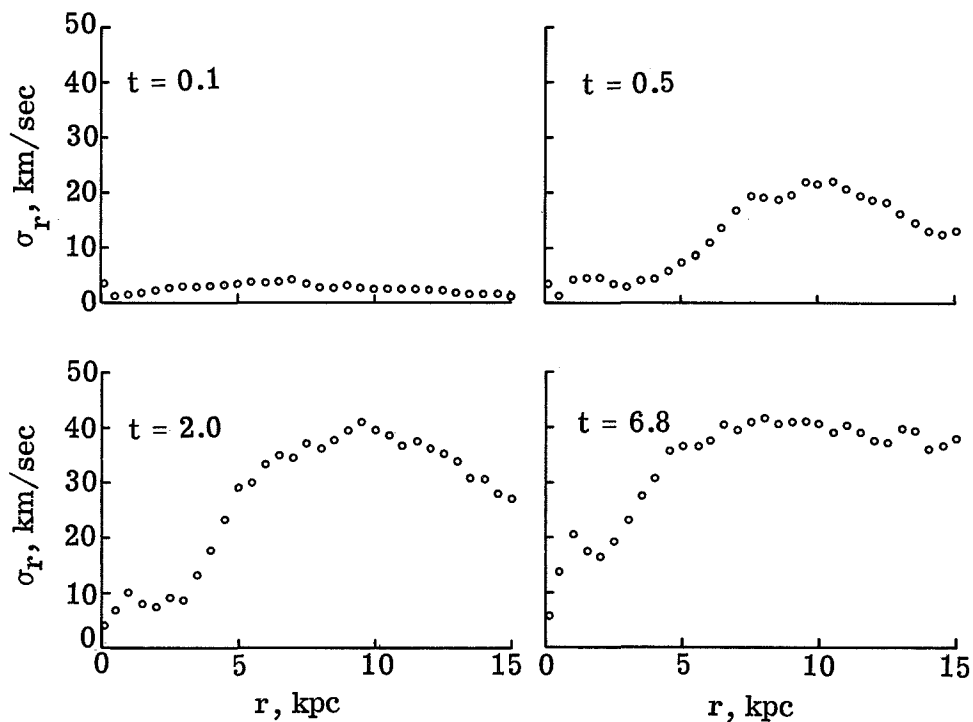
Figure 67.- Variation of the radial velocity dispersion with radius for the galaxy in figure 61. (Time in rotational periods of the initial balanced disk at r = 10 kpc.)
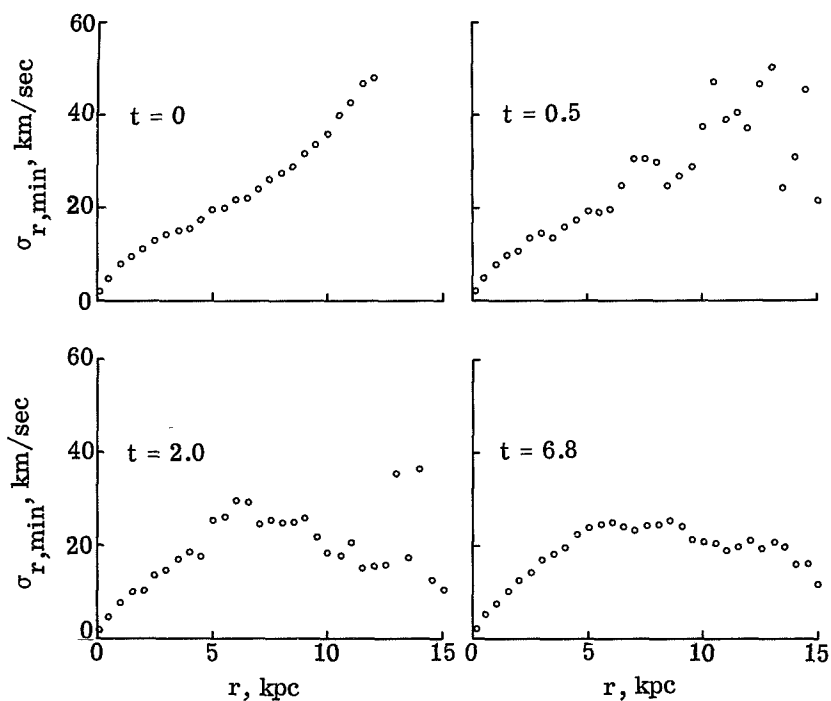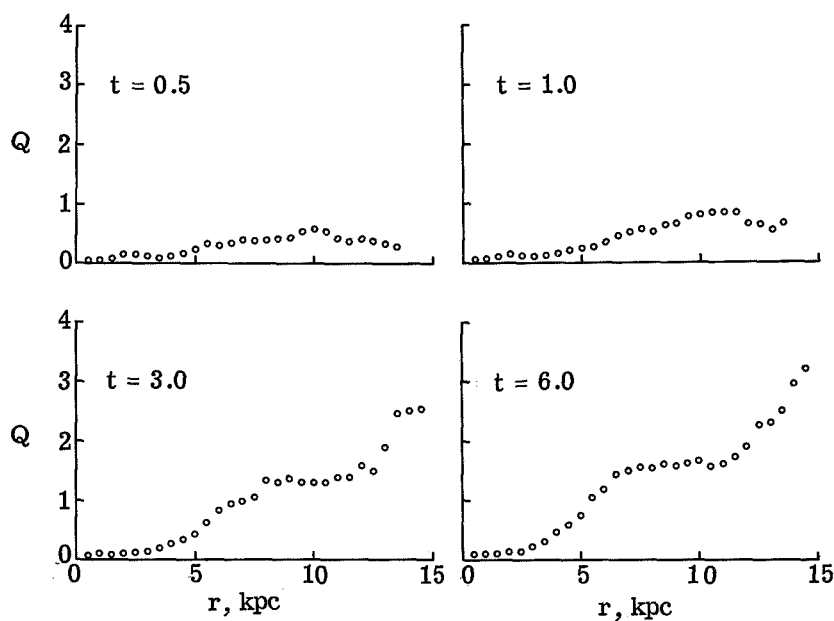
Figure 68.- Variation of $\sigma_{r,min}$ with radius for the galaxy in figure 61. (Time in rotational periods of the initial balanced disk at r = 10 kpc.)
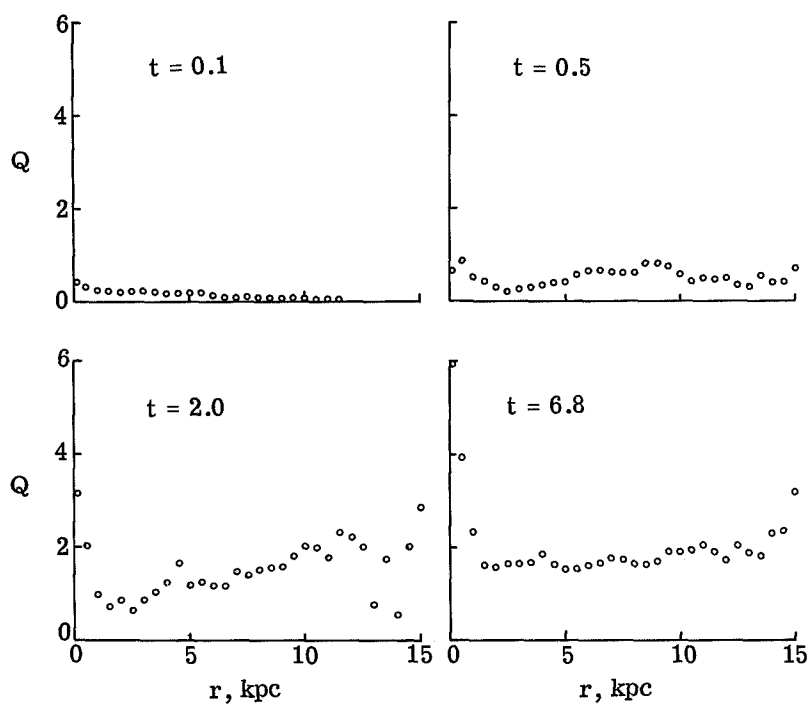

Figure 69.- Variation of $Q = \sigma_r/\sigma_{r,min}$ with radius for the galaxy in figure 61. (Time in rotational periods of the initial balanced disk.)
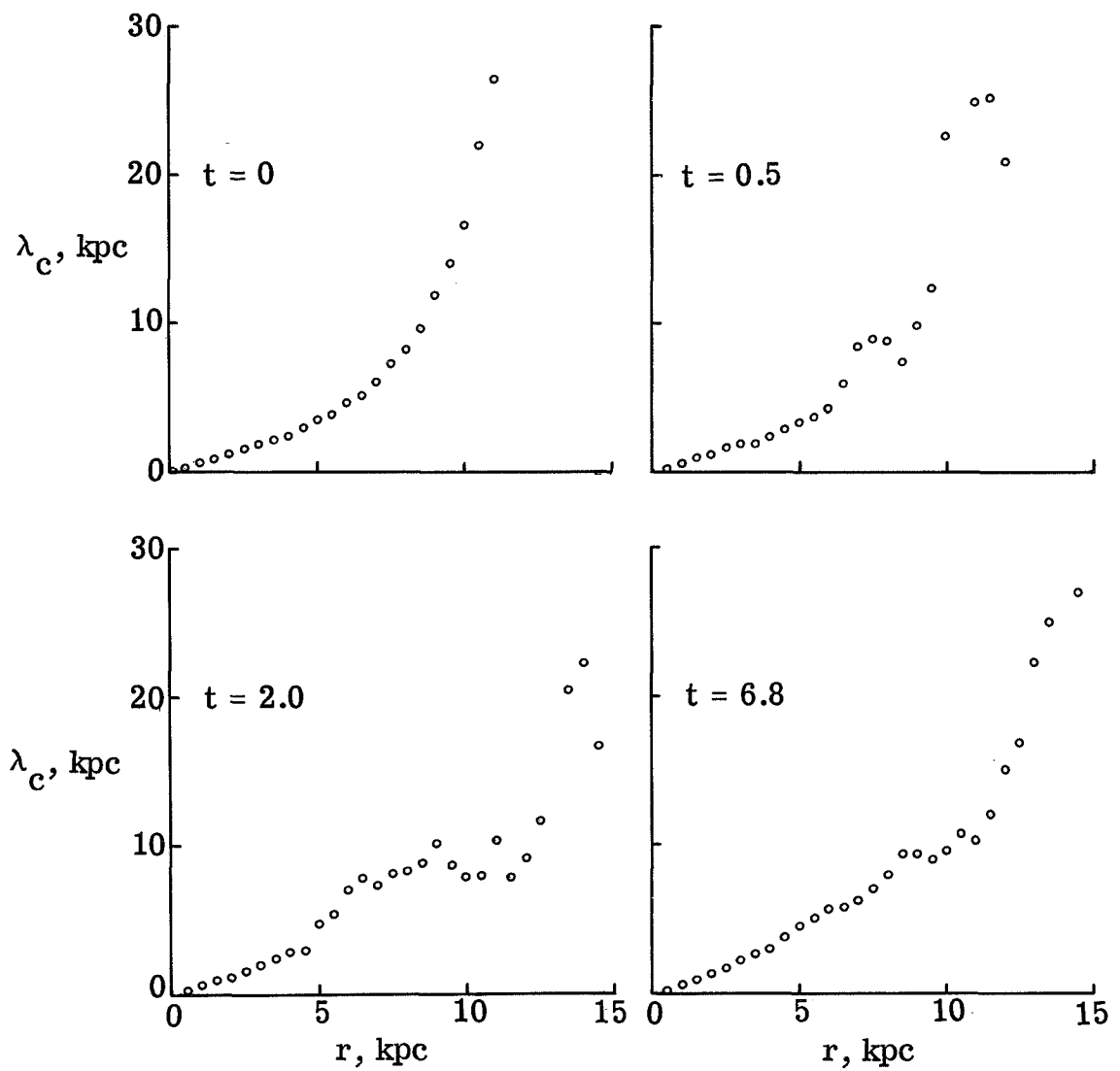
Figure 70.- Variation of the largest unstable wavelength λ_c with radius for the galaxy in figure 61. (Time in rotational periods of the initial balanced disk at r = 10 kpc.)

Figure 71.- Evolution of an initially balanced cold disk of stars under the influence of a fixed central force corresponding to the rotation curve given by equation (64). The 50000 disk stars contain 10 percent of total mass of the galaxy. (Time in rotational periods of the initial balanced disk at r = 10 kpc.)

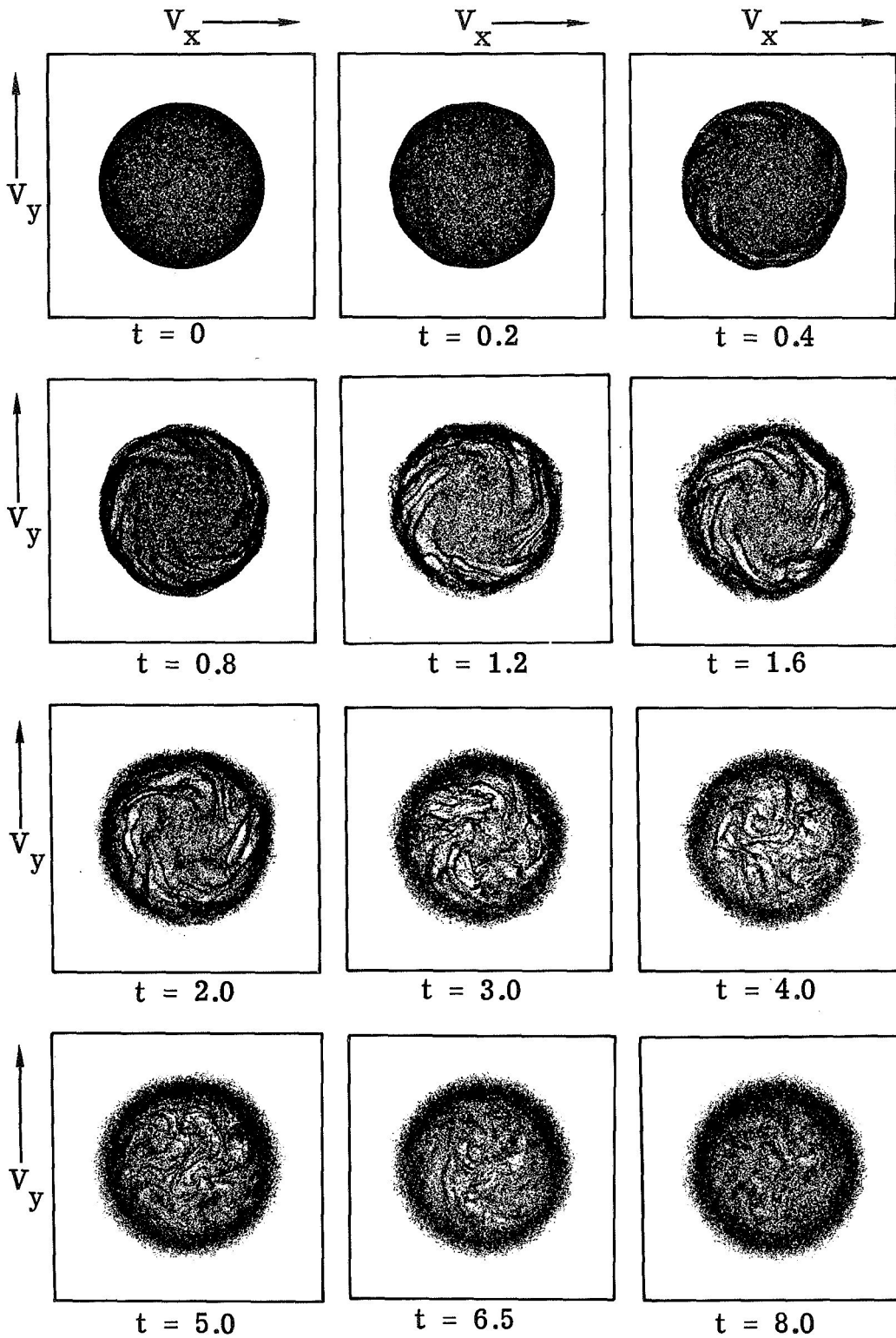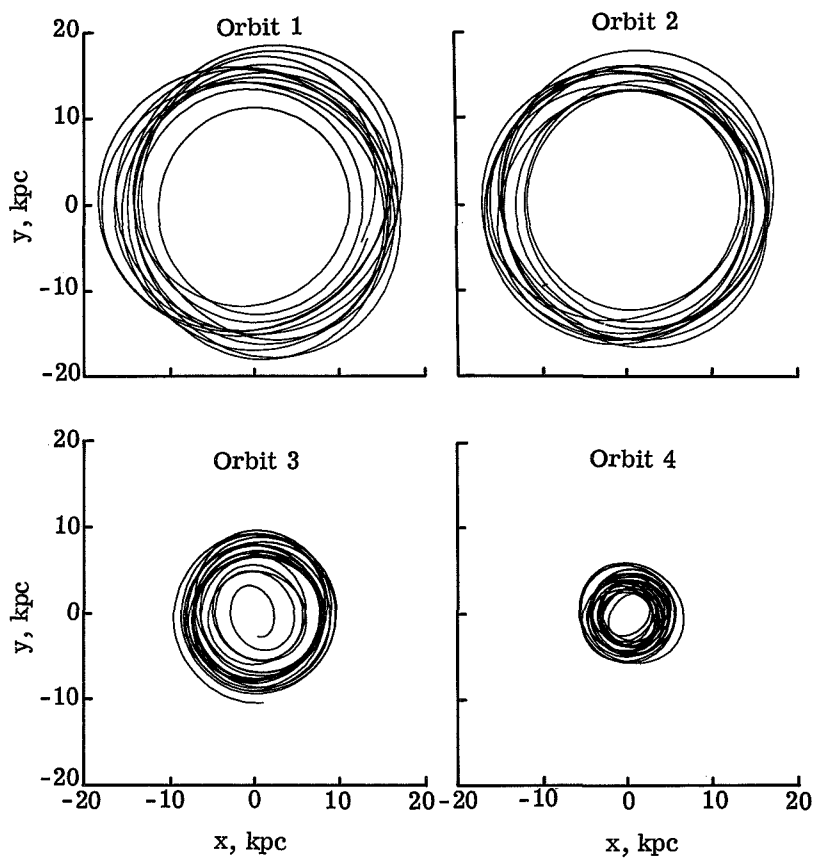Figure 72.- Four individual star orbits from the galaxy in figure 71.
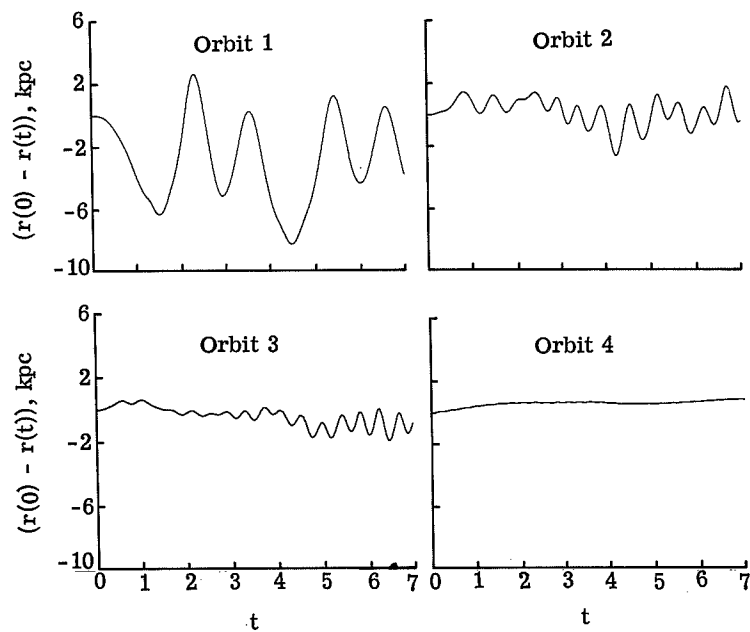
Figure 73.- Deviations of the star orbits in figure 72 from circular orbits. (Time in rotational periods of the initial balanced disk at r = 10 kpc.)
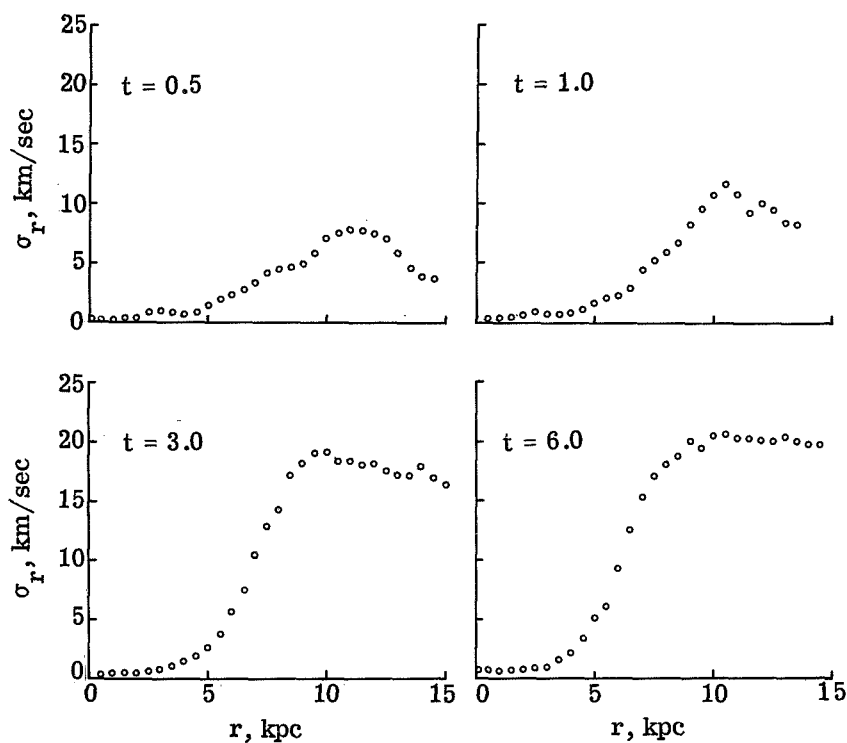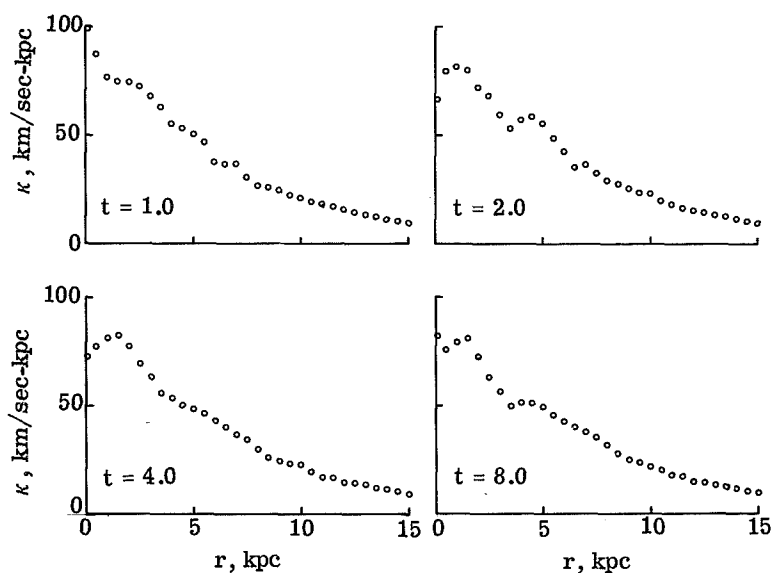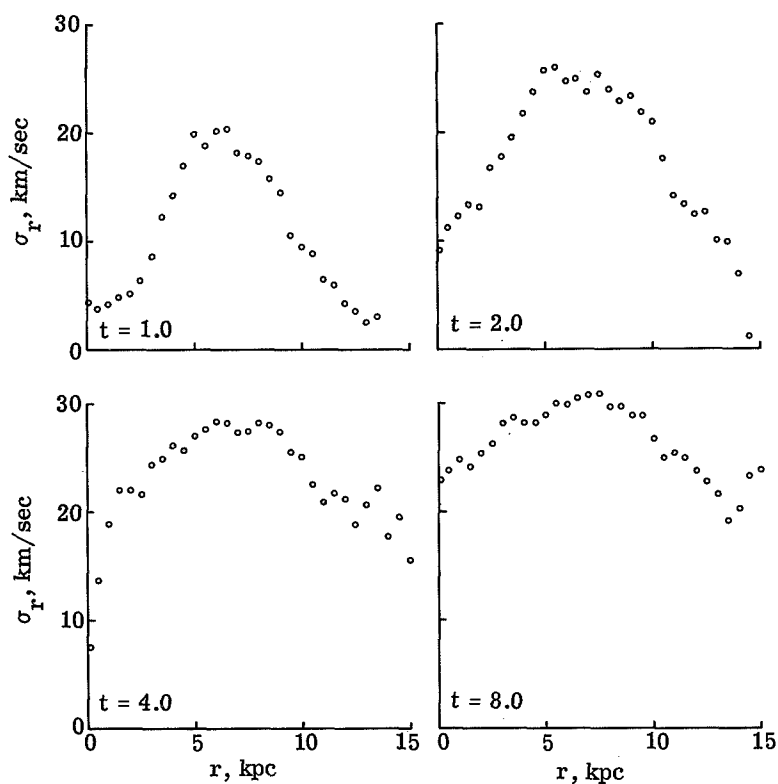
Figure 74.- Variation of the radial velocity dispersion with radius for the galaxy in figure 71. (Time in rotational periods of the initial balanced disk at $r = 10$ kpc.)

Figure 75.- Variation of $Q = \sigma_r/\sigma_{r,min}$ with radius for the galaxy in figure 71. (Time in rotational periods of the initial balanced disk at $r = 10$ kpc.)
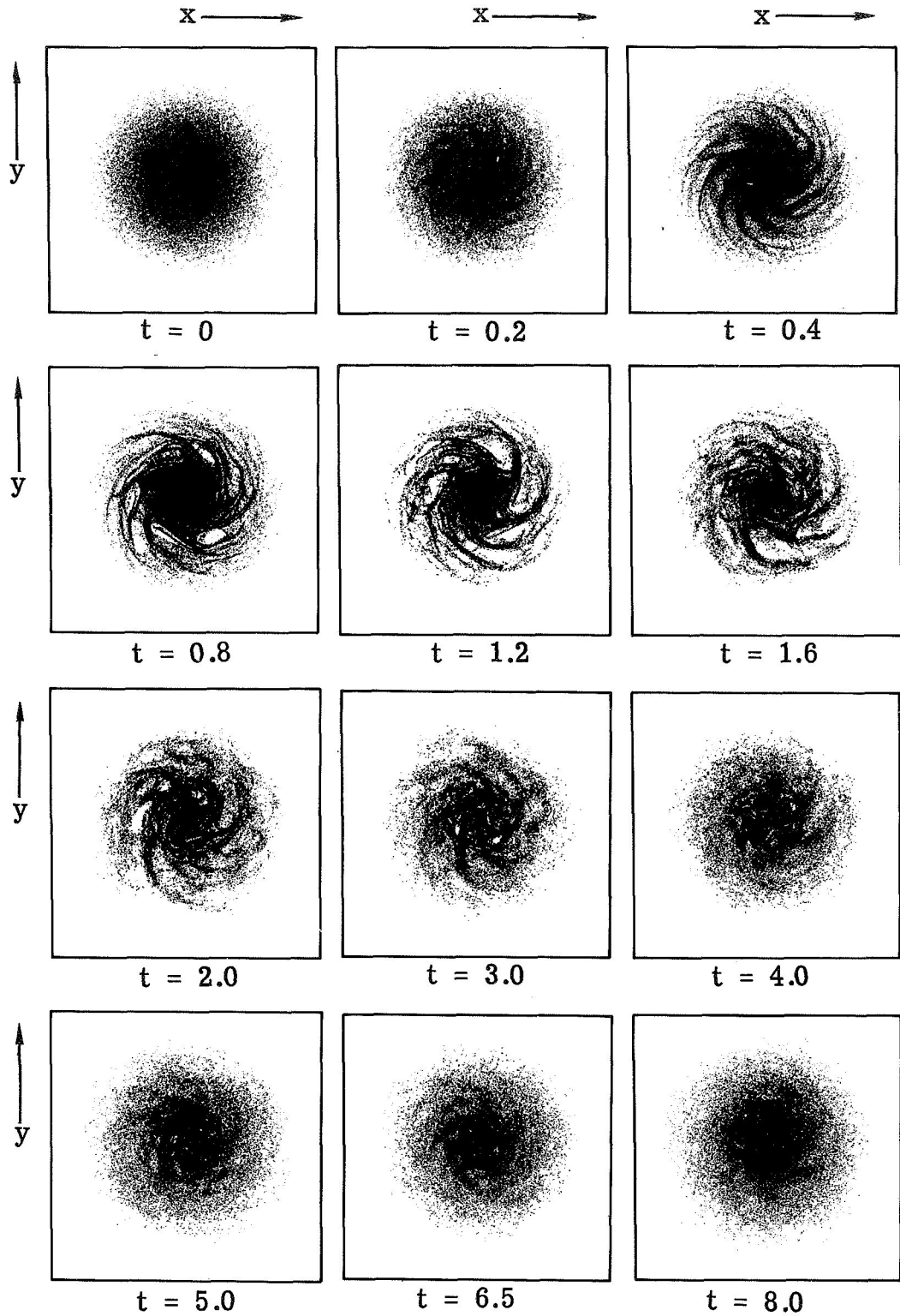
Figure 76.- Evolution of a disk of stars with a Gaussian mass distribution under the influence of a fixed radial force corresponding to the rotation curve given by equation (64). The 50000 disk stars contain 20 percent of the total mass of the galaxy. (Time in rotational periods of the initial balanced disk at r = 10 kpc.)

Figure 77.- Evolution of the disk of stars in figure 76 in V_x, V_y space. (Time in rotational periods of the initial balanced disk at $r = 10$ kpc.)

Figure 78.- Four individual star orbits from the galaxy in figure 76.
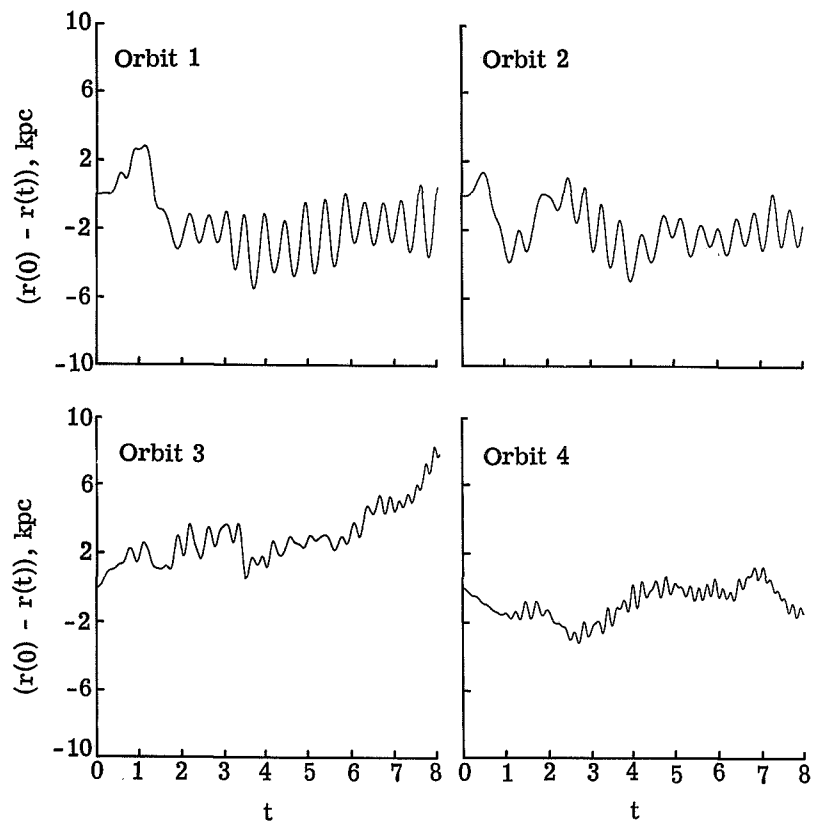
Figure 79.- Deviations of the orbits in figure 78 from circular orbits. (Time in rotational periods of the initial balanced disk at r = 10 kpc.)

Figure 80.- Variation of the epicyclic frequency with radius for the system in figure 76. (Time in rotational periods of the initial balanced disk at $r = 10$ kpc.)
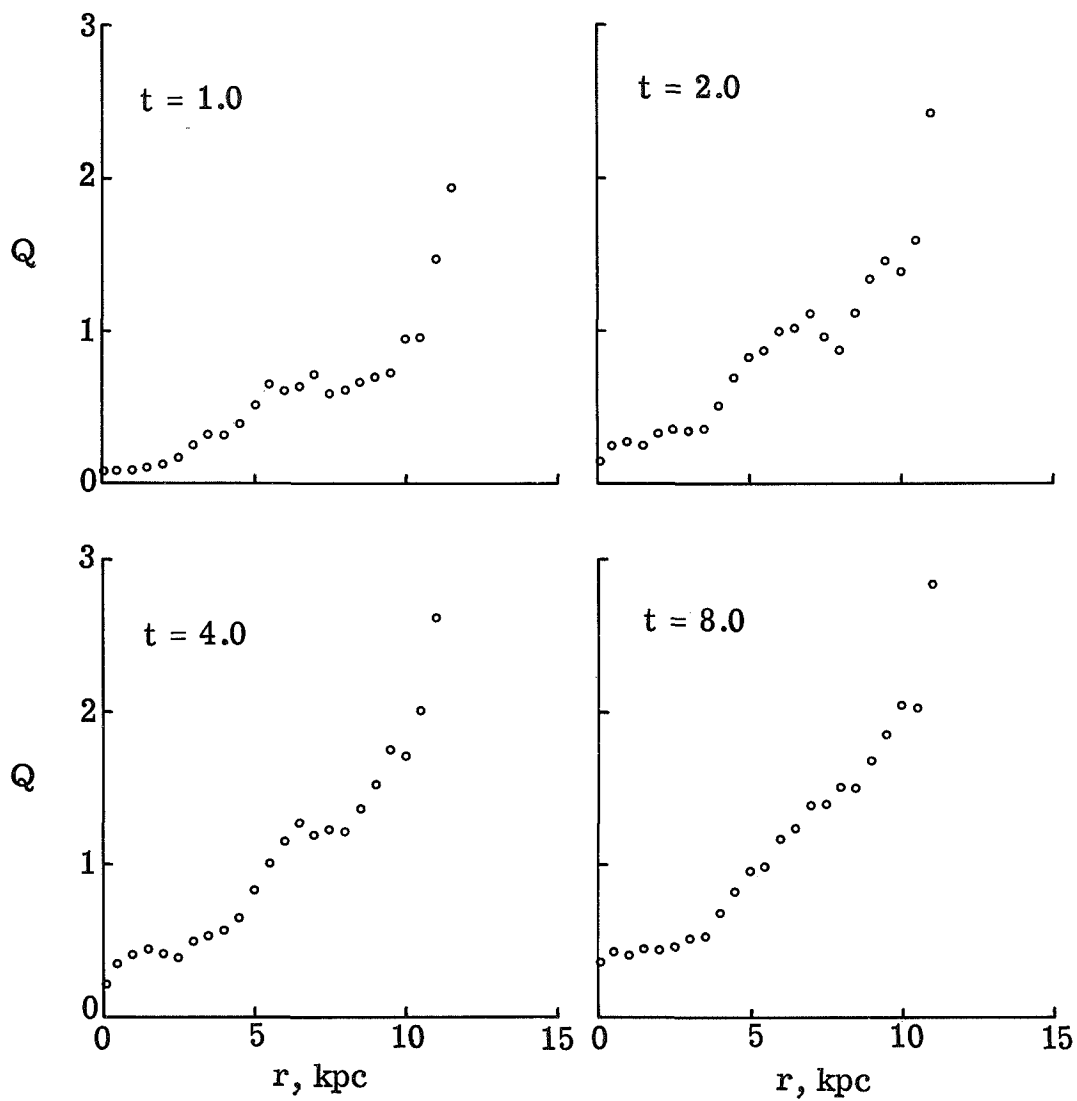

Figure 81.- Variation of the radial velocity dispersion with radius for the system in figure 76. (Time in rotational periods of the initial balanced disk at $r = 10$ kpc.)
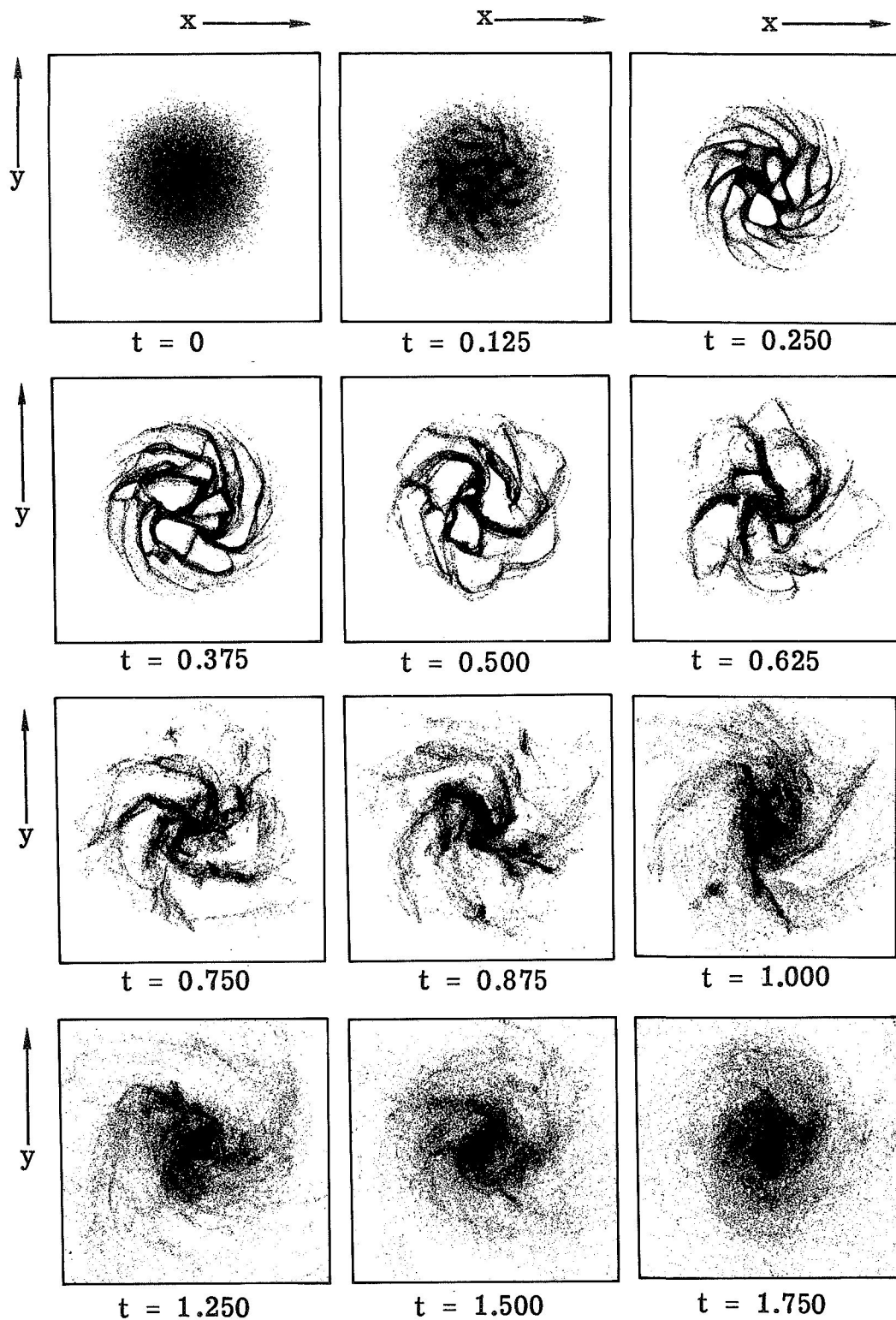
Figure 82.- Variation of $Q = \sigma_r/\sigma_{r,min}$ with radius for the system in figure 76. (Time in rotational periods of the initial balanced disk at $r = 10$ kpc.)

Figure 83.- Evolution of the stellar system displayed in figure 76 except that the 50000 disk stars contain 50 percent of the total mass of the galaxy. (Time in rotational periods of the initial balanced disk at r = 10 kpc.)

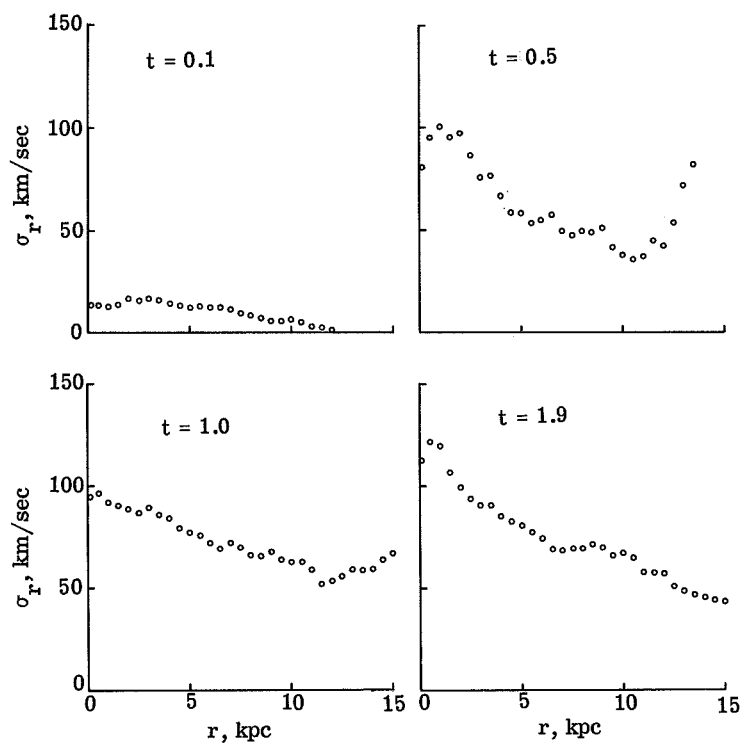Figure 84.- Variation of the radial velocity dispersion with radius for the system in figure 83. (Time in rotational periods of the initial balanced disk at r = 10 kpc.)
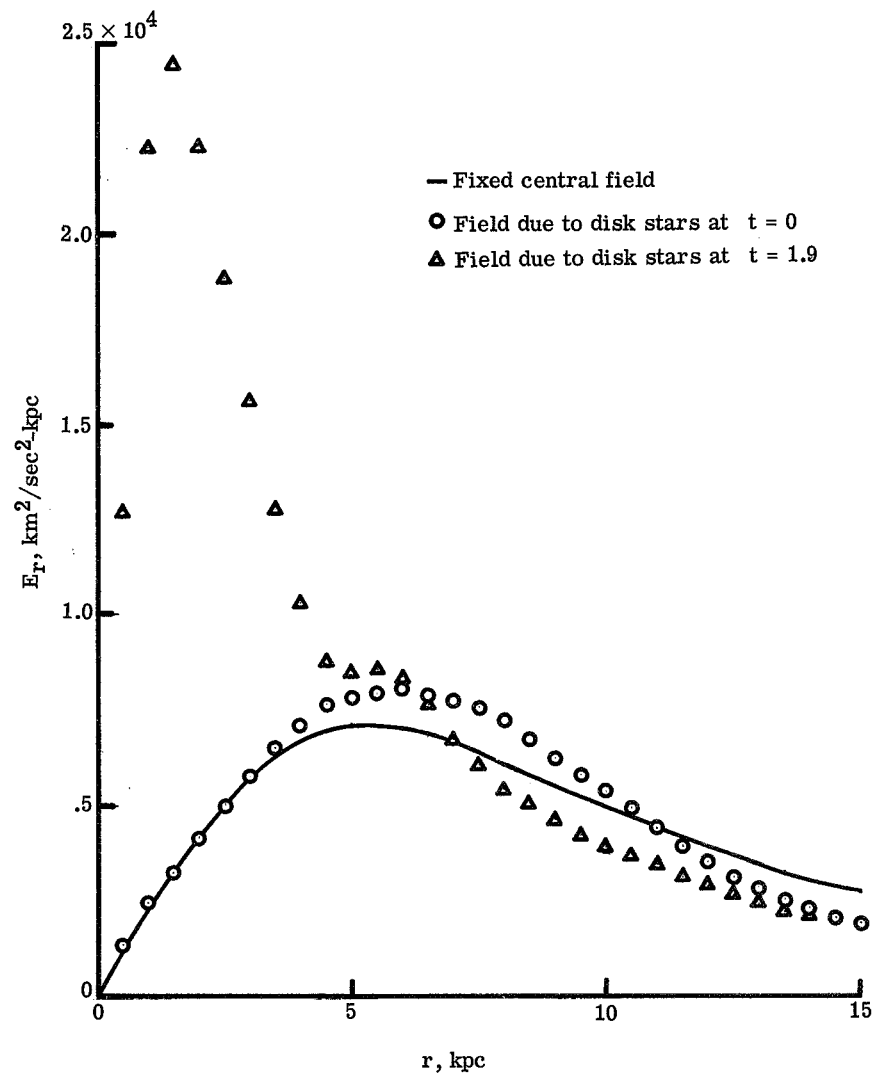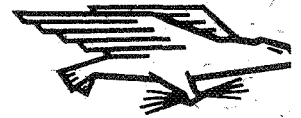

Figure 85.- Variation of the radial gravitational field with radius for the system in figure 83. (Time in rotational periods of the initial balanced disk at r = 10 kpc.)

*"The aeronautical and space activities of the United States shall be
conducted so as to contribute . . . to the expansion of human knowl-
edge of phenomena in the atmosphere and space. The Administration
shall provide for the widest practicable and appropriate dissemination
of information concerning its activities and the results thereof."*

— NATIONAL AERONAUTICS AND SPACE ACT OF 1958

NASA SCIENTIFIC AND TECHNICAL PUBLICATIONS

TECHNICAL REPORTS: Scientific and
technical information considered important,
complete, and a lasting contribution to existing
knowledge.

TECHNICAL NOTES: Information less broad
in scope but nevertheless of importance as a
contribution to existing knowledge.

TECHNICAL MEMORANDUMS:
Information receiving limited distribution
because of preliminary data, security classifica-
tion, or other reasons.

CONTRACTOR REPORTS: Scientific and
technical information generated under a NASA
contract or grant and considered an important
contribution to existing knowledge.

TECHNICAL TRANSLATIONS: Information
published in a foreign language considered
to merit NASA distribution in English.

SPECIAL PUBLICATIONS: Information
derived from or of value to NASA activities.
Publications include conference proceedings,
monographs, data compilations, handbooks,
sourcebooks, and special bibliographies.

TECHNOLOGY UTILIZATION
PUBLICATIONS: Information on technology
used by NASA that may be of particular
interest in commercial and other non-aerospace
applications. Publications include Tech Briefs,
Technology Utilization Reports and Notes,
and Technology Surveys.

Details on the availability of these publications may be obtained from:

SCIENTIFIC AND TECHNICAL INFORMATION DIVISION

NATIONAL AERONAUTICS AND SPACE ADMINISTRATION
Washington, D.C. 20546